

AD-A142 682

GEOKINETIC EFFECT ON MOTION SENSITIVE INSTRUMENTATION
SYSTEMS AND FACILITIES(U) WESTON OBSERVATORY MA
F A CROWLEY ET AL. 15 JAN 84 AFGL-TR-84-0031

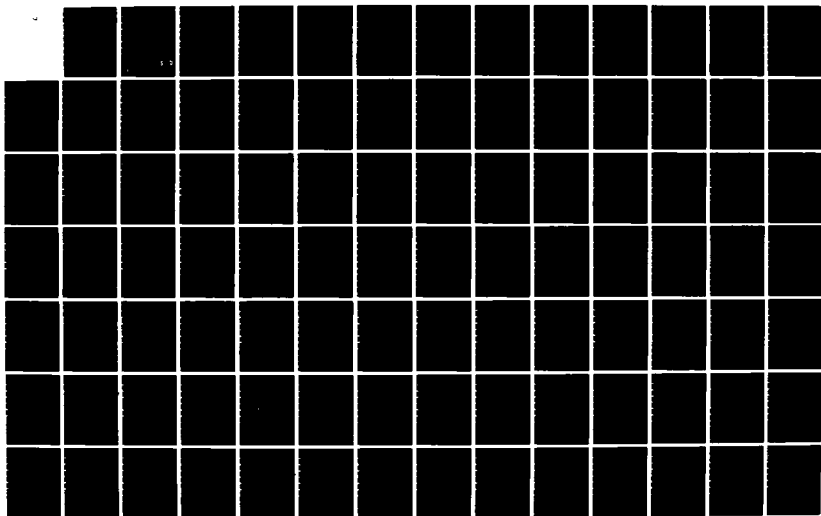
1/2

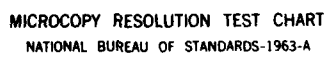
UNCLASSIFIED

F19628-81-K-0005

F/G 8/11

NL





MICROCOPY RESOLUTION TEST CHART
NATIONAL BUREAU OF STANDARDS-1963-A

12

AFGL-TR-84-0031

Geokinetic Effects on Motion Sensitive Instrumentation, Systems and Facilities

Francis A. Crowley
Eugene B. Hartnett
Joseph I. Blaney

Weston Observatory
Department of Geology and Geophysics
Boston College
381 Concord Road
Weston, Massachusetts 02193

15 January 1984

Final Report for period 1 October 1980 - 30 September 1983

Approved for Public Release; Distribution Unlimited

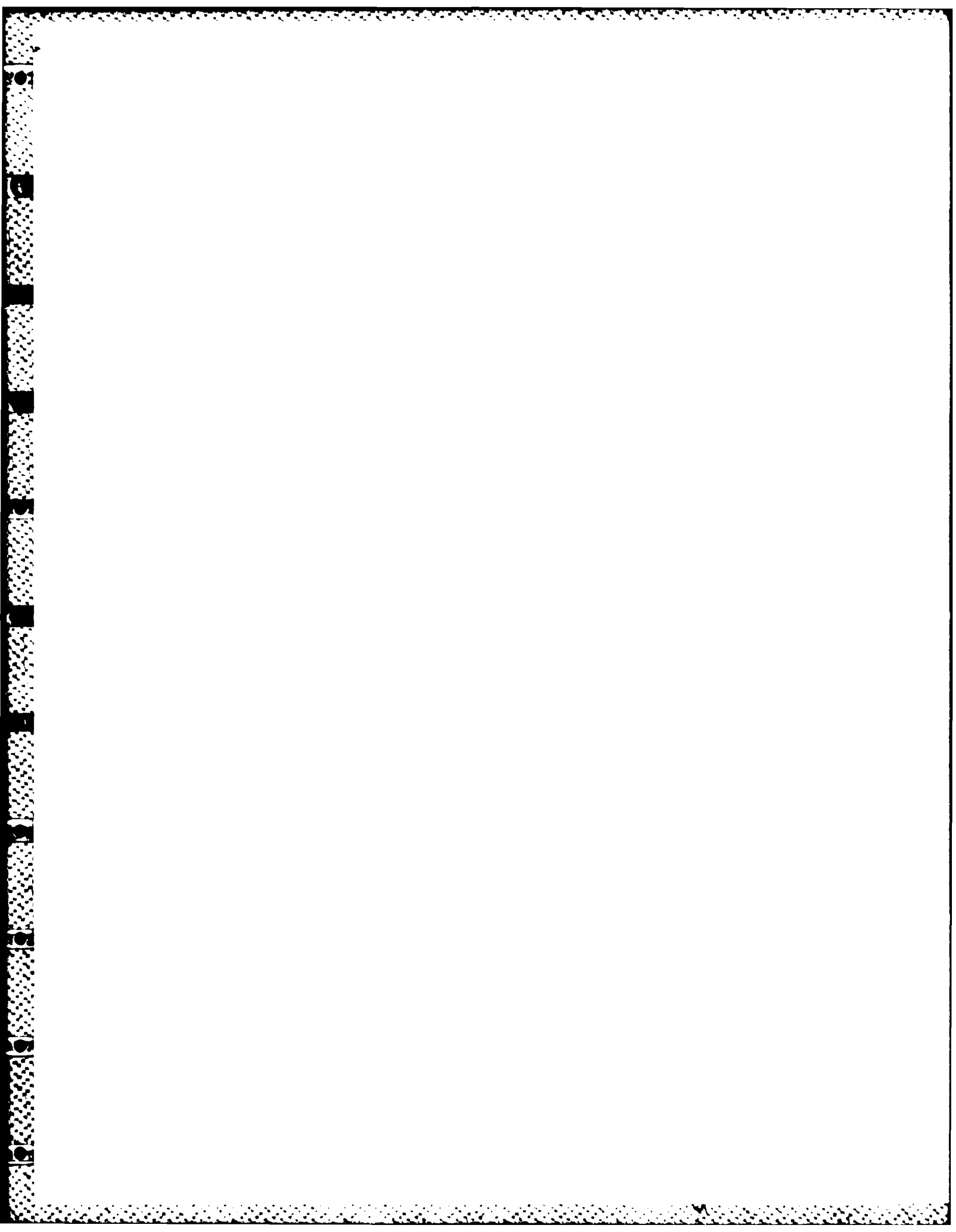
Air Force Geophysics Laboratory
Air Force Systems Command
United States Air Force
Hanscom AFB, Massachusetts 01731

DTIC
ELECTE
JUL 06 1984
S D E

DTIC FILE COPY

AD-A142 682

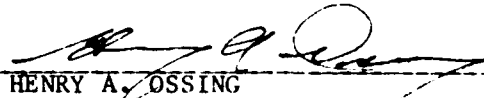
84 07 05 062



This report has been reviewed by the ESD Public Affairs Office (PA) and is releasable to the National Technical Information Service (NTIS).

This technical report has been reviewed and is approved for publication.


HENRY A. OSSING
Contract Manager


HENRY A. OSSING
Branch Chief

FOR THE COMMANDER


DONALD H. ECKHARDT
Division Director
Earth Sciences Division

Qualified requestors may obtain additional copies from the Defense Technical Information Center. All others should apply to the National Technical Information Service.

If your address has changed, or if you wish to be removed from the mailing list, or if the addressee is no longer employed by your organization, please notify AFGL/DAA, Hanscom AFB, MA 01731. This will assist us in maintaining a current mailing list.

Do not return copies of this report unless contractual obligations or notices on a specific document requires that it be returned.

UNCLASSIFIED

SECURITY CLASSIFICATION OF THIS PAGE (When Data Entered)

REPORT DOCUMENTATION PAGE		READ INSTRUCTIONS BEFORE COMPLETING FORM	
1. REPORT NUMBER AFGL-TR-84-0031	2. GOVT ACCESSION NO. AD-A142 687	3. RECIPIENT'S CATALOG NUMBER	
4. TITLE (and Subtitle) Geokinetic Effects on Motion Sensitive Instrumentation, Systems and Facilities		5. TYPE OF REPORT & PERIOD COVERED Final Report 15 Oct 1980-30 Sep 1983	
7. AUTHOR(s) Francis A. Crowley Eugene B. Hartnett Joseph I. Blaney		6. PERFORMING ORG. REPORT NUMBER	
9. PERFORMING ORGANIZATION NAME AND ADDRESS Weston Observatory, Department of Geology and Geophysics, Boston College 381 Concord Road, Weston, MA 02193		8. CONTRACT OR GRANT NUMBER(s) F19628-81-K-0005	
11. CONTROLLING OFFICE NAME AND ADDRESS Air Force Geophysics Laboratory Hanscom AFB, MA 01731 Contract Manager: Henry A. Ossing /LWH		10. PROGRAM ELEMENT, PROJECT, TASK AREA & WORK UNIT NUMBERS 62101F 7600-09-AD	
14. MONITORING AGENCY NAME & ADDRESS (if different from Controlling Office)		12. REPORT DATE 15 January 1984	
		13. NUMBER OF PAGES 115	
		15. SECURITY CLASS. (of this report) UNCLASSIFIED	
		15a. DECLASSIFICATION/DOWNGRADING SCHEDULE	
16. DISTRIBUTION STATEMENT (of this Report) APPROVED FOR PUBLIC RELEASE-DISTRIBUTION UNLIMITED			
17. DISTRIBUTION STATEMENT (of the abstract entered in Block 20, if different from Report)			
18. SUPPLEMENTARY NOTES			
19. KEY WORDS (Continue on reverse side if necessary and identify by block number) Geokinetics Rocket Plume Acoustics Motion Spectra STS Launch Environment Basin and Range Province STS Seismic/Acoustic Field Seismic Communication			
20. ABSTRACT (Continue on reverse side if necessary and identify by block number) This report describes research supporting continued refinement and expansion of ground motion knowledge crucial to USAF/DoD/NASA operations and plans. Primary emphasis was directed towards the seismic and seismo-acoustic attributes of field sites and facilities. The effects of ground motion, natural and man-made, on the performance of motion sensitive components, instrumentation and strategic systems were also investigated.			

UNCLASSIFIED

SECURITY CLASSIFICATION OF THIS PAGE (When Data Entered)

UNCLASSIFIED

SECURITY CLASSIFICATION OF THIS PAGE(When Data Entered)

Research studies included upgrading the Geokinetic Data Acquisition System (GDAS); operating the system at USAF designated field sites; developing and implementing computational techniques for data analysis; investigating the information capacity for communicating seismically in Basin and Range Valleys; and forecasting the seismo-acoustic environment for Space Transportation System (STS) launches at Vandenberg AFB.

Also considered in lesser detail was the improvement of intrusion detection systems; evaluation of seismo-acoustic waves; and the expansion and upgrade of archival seismic files.

UNCLASSIFIED

SECURITY CLASSIFICATION OF THIS PAGE(When Data Entered)

SUMMARY

USAF initiatives in developing and producing sophisticated aerospace components, systems and facilities demand continued emphasis on maintaining a current, relevant technology base. One element associated with such efforts is the effect of natural and artificial geokinetic inputs on motion sensitive systems. This report documents the overall results of a three year investigation whose purpose was the continued definition, refinement and expansion of the geokinetic technology base in support of conceptual, proposed and operational aerospace systems.

Weston Observatory participated in the development of the Geokinetic Data Acquisition System (GDAS) under a previous Air Force contract. The system was used and upgraded in the current study. Field tests and experiments were carried out at AFGL designated locations within the continental United States. The work described herein supports several USAF/DOD/NASA planning and operational concepts which involve investigating the ground motion environment at candidate sites for proposed strategic USAF systems in the Basin and Range Province of the U.S.; forecasting the seismo-acoustic environment for STS operations at Vandenberg AFB (VAFB) and determining the intensity and frequency content of air-coupled seismic waves caused by USAF overflights.

Also studied were the effects of static and dynamic loads on the motion environment (i.e. those caused by heavy vehicles, trains and wind turbulence). The seismic aspects of physical security and intrusion detection systems used by USAF were also investigated.

In compliance with a Ballistic Missile Office (BMO) Task Order, Weston Observatory conducted field test programs at locations in southwestern U.S. centered around Ely, Nevada. The purpose of these studies was to characterize local seismic affects on various missile basing modes. Additionally, ambient ground motion was monitored, collected and analyzed for inclusion in Weston Observatory archival files.

Weston Observatory supported a Space Division (SD) Task Order by deploying the GDAS at Kennedy Space Center, Florida to measure launch acoustics for STS-5 and STS-8. The program called for the measurement and evaluation of pressure generated during STS launches at KSC and defining an equivalent source term for forecasts at Vandenberg AFB, California.

Geokinetic measurements from seismic frequencies to quasi-static ground tilts were obtained to establish the deformation characteristics of surficial materials to time rate of loading.

A full duplex telemetry system, capable of accommodating eight data channels and suitable for master/slave operations with GDAS at remote field stations, was designed and fabricated under a sub-contract with Monitron Corporation.

A seismic test/calibration facility was maintained at Weston Observatory. This in-house capability provides a standard means for calibrating seismic and acoustic sensors. It also enables test and adjustment of various components prior to, and after deployment to field locations.

The acquisition and transcription of seismic and vibro-acoustic data into archival files was continued. Data documenting almost four decades of

seismic activity are maintained and updated periodically at Weston Observatory as dictated by observatory and contract requirements.

Prior to the Final Report, four other scientific reports were published under the contract. They are as follows:

Scientific Report No. 1, Seismic Transmission in Jackass Flats and Steptoe Valley, Nevada, by F.A. Crowley, E.B. Hartnett, and H.A. Ossing, 1 Dec 1981, AFGL-TR-82-0023.

Scientific Report No. 2, Seismic Communication in Basin and Range Province Valleys, by F.A. Crowley, Sep 1982, AFGL-TR-83-0014. ADA 115820.

Scientific Report No. 3, Amplitude and Phase of Surface Pressure Produced by Space Transportation System - Mission 5, by F.A. Crowley, E.B. Hartnett, and H.A. Ossing, Jan 1983, AFGL-TR-83-0039. ADA 125846.

AIAA Paper No. 83-2638, STS Vibro-Acoustics, H.A. Ossing and F.A. Crowley, AIAA Shuttle Environment and Operations Meeting, 31 Oct 1983.

The contract partially supported requirements for a Master of Science thesis in Geophysics entitled, The Seismic Response of a Layer Over a Half Space to an Air Blast, by Parker Mann, Jr., Boston College.

Accession For	
NTIS GRA&I	<input checked="" type="checkbox"/>
DTIC TAB	<input type="checkbox"/>
Unannounced	<input type="checkbox"/>
Justification	
by _____	
Distribution/	
Availability Codes	
Dist	Avail and/or Special
A-1	



PREFACE

Weston Observatory, an adjunct of Boston College Department of Geology and Geophysics, was responsible for performing this study. Research was sponsored by the Earth Sciences Division, Air Force Geophysics Laboratory, with Mr. Henry O. Ossing as the Contract Manager. The work was primarily carried out at the Observatory located in Weston, Massachusetts. Supporting field efforts were conducted in the vicinity of Ely, Nevada and at Kennedy Space Center, Florida.

This report documents original research and technological initiatives utilizing government furnished equipment jointly developed by AFGL and Boston College under previous USAF sponsorship. Results of the study suggesting additional research of potential significance to DOD plans and programs are:

- a. Continue to upgrade the GDAS to improve its reliability and utility, along with new work to expand its capabilities in response to AFGL mission requirements.
- b. Develop and demonstrate viable techniques to forecast the motion environment of structures and facilities excited by rocket launches, aircraft overflights and atmospheric explosions.
- c. Investigate limitations imposed by real world seismic propagation and noise effects upon surveillance/intrusion-detection systems.
- d. Establish the potential capacity of seismic communication links operated in geological structures suitable for "deep-basing".

TABLE OF CONTENTS

		Page
	Summary	1
	Preface	5
1.0	<u>GEOKINETIC DATA ACQUISITION SYSTEM</u>	9
1.1	Certified Laboratory Test of GDAS	10
1.2	System Performance	11
1.3	Transducer Elements	12
1.4	J Box	14
1.5	Signal Conditioning Hardware	16
1.6	Software	20
1.7	Memory	23
1.8	Storage	23
1.9	Graphics	24
1.10	Telemetry Sub-System	24
1.11	Central Processing Unit	25
1.12	Operational Features	25
1.13	References - Section 1	27
1.14	Illustrations - Section 1	29
2.0	<u>FIELD OPERATIONS</u>	37
2.1	Railroad and Steptoe Valley Operations	37
2.2	Calibration	39
2.3	Kennedy Space Center	39
3.0	<u>PHYSICAL SECURITY/INTRUSION DETECTION</u>	41
3.1	Field Studies	41

	Page
4.0 <u>SEISMIC COMMUNICATION</u>	43
4.1 Approach	43
4.2 Seismic Noise in Basin Valleys	44
4.3 Seismic Signals	45
4.4 Channel Information Rates	50
4.5 Transmitter and Receiver Arrays	52
4.6 Site Effects	53
4.7 Findings	53
4.8 References - Section 4	55
4.9 Illustrations - Section 4	57
5.0 <u>SPACE TRANSPORTATION SYSTEM</u>	73
5.1 Approach	73
5.2 Measurement System	74
5.3 Analysis of Surface Pressure	76
5.4 Plume Spectra in Standard Form	79
5.5 Comparison of Forecasted Values	82
5.6 Findings: STS-5	82
5.7 Conclusions: STS-5	83
5.8 References - Section 5	85
5.9 Illustrations - Section 5	87
6.0 <u>SEISMIC PIER ROOM</u>	107
7.0 <u>SONIC BOOMS</u>	109
7.1 References - Section 7	111
<u>APPENDIX A-DEFINITIONS</u>	113

1.0 GEOKINETIC DATA ACQUISITION SYSTEM, GDAS

GDAS is a system to measure, analyze, store and display geophysical phenomena. It consists of three similar hardware units functioning either independently or in consort. GDAS is permanently packaged in shock isolation cases, ready for transport. During the contract period, components were upgraded in response to program needs. Major improvements have been made to support a greater diversity of sensors; accommodate higher data rates; incorporate an expansion in storage; and improve system reliability, particularly when operating in a harsh field environment.

The GDAS Central Processing Unit (CPU) has been upgraded by replacing the Digital Equipment Corp microprocessor LSI-11-03 with a LSI-11-23. Disk storage capacity has been expanded by implementing a Charles River Data System Winchester HD-11 disk unit. These hardware changes are an initial step towards increasing system bandwidth to 100 Hz.

An important aspect of this effort was to physically strengthen the units for shipment back and forth to field sites and for operation at remote locations under unfavorable conditions. This involved installing more sturdy electronic parts, reinforcing structural members, providing locking electrical connectors and fabricating and installing restraining devices for P/C modules and components.

The predicted vibrations at Kennedy Space Center (KSC) for STS launches required hardening and dampening of components located close to the launch pad. Physical restraints were installed and component carriers in the filter section were replaced by full circuit headers. An added bonus of this modification was a reduction in noise. Foam block card

restraints were strengthened to support the weight of the Kennedy recorder. Calls to individual manufactures of equipment used in the system were made to verify vibration and shock specifications. Suggestions made by the environmental testing departments of these companies were implemented as needed.

1.1 CERTIFIED LABORATORY TEST OF GDAS

Because of the proximity of the GDAS to the launch pad at KSC, full scale vibration testing was conducted 8 Oct 1982 at the certified test laboratory of the Acton Environmental Test Corp (AETC). These tests were documented and a report was prepared by AETC describing the methods used and the overall results. Analysis of the actual STS-5 vibration environment at Kennedy Space Center showed the environment was less severe than forecast. The following information relative to pre-launch shake tests was derived from AETC Test Report No. 17818-83D, 26 Oct 1982 (1).

Test Procedure - The GDAS under test was housed in two fiberglass cabinets mounted side-by-side on an aluminum I-Beam fixture. Forty Durometer rubber strips were placed on the cabinet side of the vertical and top supports for damping and tightness. The test item and fixture assembly were clamped to the AETC 45° biaxial shaker table.

Test Monitoring - The test used six accelerometers, two of which were attached to the shaker table to monitor the test input. A second biaxial pair monitored the response of the top of the mounting rack in cabinet No.1, while a third pair monitored the top of the rack in cabinet No.2.

Functional and Operational Test - Set up of the monitoring computer was accomplished by Boston College personnel. They also performed pre, post and operational testing. Evaluation traced noise on the data line to a switching power supply and to line pickup from many arbitrary sources.

Sine Sweep Test - The sine sweep test consisted of a sinusoidal input of equal in-phase vertical and horizontal accelerations at frequencies from 1 to 33 Hz. The sine sweep was conducted at a maximum sweep rate of 1 octave/minute. Sweeps were done at .25g peak-to-peak and .5g peak-to-peak accelerations. The input was applied by the AETC 45° biaxial table in two orientations as follows: 1) Front-to-back & Vertical, 2) Left-to-right & Vertical. Resonance frequencies were determined by a 90° phase lag between the response waveform and the input waveform. All amplifications were also noted. The accelerometer outputs were permanently recorded by an oscillographic recorder.

1.2 SYSTEM PERFORMANCE

Overall performance of the GDAS electronics and associated components during STS-5 was as expected. The quality and quantity of data collected more than met the needs of the field test program. Steps taken to strengthen structural parts of the GDAS chassis and to dampen excessive vibration during launch were effective. The pre-launch shake tests at AETC and the actual launch at KSC show that with proper precautions that the GDAS can operate successfully in a relatively severe vibration environment.

Because of a discrepancy between our measurements and those reported by NASA, we elected to recertify our KSC pressure readings by returning the MLR transducers to the manufacturer for recalibration and recertification following the launch of STS-5. A reevaluation of all transducers was made at the vendor's test facility by Weston personnel. All units were found to be well within specifications and tracked quite closely with the original performance estimate. Verification and recertification of sensor performance supports the validity of Weston pressure data.

1.3 TRANSDUCER ELEMENTS

1.3.1 Seismometers - For most study applications seismometers are buried in shallow holes over extended periods to ensure continuous, real-time monitoring and recording of seismic occurrences. In the past, there have been problems caused by moisture seeping into the sensors, primarily around electrical connector seals because of shrinkage and/or deterioration of sealing material. In order to resolve this, LASA geophones used by another group at Weston Observatory were examined and tested. These sensors, electrically and physically identical with our units, are encased in a steel housing completely waterproofed and capable of withstanding relatively high pressure differentials. We are investigating options for replacing older geophones with these ruggedized models.

Test and calibration of Hall-Sears seismometers has continued and a set of units was designated to be a comparative standard. A set of Mandrel Industries EV-17 horizontal seismometers was tested and calibrated against

these standards. The EV-17 seismometers were subsequently implanted in Railroad Valley.

1.3.2 Seismic Calibration - A means for calibrating seismometers during field studies was incorporated into the J Box. The calibration hardware uses a unit gain differential amplifier to isolate the power source from the J Box circuitry. The current capability of the calibration unit is 100 ma. This is sufficient to concurrently run 16 seismometer calibrations or deliver calibration signals to all external preamplifiers. The unit resides in slot 17. (Figure 1-1)

1.3.3 Pressure - Eight pressure transducers, Model MLR 1.5 PSID, were purchased from D.J. Instruments to expand our measurement capacity in support of the STS launch program. Hardware for sixteen additional channels was constructed and tested. Weston Observatory again expanded its pressure collection capability for the STS-8 launch (3rd quarter, 1983).

New pressure transducer amplifiers were constructed with better reliability, noise and drift characteristics. The primary operational amplifier in these new units is an Analog 714/OP07. A second operational amplifier, Analog 725, was evaluated as a substitute. Mounting requirements for the 725 amplifier were included in the design of the circuitboard. Use of the 725 is favored when extremely high gain is required.

A fixed three terminal voltage regulator, LM 7805 uc, replaced the 723 precision regulator to decrease noise and temperature related drift in the excitation voltage.

The new pressure amplifier employs the bridge network shown in Figure

1-2. The network uses a resistor network that allows a single resistor gain control given by:

$$A_v = \frac{R_3}{R_1} \left(\frac{1+R_5}{R_3 \parallel R_6} \right)$$

The network R9, R10 balances the D.C. output. C1, R11 is the compensation network needed with the 725 amplifier. Also provided on the printed circuitboard but not implemented is an etchout for an additional amplifier/filter section.

Pressure Transducer Calibration - Several methods of calibrating pressure transducers were investigated including: a) Periodic calibration by an approved test facility, b) return to the manufacturer for calibration and re-certification, c) comparison with barometric transducers and d), construction of a calibration unit. The last proved to be the most convenient, reliable and compatible with field operations. Various devices were tested, including flexible transparent tubing, a hand blown glass tube and finally a commercial manometer. The manometer was affixed to a mounting board and treated as a laboratory standard. The system was used in field calibrations at Kennedy Space Center with a manifold that allowed a common input to all sixteen pressure sensors.

Pressure Sensor Box - Figure 1-3 shows the pressure transducer and its related amplifier. These sensors-amplifier units are hardwired to a bank of amplifiers in the J Box.

1.4 J BOX

The present junction box is the fourth such unit that has evolved over

the years. Although larger and heavier than earlier models, the latest box has greater flexibility. The entire array can now be serviced, tested or changed without disturbing a sensor.

The box is a stainless steel Hoffman-type 4X enclosure with a hinged top sealed by a full waterproof gasket. Watertight input/output connectors pass through the sides. The entire box can be buried for extended time periods in drained soil. The J Box has a dual card cage and power supply on a removable panel which also serves as a heat sink. The R.O. Associates model 303 power supply provides ± 12 V with a current margin well in excess of present requirements. In hot climates, deep burial is necessary to insure proper ambient temperature.

The dual cage card holds 16 preamplifier channels, one calibration driver and one empty slot for storage. Additional wiring for running remote preamps is included. Signal conditioning can be accomplished within the J Box or at the recovery amplifiers. A 110 VAC service outlet is provided for test and repair of internal components without the need to connect/ disconnect the unit to accommodate test equipment.

1.4.1 J Box Modifications - Modifications made to the J Box are shown in the wiring diagram, Figure 1-4. A shielding wire connecting various sensor cases and the J Box was added to the system. The need for this evolved from tests that showed noise induced by individually grounded seismometers could be suppressed by using a common ground throughout.

1.5 SIGNAL CONDITIONING HARDWARE

1.5.1 Preamplifiers and filters - A bank of 16 preamplifiers was designed, constructed and tested. The new design features a temperature compensation circuit and a precision current source for system calibration.

The preamplifier has three stages, Figure 1-5. Stage 1 (A1 and A2) is a high input impedance full differential amplifier. Stage 2 is a two pole low pass Butterworth Filter (A3). Stage 3 (A4) is a buffer driver that decouples the preamp from the line. Also on the board is a current source (A5) for calibration.

Multi-stage amplifiers were selected because of their low drift, low noise and input overload protection characteristics. Input stage (A1 & A2) exhibits high common mode rejection independent of gain. A single common mode adjustment (R5) balances the gains of the two halves of the stage. The circuit is inherently low drift, especially at low gain. Resistors were chosen to balance the sensor impedance and bias currents. Equal gains in A1 & A2 insure cancellation of bias drift. A cross coupled single balance resistor (R15) in this circuit insures minimal drift. The additional circuits (A3 & A4) are sign opposing to further cancel drift.

Compromises made to increase temperature stability are not without penalty. The balance technique causes some reduction in open loop gain and high frequency response. The use of equal gain units limits the common mode handling of the overall circuit. If a common mode voltage in excess of 5 volts is present, A1 will cause saturation. Such penalties are relatively insignificant when using short lines.

Resistor network R1 thru R4 is a damping network consisting of four resistors. As represented, damping is halved and balanced effectively by forcing the seismometer or other sensor to be a balanced source; i.e., a phantom ground is reflected in the source by virtue of the grounding of junction R2 and R4. This grounding offers a return for the non-inverting inputs of A1 and A2, and references the sensor to ground. Also, for high signal input, the damping section can function as a voltage divide network. When this preamplifier is used as a recovery amplifier, the network can be changed to allow high pass or low pass amplification. Such combinations result in a single pole filter. Resistor/capacitor combinations used with this application call for $R_1 C_1 = R_2 C_2$.

As mentioned, resistor selection with the A1, A2 circuit is made to balance bias current and equalize gain. In the circuit, R5 is the common mode adjust. A common mode rejection ratio of 60 db is easily obtained. Gain can be changed by the addition of a single resistor across the two summing junctions. This resistor increases the differential gain, but not the common mode gain. Therefore, common mode balance and handling capability remain constant over gain changes. The resistor affects both halves of the amplifier, holding drift cancellation. For gain purposes, this resistor (R9) is effectively across R5, R6 and R9.

A two pole Butterworth Filter was devised using A3 as an active element. The circuit is in standard form as shown on the schematic. Provisions are made on the board for filter changes by soldered jumpers.

The output stage is an inverting unity gain amplifier. Resistor R26 equals the combination of R24 and R25 for bias balancing. Capacitor C5 is for oscillation suppression. Resistor R27 decouples the op-amp from the

large capacitive load presented by long signal lines. It is included within the feedback loop to prevent its appearance as a finite resistance in the line. The circuit can be used for additional amplification, if needed. The total circuit has a zero phase shift at DC.

The current converter (VIC) used for calibration is mounted on the preamplifier board using A5 as an active element. It is designed for a floating load. In the circuit, the calibration current is supplied by the op-amp and driver. This only draws ECal/R28 amperes from the cal driver, which in turn isolates the calibration source from the J Box. The circuit supplies the entire calibration current to the load. A complementary symmetry pair, (Q1,Q2) was added to support currents as large as 100 ma. Resistors R31 and R32 reduce the possibility of thermal runaway in case of overload without limiting the current capacity of the transistors. Capacitors C10 and C11 are oscillatory suppressing and bandpass limiting. In operation, the input current is amplified by the ratio of R29 and R30.

Resistors R28 and R30 are standoff mounted to facilitate change. The voltage constraint on the circuit is the limiting factor on the size of either resistor. For normal calibration frequencies the inductance of the seismometer calibration coil can be neglected. This circuit uses its own ground line to eliminate voltage drops on the seismic amplifier ground line when large calibration currents are needed.

Standard 4.5" x 6.5" circuit cards were used with a two sided, 22 pin (4 total) etched edge connector having .156" spacing. A single dog-eared extractor is mounted on one corner. Input circuitry of A1 and A2 have been ringed with ground planes to eliminate leakage current with high input impedances. Included within these loops are the damping resistors, R1 thru

R4, and the addition gain resistors R20 thru R24. The calibration source is isolated from the amplifier by a ground plane and separately bypassed supply voltage lines.

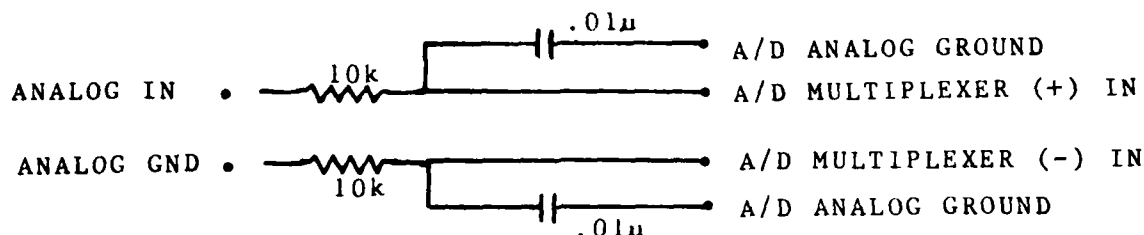
Component layout for the A1, A2 circuit was compacted for noise reduction. Due to low density on the card, layout and schematic follow fairly well. The balance potentiometer is functionally more prominent and accessible than the common mode adjust potentiometer. Both are readily accessible from the rear. Ground and output test points are provided. Placement of the two pole filter provides access to check the differential stage. Comparison of the card and schematic (Figure 1-5) locates specific jumpers or resistors.

1.5.2 A/D Converter - Considerable effort was directed toward isolating and resolving intermittent noise in the GDAS A/D converter. This effort is part of a continuing drive to reduce overall noise in the system. Ground loop problems between the A/D module and the filter-amplifier deck necessitated redesign of the calibration driver used in the filter-amplifier deck. This circuit accepts the D/A output of the A/D module, decouples it from the digital system, and supplies some signal filtering and gain adjustment. It then acts as a buffer-driver to supply the calibration signal to the J Box. In addition, the unit supplies a buffered return to the A/D for recording the absolute calibration signal.

1.5.3 A/D Noise - As noise reduction within the analog sub-system progressed, the A/D module evolved as the major contributor. When active, the unit must draw a charge from the driving circuit. A relatively large current spike then develops to contribute to noise. Consultation with the manufacturer confirmed this and they suggested a modification which had

minimal results.

Because of the nature of the noise it was decided to install a single-pole, low pass filter as close as possible to the A/D input. The filter not only reduces interactive noise but presents a capacitive load to the multiplexing capacitance for charge transfer. This filter is set at 1.59 KHz, well above our present maximum measurement frequency. A single channel presentation of this filter is as follows:



Remaining noise within the A/D is caused by switching pulses from the computer and the control circuitry on the A/D itself. Noise specification for the A/D is $\pm \frac{1}{2}$ LSB, a figure we have not been able to meet except in a special test setup at the manufacturers facility.

In the actual filter, analog grounds from the filter deck are tied together at the output of the 10k resistor and subsequently, only one capacitor is used on the negative side. This is due to the constraint of the A/D working in a psuedo-differential mode.

Additional noise reduction within the A/D was realized by placement of ceramic bypass capacitors on the supply bus and on the output of the DC-DC converter used in the analog section of the A/D module.

1.6 SOFTWARE

System identification software was extended to document electronic

elements as well as provide estimates of overall systems response. This effort was divided into three areas: a) Calibration - The program that calibrates the sensor was split into two versions to allow output to either the printer-plotter or the hard copy unit. The program has also been adapted to estimate the overall electronic response; b) Electronic Components - Several existing programs were used to design or to change the parameters of the filter cards and record these parameters; c) Graphics - Work was completed on a new plotting library compatible with the existing LSI libraries.

1.6.1 Implementation and Upgrade - Data acquisition software and clock hardware for GDAS were altered to permit analog sampling to 8000 samples per second with output to disk, or 3000 samples per second with output to tape. The maximum number of scans per second is 500; maximum number of channels per scan is still 16. The ERC calendar clock was modified to support different sample rates, selectable by a switch.

A package of programs has been developed to analyze data and produce plots for scientific reports much quicker than before. Additionally, we continued to make revisions, additions and improvements to our plotting libraries. One significant change reduced the amount of computer memory required to allow larger, more powerful programs to be run. In specific circumstances, an unlimited number of points can now be plotted.

Event detection algorithms were applied and tested for effectiveness in measuring strong motions, given ground response characteristics of the site. Ground motion data were analyzed to upgrade the data acquisition, formatting and storage required for future operations. Work on refining a standard structuring of the data file was continued and a brief library of programs that allows easy access to the data files has been written.

License upgrade of the DEC LSI-11/23 was completed. Software was upgraded by the installation of RT-11 Version 4. In addition, the Fortran library was rebuilt with "virtual arrays" enabled. This allows the use of upper memory to hold data arrays. Larger quantities of data can be processed and lower memory is freed for more executable code. The Fortran compiler and library were rebuilt to produce threaded code with floating-point unit subroutines. This results in faster execution of floating point arithmetic.

Data analysis techniques to determine the following site characteristics continued: a) Ground response to static and dynamic loads, b) effectiveness of a small seismic array to detect, identify and locate nearby surface sources, c) normal impedance of a site to acoustic inputs and d), source description of the STS exhaust plume.

Synthesizing a prediction operator for seismics in Railroad Valley was accomplished. Approximation operators were formed and used to predict the responses for actual hammer-blows. Tiltmeter data from truck runs were frequency scaled to enable comparison to a common vehicle speed.

A modified data acquisition program was produced which uses extended memory for storing samples until memory is full before writing a file. The unmodified version can sample 16 channels at 100 samples/second for about 10 seconds. The modified version can sample for about 57 seconds.

Also completed was the analysis of KSC data to provide control for structure response measurements at VAFB.

The data acquisition program "SAMPLE" was modified to respond to remote control for the STS launches at Kennedy Space Center (KSC). Data acquisition program "DKSAMP" was modified to accept data from the Monitron telemetry hardware.

1.7 MEMORY

LSI-11/03 units were replaced by more powerful LSI-11/23's. The new CPU's permit faster data acquisition and, when used with the floating point instruction set, provide faster processing. New memory management allowed an expansion of each unit from 32K to 128K words. This feature enables data acquisition of over 90,000 samples in memory at rates up to 500 samples/second. Implementation of new peripheral units into the GDAS also permits more rapid processing of greater amounts of data by providing larger disk storage, more core memory and faster graphics. The upgrade also included hardware retrofit of more technically obsolete components.

1.8 STORAGE

1.8.1 Data Storage - Systems storage capabilities were increased through the incorporation of "Winchester" technology. The Weston Observatory based unit was upgraded with a Charles River Data Systems HD-11 Winchester disk having 70 megabytes of storage. The FD-11 dual double-density floppy disk system provides a common storage medium for all subsystems. Two field units were upgraded with the more compact Data Systems Design model 880 which has an 8 megabyte Winchester and single double density floppy disk.

1.8.2 Bubble Memory - Winchester disks are too vibration sensitive for use in motion environments encountered near STS launches. Upgrading of GDAS for STS applications was accomplished by QBC-11/02 bubble memory devices produced by Bubbl-Tec. The devices are highly resistant to vibration since they are without any moving mechanical parts.

1.9 GRAPHICS

Graphics and control capabilities were expanded by the addition of Tektronix 4025 display terminals to each system. These units function as the operator's command console and display device for computer generated graphics. The unit can operate at 9600 baud and has 32K bytes of graphic memory. Hardcopies of graphic displays or alphanumeric output are made by Tektronix 4631 electrostatic hard copy units. The combination allows for rapid display and print of all 16 channels when operating in the normal sample-to-tape mode.

1.10 TELEMETRY SUB-SYSTEM

A digital data telemetry system capable of direct interface with GDAS was designed and constructed by Monitron Corp under a Weston Observatory sub-contract. It expands the data collection potential of the system by accommodating a sensor array positioned within a 15-20 mile radius of the master data collection station by transmission of realtime information. The effort called for defining and demonstrating the equipment with the GDAS. Phase I included a Technical Design/Evaluation Report describing the theory of operation, techniques, salient characteristics of components and preliminary block diagrams and schematics. Phase II covered fabrication. Phase III documented the operational/maintenance/repair functions of the system and provided final drawings, schematics and operational write-ups and descriptions. The telemetry transmits/receives in the 425-435 MHz band.

1.11 CENTRAL PROCESSING UNIT (CPU)

Several major components of the government owned PDP-11/20 computer failed catastrophically while other units became inoperable or unreliable. The age of these items was 8-10 years. Digital Equipment Corporation (DEC) advised us that because of age and technical obsolescence it did not appear cost effective to troubleshoot, modify, update and repair the system. Their recommendation was to replace the PDP-11/20 with current equipment which could be properly documented and periodically updated. The inoperable computer and associated units were returned to AFGL for disposition early in 1983. Weston Observatory submitted a contract modification to purchase a replacement computer but the request was not approved.

Weston Observatory solicited and received a new DEC PDP-11/34 computer as an educational gift from Digital Equipment Corporation. This unit has been installed at the Observatory. The equipment is primarily committed to hands-on training of students in scientific research and computer techniques. Graduate Research Assistants use the new computer to support their master's theses. Residual DEC model TU-10 tape decks and RK05 disk drives from the defunct AFGL PDP-11/20 system have been interfaced with the DEC PDP-11/34. The system allows continued access to archival tapes obtained under current and previous contracts.

1.12 OPERATIONAL FEATURES

1.12.1 ERC Clock - The ERC clock was re-configured to make all units fully compatible. Also completed was a timing system for the helicorders.

Repairs and changes were made to the accelerometer system to permit use in soft soil areas. The accelerometer preamplifier was modified to remove a microphonic condition and a new type of cable was installed to reduce noise.

1.12.2 GDAS Main Frame Rewire - High noise spikes approaching the noise immunity level of the digital circuitry were found on the power busses of the DEC backplane. The system was rewired to reduce this noise before it became a major problem as it would with aging components.

The main frames were completely stripped, rebuilt mechanically to make them more functional, and facilitate trouble shooting. Added to the system were ceramic bypass capacitors to reduce the inductive effect of the wiring. All power leads were twisted to a maximum of 1 twist per 3 inches to reduce line inductance. Ammeters in the sense lines of the power supplies were removed to reduce the impedance of other lines. The new power distribution schematic is shown in Figure 1-6.

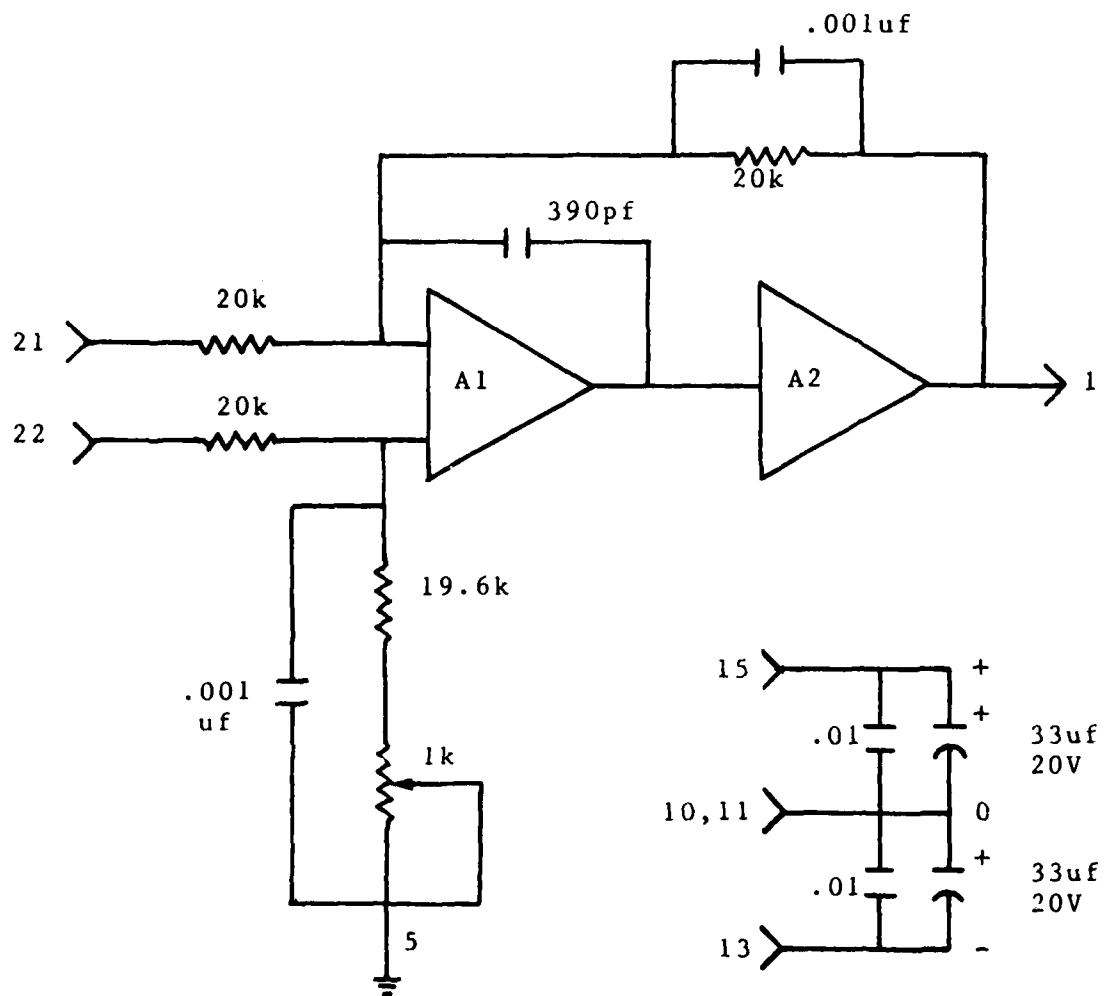
1.13 REFERENCES - SECTION 1

1. Acton Environmental Testing Corporation Test Report, Sine Sweep Testing of a Monitoring Computer System in Two Cabinets, Report No. 17818-83D, Oct 1982.
2. Scientific Report No. 1, Seismic Transmission in Jackass Flats and Steptoe Valley, Nevada, by F.A. Crowley, E.B. Hartnett, and H.A. Ossing, 1 Dec 1981, AFGL-TR-82-0023.

1-14 ILLUSTRATIONS-SECTION 1

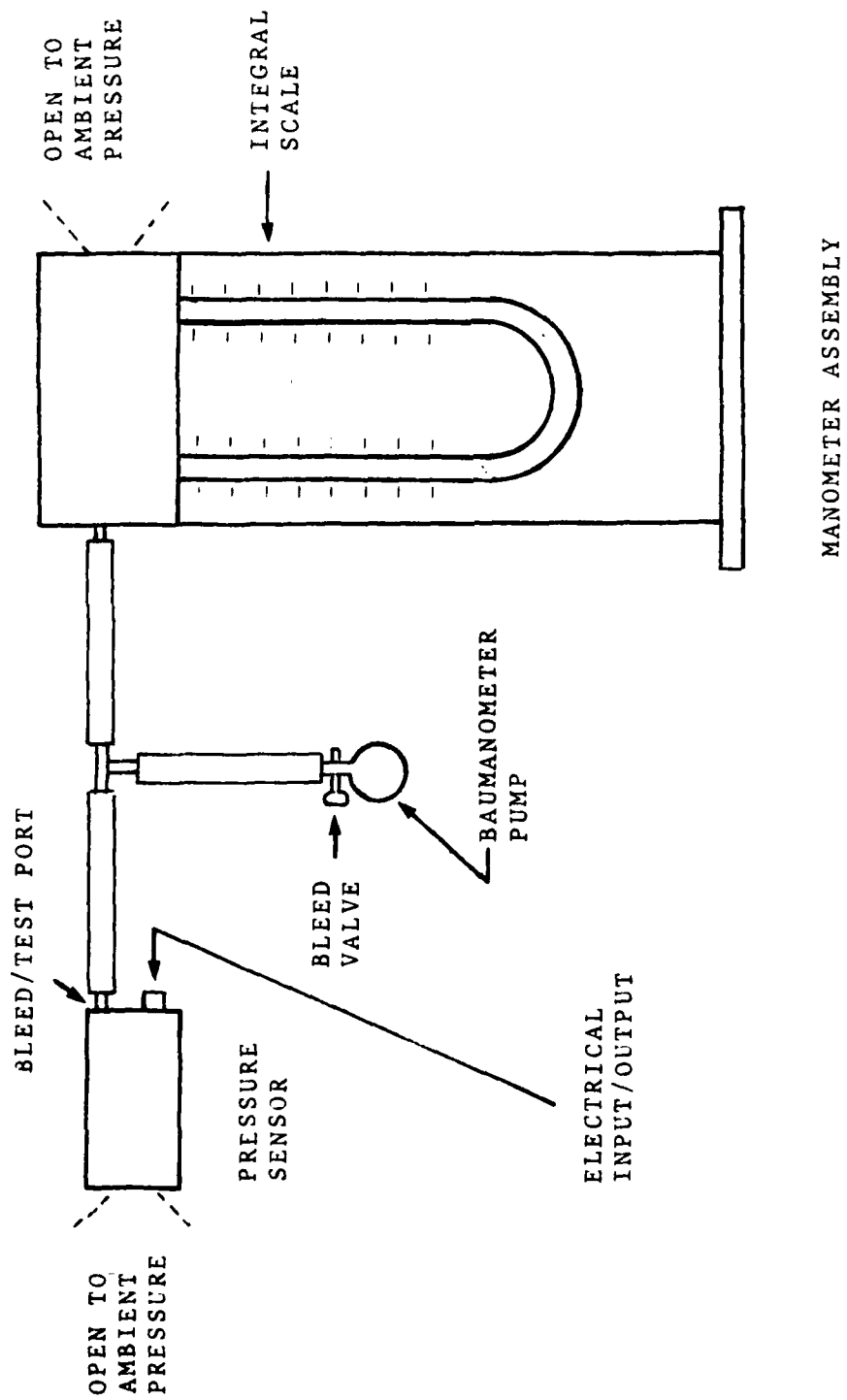
1. Calibration Receiver/Driver, New J Box
2. Pressure Transducer Preamplifier
3. Pressure Transducer Calibration
4. Wiring Diagram Schematic
5. Seismic Preamplifier
6. System Controller Chassis Power Distribution
Schematic (Part 1)
7. System Controller Chassis Power Distribution
Schematic (Part 2)

A1 FAIRCHILD 714HC
 A2 BURR BROWN 3329/03
 ALL RESISTORS RN55C



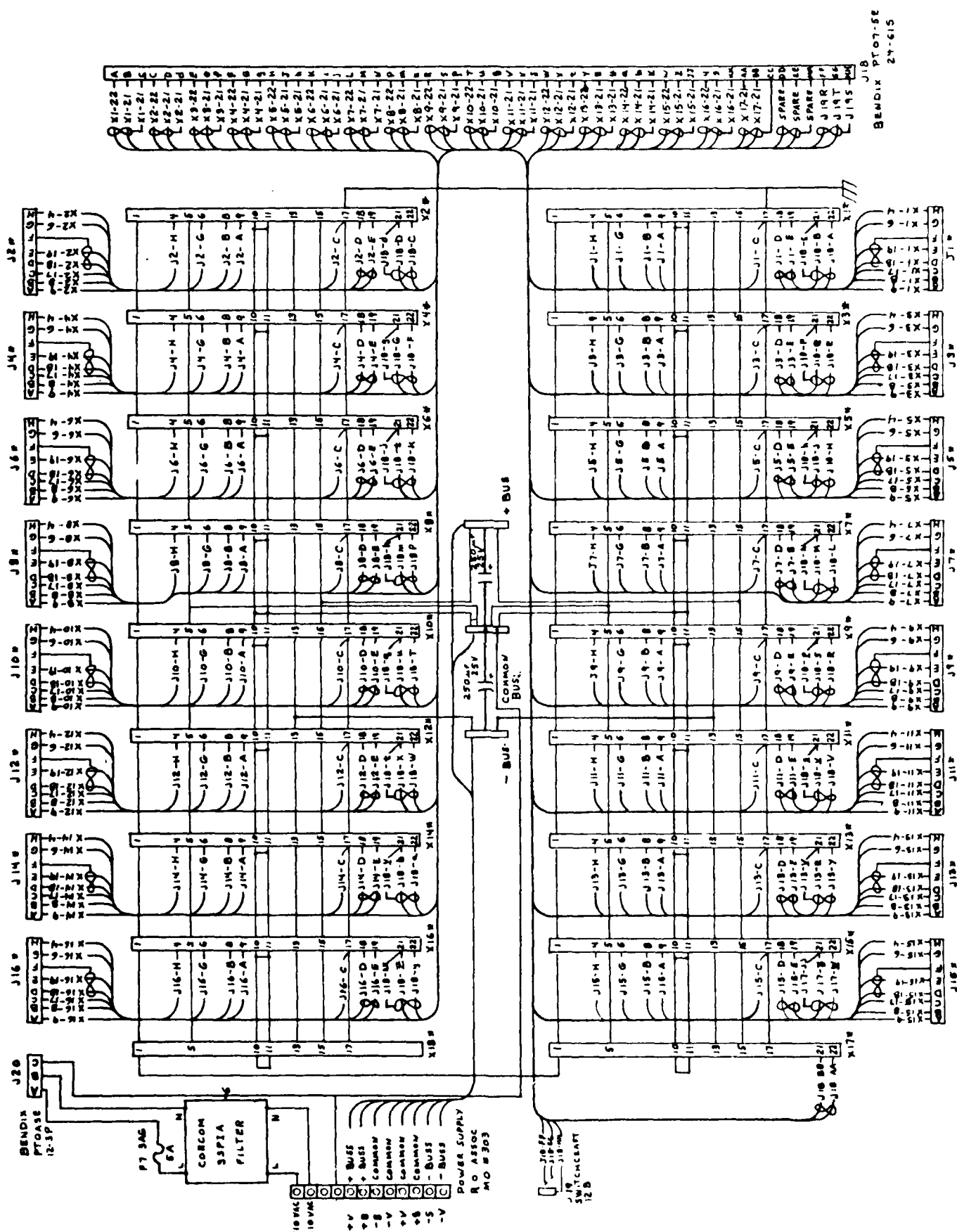
CALIBRATION RECEIVER/DRIVER, NEW J BOX

Figure 1-1



PRESSURE TRANSDUCER CALIBRATION

Figure 1-3



WIRING DIAGRAM SCHEMATIC

CONNECTORS J1 THRU J16
BENDIX PTO7A-12-103
SOCKETS X1 THRU X18
CINCH 50-44A-20

Figure 1-4

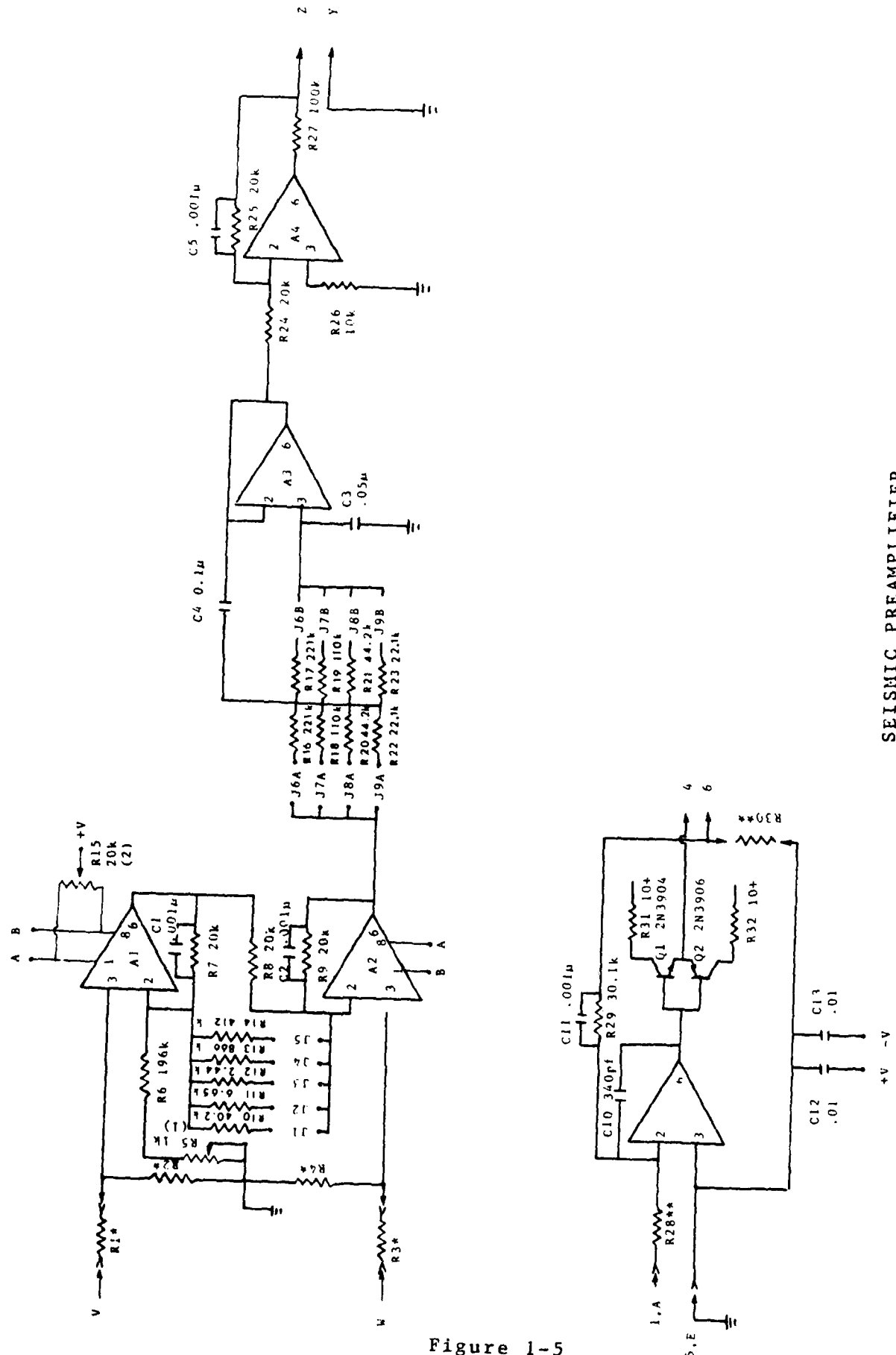
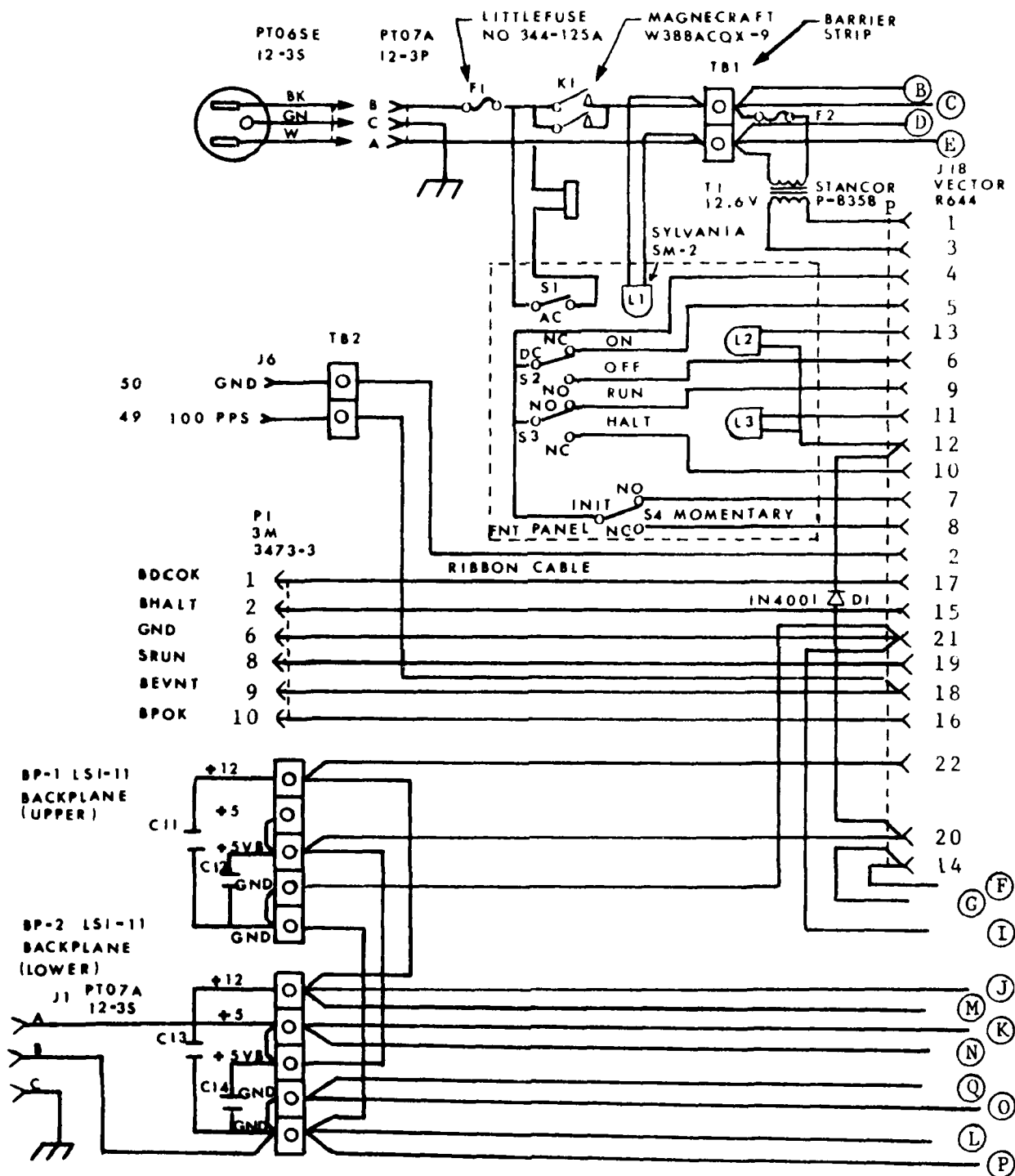
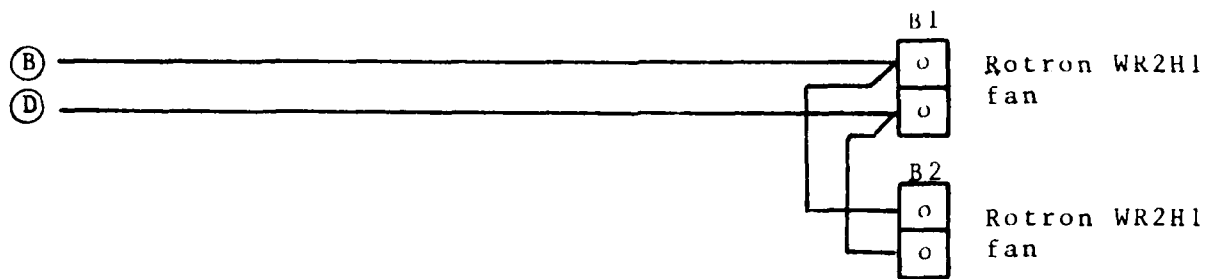


Figure 1-5
34

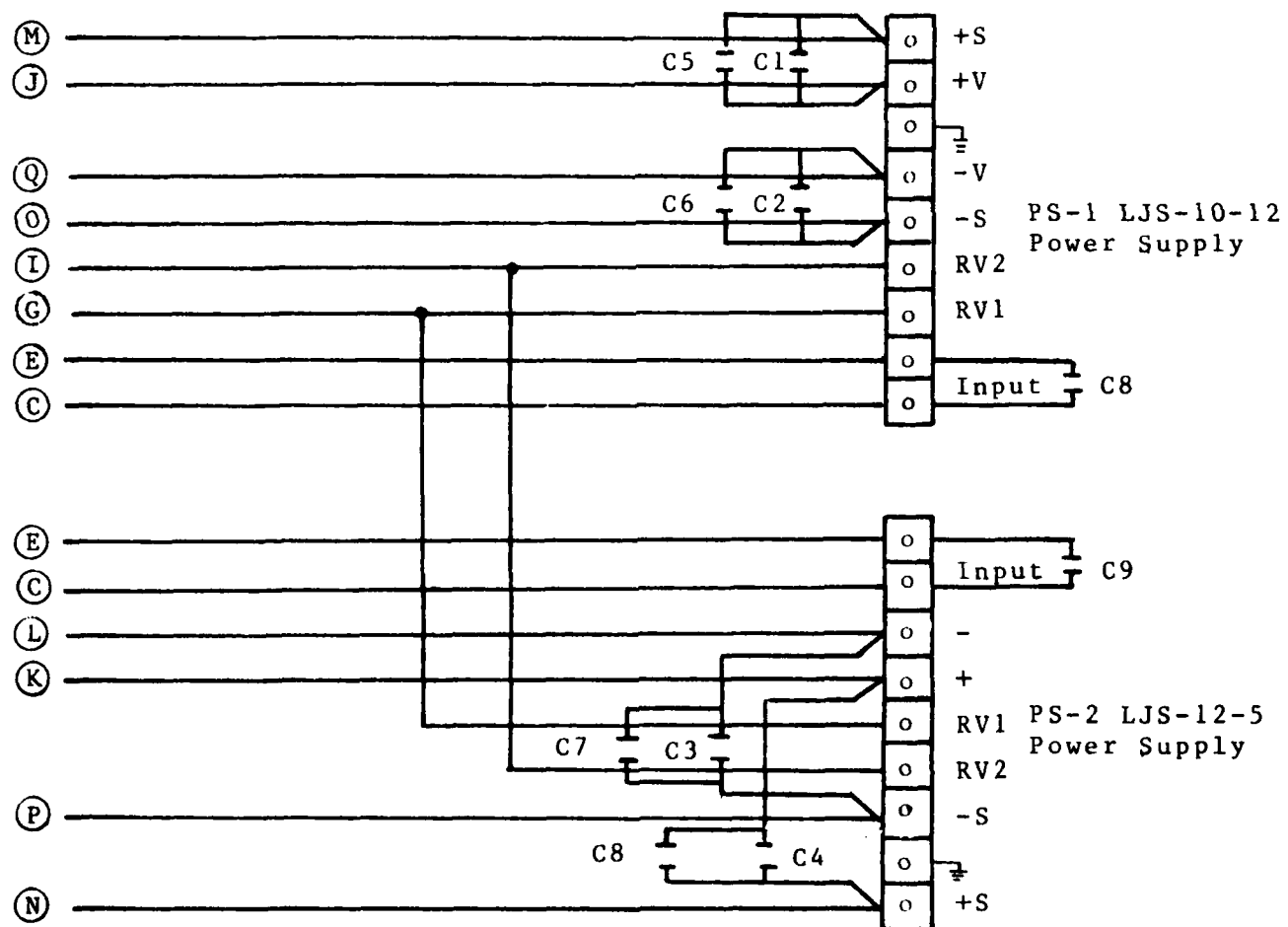


SYSTEM CONTROLLER CHASSIS POWER DISTRIBUTION SCHEMATIC

Figure 1-6, Part 1



C1-C4 2.2 μ f 35v
 C5-C8 .01 μ f 50v
 C9-C10 .01 μ f 1kv
 C11-C14 .01 μ f 50v



SYSTEM CONTROLLER CHASSIS POWER DISTRIBUTION SCHEMATIC (CONT.)

2.0 FIELD OPERATIONS

Field test programs were centered in Steptoe and Railroad Valley (RRV), Nevada. The contract called for the establishment, calibration and operation of a semi-permanent seismic field station to support geokinetic measurements from seismic to quasi-static ground motion caused by slowly moving loads. The locations were chosen as representative of actual and potential environmental scenarios. The purpose of the research was to determine the spacial and temporal attributes of seismic noise and to measure site ground response to surface loading.

2.1 RAILROAD AND STEPTOE VALLEY OPERATIONS

2.1.1 Theft of Material - Upon arrival at the Railroad Valley site (8 June 1982) it was discovered that approximately 750 feet of multi-conductor cable and minor parts valued at \$800-1,000 had been stolen. All items were stored outside the trailer. A written report was submitted to the Sheriffs Office in Tonapah, Nevada.

2.1.2 Seismic Station - A seismic array station was emplaced in RRV in January 1981. The site was intermittently occupied by Weston personnel until June 1982. AFGL Space Physics Division scientists and TRW personnel also used the facility during the period to conduct studies sponsored by BMO.

The following investigations were carried out in RRV : a) Normal acoustic impedance at the site was measured for sonic booms caused by

supersonic overflights; b) methods for estimating spacial Q_R from array measurements were tested; c) propagation parameters were used to extrapolate ground response and simulate seismic events generated by distributed, moving surface loads of known dynamic properties; d) event detection algorithms were applied and tested, and e), ground motion characteristics were accumulated, analyzed and stored for subsequent usage. The effort also supported AFGL/LWH earth-tilt studies.

During the first phase of the study (January 1981), an eleven element seismic array station was installed, calibrated and operated to determine the statistical attributes of the seismic background noise and to define seismic propagation excited by surface sources in the general neighborhood of the seismometer array.

The original array was subsequently expanded to include a 5 element pressure configuration and a 10 meter tower supporting instruments for wind measurements. Data taken during this phase were analyzed to separate the pressure spectrum due to turbulence from that due to acoustics. Using sources of opportunity (aircraft, local traffic), the acoustic impedance of the site to pressure loads traveling near the speed of sound in air was established.

The RRV station was again occupied in June 1981 and tiltmeters and traffic location monitors were installed along the road between Duckwater and Current, Nevada. The work supported AFGL efforts to predict and measure ground deformation caused by slowly moving loads. An array of five Hall-Sears 10-1 vertical seismometers and four Electro Technical EV-17 swinging gate seismometers provided measurements of ground motion in the near-field of a load. Of particular interest was the deformation

characteristic of soil under the action of static and dynamic loads.

2.2 CALIBRATION

2.2.1 Calibration - Calibration of the site was densified to provide data to test the ability of a small array to locate surface sources by path matched filtering. Studies were initiated to determine seismic Q losses, location errors and detection ranges for "intruder class" sources. The effort supports isolating source and transmission attributes in noise corrupted observations.

2.2.2 Ground Response - Ground response around the AFGL seismic array was obtained for nearby sources. The propagation characteristics of seismic waves excited by surface sources over a wide suite of headings was determined. The results are available to construct site compensation operators essential in seismic source studies.

2.3 KENNEDY SPACE CENTER

2.3.1 STS Planning - Participation in the STS launches at KSC, Florida included modification and redesign of units to insure reliable operation as close as 250 meters from the launch pad. Weston also assisted AFGL in: a) defining a plan to estimate spacial coherency, phasing and spectral intensity of the surface pressure excited by an STS launch, b) coordinating these plans and activities with NASA and c), insuring that effects of the KSC vapor cloud are properly included in Vandenberg AFB forecasts. This work supports the construction of an "Equivalent STS Plume Pressure Source" for the early portion of the launch.

2.3.2 STS Launch Summary - Weston Observatory participation in the STS-5 launch at Kennedy Space Center resulted in the publication of a technical report entitled, "Amplitude and Phase of Surface Pressure Produced by Space Transportation System Mission 5" AFGL-TR-83-0039. This report describes surface pressures produced at distances of 150-300 meters from the launch pad. We find that the attenuation, phasing and spacial coherency of surface pressure observations are consistent with acoustics propagating outward from a single, small source moving with the rocket. The OASPL (overall sound power level) estimates for STS-5, calculated from standard form spectra, point to low acoustic efficiency or axially asymmetric acoustics for the shuttle at KSC.

Data obtained from array measurements of surface pressure during the STS-5 launch at KSC permit an estimate of the amplitude and phase of the pressure for an area, orientation, and distance of interest to Space Division. Of particular concern to vibration forecasts is the spacial coherency and equivalent source height for plume generated pressures at a range of 150-300 meters.

3.0 PHYSICAL SECURITY/INTRUSION DETECTION

During the last quarter of 1981 a meeting was held at Hanscom AFB, ESD/CCB, Physical Security System Directorate. The purpose of this consultation was possible utilization of the unique technical competence and initiative of AFGL/Boston College in the "Maid Miles" program directed by ESD. This meeting, attended by AFGL/LWH and Boston College Weston Observatory personnel, was presided over by Lt. Col. Moses and Captain Davis (ESD/OCB). Some of the conclusions resulting from this exchange are: a) ESD/OCB is extremely well versed in the tactical requirements for multi-sensor intrusion detection, but its efforts are primarily engineering, b) the program is staffed by Air Police and engineering personnel, who have limited technical knowledge of the geophysical aspects of seismic detection.

3.1 FIELD STUDIES

Field studies show that in low noise areas like Railroad Valley it is possible to detect an individual running at a distance of up to a mile using a single seismometer, without any serious preprocessing. Future investigations should be directed towards determining bandwidth loss, location error and detection range for such "weak class sources".

4.0 SEISMIC COMMUNICATION

It has long been recognized that the Earth provides a virtually indestructible full duplex path for communicating with hard buried facilities (1). Work on the subject has highlighted estimates of channel capacity when communicating in competent rock (2), or the performance of specific hardware and coding at short and long ranges (3,4).

There is a need to determine the information capacity for communicating seismically in a landform suitable for basing MX (5). Of paramount interest is the potential information capacity of seismic communication links in deep, dry alluvial valleys of the Basin and Range Province, a leading landform for MX basing. To this end we established a maximum information rate for sites in Railroad Valley, Steptoe Valley and Jackass Flats, Nevada over a range of source strengths, bandwidths and distances.

4.1 APPROACH

We treat the Earth to be a linear, time invariant transmission path defined by its Green's Function. Seismic signals observed at a distant receiver point are delayed, colored versions of those generated by the source obscured by additive noise. For surface sources and surface observers, the strength of seismic signals at a distance is dominated by Q losses and cylindrical spreading.

Seismic noise at the candidate sites is well represented by a stationary, independent, Gaussian process convolved with the appropriate site-sensitive shaping operator.

Maximum capacity seismic channels are computed after Hartley-Shannon for the seismic signals and noise terms in each area. At high signal-to-noise ratios optimum transmission is tantamount to matched filtering. The effect of source and receiver arrays on communication is also considered for the simple case of coherent signals and incoherent additive noise.

4.2 SEISMIC NOISE IN BASIN VALLEYS

4.2.1 Statistical Classification - Seismic noise is sensitive both to local structure and the kinds and distribution of noise sources. For sites excited by a large number of independent sources we can anticipate Gaussian attributes. If the noise sources are also well distributed about an observer, the seismic noise field has well defined spacial properties for uniformly layered structures (6).

Figure 4-1 shows the distribution of the ground's particle velocity during event free intervals at a site in Steptoe Valley near Ely, Nevada. The plot is arranged to give a straight line relation for Gaussian variates. The observed distribution is well represented by a zero mean Gaussian process, $N(0, S^2)$, $S^2 = .02 \text{ (microns/sec)}^2$ (7). In remote areas, seismic noise tends to exhibit Gaussian attributes (8). Seismic noise in these rural valley areas also tests stationary (7,9). In contrast, noise in urban areas more often is non-stationary, reflecting the rhythms of the work cycle (8).

4.2.2 Spectral Estimates - Being both stationary and Gaussian, seismic noise at a point can be fully characterized by spectra (10). Figure 4-2 is a large average, spectral estimate of base level seismic

noise measured in Railroad Valley. For frequencies much above 1 Hz, the spectra are relatively flat when cast into terms of particle velocity. The modest bulge just above 10 Hz coincides with a ground resonance term excited by acoustic loads. The frequency of these air-coupled seismics is determined by the velocity and density structure neighboring the site.

For the sites considered, Railroad Valley is much the quietest. The seismic level here compares favorably to the level forecast for quality seismic detection sites in the southwestern United States (11). In turn, the seismic noise spectra at depth can be expected to be reddened versions of those measured at the surface in that the shorter wavelength, higher frequency components are almost always proportionately more attenuated at depth (12,13).

4.3 SEISMIC SIGNALS

4.3.1 Elastic Response - For an elastic body with homogeneous boundaries, the displacement at time, T' , for a point located at $X'(x',y',z')$ relates to forces within a source region located at $X(x,y,z)$ acting at time, T , through the temporal convolution of the force with the appropriate Green function (14,15).

$$u_k(X',T') = \iiint_V G_{k1}(X',T';X,T) \cdot f_1(X,T) dV dT$$

In elastodynamics the convention is to let the displacement at a field point caused by a force applied within the source region define response, Figure 4-3. The elastic response is causal, linear and time invariant. Also, the source time-history can be recovered by linear deconvolution (16)

when the source is slowly moving and small with respect to the radiated seismic wavelengths.

For uniformly layered areas and vertical surface loads, ground response is insensitive to azimuth. Placing the source at the origin, we then express the ground response solely as a function of distance, r and retardation time, t .

4.3.2 Normal Mode Representation - We represent the Fourier transform of $G_{33}(r,t)$, the vertical displacement of the ground surface at a "large" distance, r , due to a vertical impulse at the origin, to be principally the sum of the normal mode contributions attenuated by a material loss factor, Q ,

$$G_{33}(r, \omega) = \sum_{j=1}^N A_j(\omega) \cdot r^{-1/2} \exp(-k_j(\omega) \cdot r / 2Q(\omega)) \cdot \exp i(k_j(\omega) \cdot r + \phi_j(\omega))$$

Here j is the mode number and A, ϕ are the apparent amplitude and phase associated with the source. As given, attenuation is governed by cylindrical spreading and a spacial Q loss defined by the fractional loss

of amplitude over one wavelength. The spacial Q term used here relates to a temporal determination of Q through the relation,

$$Q^{-1}(\text{temporal}) = \frac{U}{c} \cdot Q^{-1}(\text{spacial})$$

with c, U the phase and group velocities of the mode in question.

For our sites experimental values of $G_{33}(r, \omega)$ are fitted to the fundamental mode representation by determining A, k, ϕ , Q over a discrete distance set, $r_\lambda, \lambda = 1, 2, 3 \dots L$

4.3.3 Propagation - The average value for unit weighted surface impacts over the distance, $r_\lambda, \lambda = 1, 2, 3, \dots, L$ is

$$F_{33}(k', \omega) = 1/L \sum_{\lambda=1}^L G_{33}(r_\lambda, \omega) \cdot \exp(-ikr_\lambda) \cdot |G_{33}(r_\lambda, \omega)|^{-1}$$

$F_{33}(k', \omega)$ has a maximum value of unity for unimodal, low noise measurements measurements when $k' = (\omega/c)$. Computation of $F_{33}(k', \omega)$ based on 50 response wavelets measured over the range $120 \leq r \leq 200$ meters is found to be quite close to unity over the passband $3.7 \leq f \leq 37$ Hz. In this passband, the seismic response to a surface load can be well represented by a unimodal surface wave. The (k', ω) pairs that generate absolute maxima for the data establish the propagation characteristics for the test site. The phase and group delay times are determined from $c = \omega/k$ and $U = d\omega/dk$ with:

$$t_p = r/c, \quad t_g = r/U$$

4.3.4 Source Phase - Once k' is determined, source phase can be calculated directly from the residual phase for $r=0$.

$$\text{ARG}(G_{33}(0, \omega)) = \text{ARG}(G_{33}(r, \omega)) \cdot \exp(ik'r)$$

Average phase residuals are independent of frequency. The theoretical value for cylindrically spreading surface waves due to a surface impact on a uniformly layered elastic half space at large distances, r , is $\pi/4$. The calculated source term is consistent with the normal mode representation.

4.3.5 Attenuation - For unimodal propagation in uniformly layered, lossy media, surface wave attenuation at a distance can be obtained from

$$|G(r, \omega)| = A(\omega) \cdot 1/r^{1/2} \cdot \exp(-kr/2Q)$$

Q is then calculated from the slope of the best fitting (least square) slope of the data. A measure of the goodness of fit, E , was also calculated from the residuals. Q estimates tend to be decreasing functions of frequency. The Q value found here for the surficial sediments is modestly larger than loss values used elsewhere (1).

4.3.6 Prediction Errors - The dispersion relation and Q values found for Railroad Valley were used to adjust individual impulse responses over $100 \leq r \leq 200$ meters to a common reference distance, $r=150$. The average amplitude response for 150 meters, $[G(150, f)]$ was then obtained.

The ground acts as a bandpass transmission element. The low frequency limb is controlled by the nature of the elastic response. The high frequency roll-off is dominated by the material quality factor, Q .

The ground disturbance predicted in Railroad Valley for a standard impulse with distance is given in Figure 4-4. The synthetic responses obey the A, k, Q parameters calculated at the site for unimodal surface waves in the range, 100 r 200 meters.

The synthetic waveforms were compared to the actual wavelets. Error wavelets, the difference between predicted and measured values, are small, Figure 4-5. The error is ascribed to additive seismic noise, higher mode responses and lateral inhomogenities.

The scatter in the individual amplitude and phase responses about an average value for Jackass Flats was computed and plotted. Scatter diagrams support the proposition that the original measurements are corrupted by additive noise for frequencies greater than 35 Hz (16).

It is worth noting that the predicted seismics at distances greater than a few hundred meters are quite sensitive to our estimate of Q . A unit difference in Q can cause almost a 6 db difference in the predicted midband amplitude response after 1 km. Indeed, a major impetus for this study was the lack of reliable attenuation data for Basin and Range Valley materials. Recent interest in mantle Q permits an upgrading of earlier work concerning communicating seismically at long range (4); it bears little on data rate estimates at modest distances (10km) in the deep alluvial valleys of the Basin and Range Province.

Even in these supposedly simple valley sites, attenuation is due to lateral structural changes as well as Q losses. To show this we determine

the phase velocity for a number of headings in Railroad Valley, Figure 4-6. The seismic response is azimuth sensitive; ground structure is not laterally uniform. Attenuation is not solely a function of distance and Q loss. The effect of heading is somewhat less severe at lower frequencies, suggesting the valley is more uniform at depth.

4.4 CHANNEL INFORMATION RATES

The capacity of a communication channel in bits/sec over the band $a \leq f \leq b$ is computed after Hartley-Shannon as

$$C = \int_a^b \log_2 \left[\frac{P_{ss} + P_{nn}}{P_{nn}} \right] df$$

where P_{ss} and P_{nn} are the power spectra of the signal and noise processes, respectively (18). Channel capacity is a maximum when $P_{ss} + P_{nn} = \text{constant}$. Constant reception spectra can be obtained either by weighting at the source or receiver. In either case, we can negate distortions due to the seismic path by application of a linear convolution operator that is the inverse of the ground response, $G(r,t)$.

4.4.1 Narrowband Sources - The center frequency for minimum strength sources and optimum transmission is illustrated for the transmission and noise characteristics found in Railroad Valley. The $P_{ss}(f)/P_{nn}(f)$ ratio for a white source of strength, $S = 6.25$ Newtons rms measured at a range of 150 meters, was computed. In this case a channel centered at 18 Hz is optimum in the sense that it maximizes channel capacity for a given source level, bandwidth and range.

In order that the maximum channel capacity for broadband sources be realized, the inverse of the path response must be known. Even the detection of signals with a peak G_{ss}/G_{nn} substantially less than unity is not without difficulty. The capacity of channels, using one or more transmitter-receiver pairs uncompensated for seismic dispersion, passes a sub-optimally coded sequence.

The maximum information capacity for a source of 31.25 Newtons rms and 1 Hz bandwidth was determined for Railroad valley. Here we can transmit and receive in excess of 2 bits/second over a 1 Hz bandwidth at a distance of 1 km using a source of only 31.25 Newtons rms, Figure 4-7.

After a few hundred meters, narrowband sources are relatively efficient seismic transmitters. The effect of source bandwidth and range on information capacity is shown in Figure 4-8 for a source strength of 9.375 Newtons rms. For this source level and locality, a bandwidth of 3 Hz is optimum at a range of 0.50 km.

In Figure 4-9 the source strength needed to maintain a channel capacity of 2 bits/second over a bandwidth of 1 Hz is shown. A source level of at least 25 Newtons rms is needed to insure a channel capacity of 2 bits/second at a range of 1 km. Under these constraints an approximately linear relationship exists between source strength and distance.

4.4.2 Broadband Sources - The information rate for a channel consisting of a broadband signal source and a receiver whose response is the inverse of that of the ground is depicted in Figure 4-10 for a range of 150 meters and source strength of 4.419 Newtons rms and frequencies less than 50 Hz.

Seismic communication is a lowpass phenomenon in that 95% of the channel capacity is obtained from frequencies less than 35 Hz. The

bandwidth for efficient seismic communication is also range dependent. To show this we compute the cutoff frequency needed to attain 98% of channel capacity for white sources, Figure 4-11. The useful information bandwidth for weak sources at distances greater than 1 km is less than 20 Hz in Railroad Valley.

To further show the impact of range on broadband communications, we estimate channel capacities in Railroad Valley as they relate to bandwidth over a suite of distances, Figure 4-12. Broadband seismic communications require relatively strong sources to excite frequencies much above 25 Hz for distances greater than 200 meters.

4.5 TRANSMITTER AND RECEIVER ARRAYS

Coherent signals embedded in additive independent incoherent noise provide a conservative basis to estimate the effect of both transmitter and receiver arrays on channel capacity. For such a construction, P_{ss}/P_{nn} increases directly as the sum of the number of receiver and transmitter elements. Channel capacity for systems employing multiple transmitter and receiver elements are shown in Figure 4-13 for narrowband transmissions at a range of 300 meters.

The prospects of surface arrays separating signals from noise are considerably better for buried sources than for surface sources. The reason for this is that both the noise and signals propagate largely as low order surface waves. Arrays cannot separate seismic waves traveling in the same direction and the same mode. In contrast, low mode surface seismics are only poorly excited by buried sources. Arrays using velocity filtering should be quite effective in separating seismic signals from noise for

buried sources (19).

4.6 SITE EFFECTS

The seismic wavelets produced by a standard impact at a distance of 150 meters are shown for Jackass Flats and Railroad valley, Figure 4-14. Seismic response is clearly site sensitive. It immediately follows that channel data rates are also site sensitive. Optimum capacity channels for a broadband transmitter operating in Jackass Flats are given in Figure 4-15. For the ranges and frequencies considered, Railroad Valley has the greater capacity. The low noise in Railroad Valley is the controlling factor.

All the estimates given in this study are for point surface sources and surface receivers. For a surface source and a buried receiver at large offset distances, both the noise and signal are attenuated in roughly similar fashion. P_{ss}/P_{nn} ratios at depth should be much the same as those found for surface sources and receivers. The results of this study should apply. In contrast, P_{ss}/P_{nn} should be significantly smaller for a source at depth and a surface receiver. Reliable assessments for communicating to the surface from a buried facility require seismic measurements at depth in the areas of interest.

4.7 FINDINGS

Communication by seismic means is as commonplace as a "knock at the door"; its feasibility is not in question. What is in question is the information capacity of seismic data links operated at specific source

strengths and distances in the landform of concern.

Information capacity for a ground path is readily calculated once the signal and noise spectra are specified. Data links can be optimized by weighting at the source and/or receiver. In any event, signal distortion due to seismic propagation can be nullified by an inverse operator of the seismic impulse response, $G(r,t)$.

Seismic waves excited by surface impacts are well represented by unimodal, Q damped surface waves. Using this representation, signal spectra can be generated over any desired range of distances, source strengths and bandwidths.

The effect of range, bandwidth and source strength on channel capacity was established for the seismic signals and noise found at each site. Seismic data links of 2 bits/second are quite realizable for ranges of a few kilometers using sources of less than 100 Newtons rms in the band $2 \leq f \leq 20$ Hz.

The major uncertainty encountered when estimating capacity arises from the uncertainty in Q and lateral inhomogeneities.

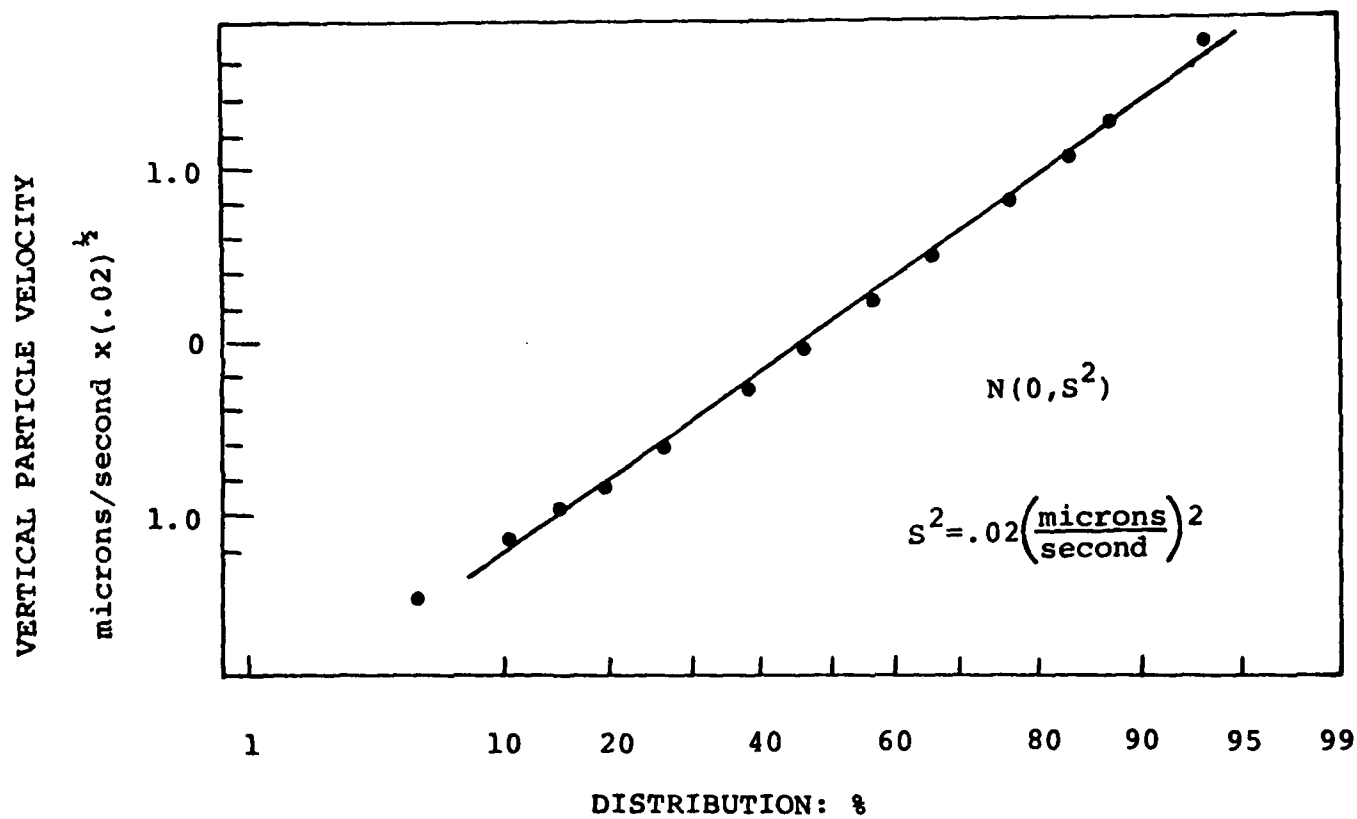
4.8 REFERENCES - SECTION 4

1. An Estimate of the Maximum Range of Detectability of Seismic Signals, N.A. Haskell, Air Force Survey in Geophysics No. 87, March 1957, AFCRL-TN-57-202, AD152610.
2. Seismic Communications Feasibility Study, Don R. Fink, Park H. Miller, Philco-Ford, Bluebell, PA, Communications and Electronics Div., May 1968, AD391651.
3. Continuous Seismic Wave Communications Experiments at 80 Hz in Diverse Terrains, F.F. Johnson et al, U.S. Army Electronics Command Research and Development Technical Report ECOM- 2921, January 1968, Fort Monmouth, N.J., AD832794.
4. Study of the Feasibility of Long-Range Seismic Communications, July 72 H.W. Briscoe, Report No. 2405, Bolt Beranek and Newman, AD904729.
5. Technical Exchange Meeting at BMO, Norton AFB, California, June 1982, Lt. Col. M. Jackson.
6. Space and Time Spectra of Stationary, Stochastic Waves with Special Reference to Micro-Tremors, K. Aki, BERI Vol. 35, 1957.
7. Temporal Attributes of Seismic Base Noise in Steptoe Valley, F. Crowley, H. Ossing, E. Hartnett, AFGL-TM-40, 1980.
8. Earth Environmental Noise Fields, F.A. Crowley, H.A. Ossing, Air Force Surveys in Geophysics No 224, AFCRL 70-0460, 1970, AD 713172.
9. Temporal Attributes of Seismic Base Level Motion, Railroad Valley, Nevada, H.A. Ossing, E.B. Carleen, 1981, AFGL-TR-81-0221.
10. Topics in the Theory of Random Noise, Volume 1, R.L. Stratonovich, Gordon and Breach, New York, 1963.
11. A Survey of the Ambient Motion Environment in the Southwestern United States, H.A. Ossing, R.A. Gray, AFGL-TR-78-0052, February 1978, ADA056872.
12. Noise Attenuation in Shallow Holes, F.J. Douze, The Geotechnical Corporation, Technical Report No. 64-135, 11 January 1965.
13. Study of Seismic Signals and Noise by Means of a Buried Array, G.C. Phillips, Changsheng, Wu, AFCRL-TR-66-578, June 1966, AD 637687.
14. Moment Tensors and Other Phenomenological Descriptions of Seismic Sources, G. Backus, 1976, Geophys. Jour. Res. Astro. Soc.
15. Quantitative Seismology, Aki, K., 1980, W.H. Freeman and Company.

16. The Determination of Source Properties, Stump, B., 1977, BSSA.
17. Seismic Transmission in Jackass Flats and Steptoe Valley, Nevada, Crowely, F.A., Hartnett, E., Ossing, H., 1 December, 1981, AFGL-TR-82-0023.
18. Principles of the Statistical Theory of Communication, Harman, W.W., McGraw-Hill, New York, 1963.
19. Seismic Detection and Location of Isolated Miners - Final Report, Arthur D. Little, Contract No. 122026 15 December 1972.

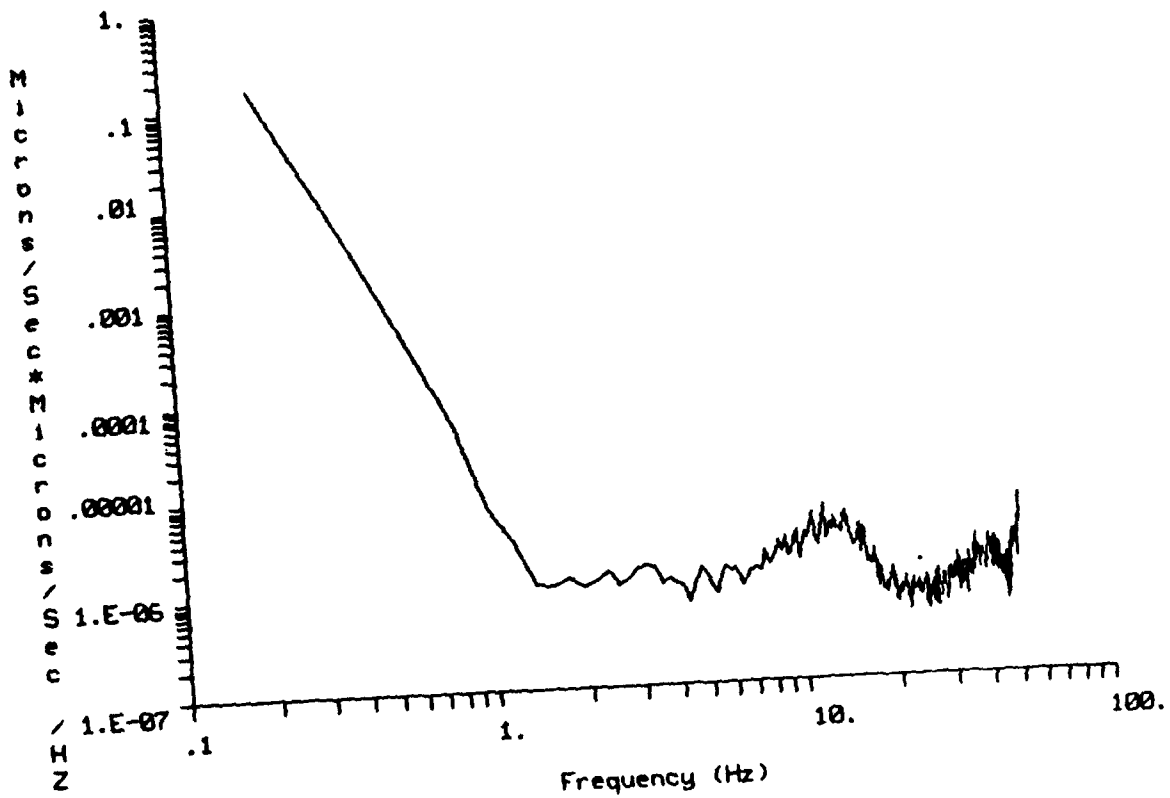
4.9 ILLUSTRATIONS - SECTION 4

1. Seismic Noise Distribution - Steptoe Valley
2. Seismic Noise Spectra - Railroad Valley
3. Green's Function Representation
4. Predicted Response - Railroad Valley (270°)
5. Error Wavelet
6. Valley Velocity
7. Channel Capacity: Narrow Band Source (RRV 270°)
8. Effect of Bandwidth
9. Effect of Source Strength
10. Ground Bandpass Characteristic: RRV (150 meters)
11. Ground Cutoff Frequency
12. Channel Capacities: Wide Band Source RRV
13. Effect of Arrays
14. Effect of Site
15. Channel Capacities: Wide Band Source (Jackass Flats)



SEISMIC NOISE DISTRIBUTION- STEPTOE VALLEY

Figure 4-1



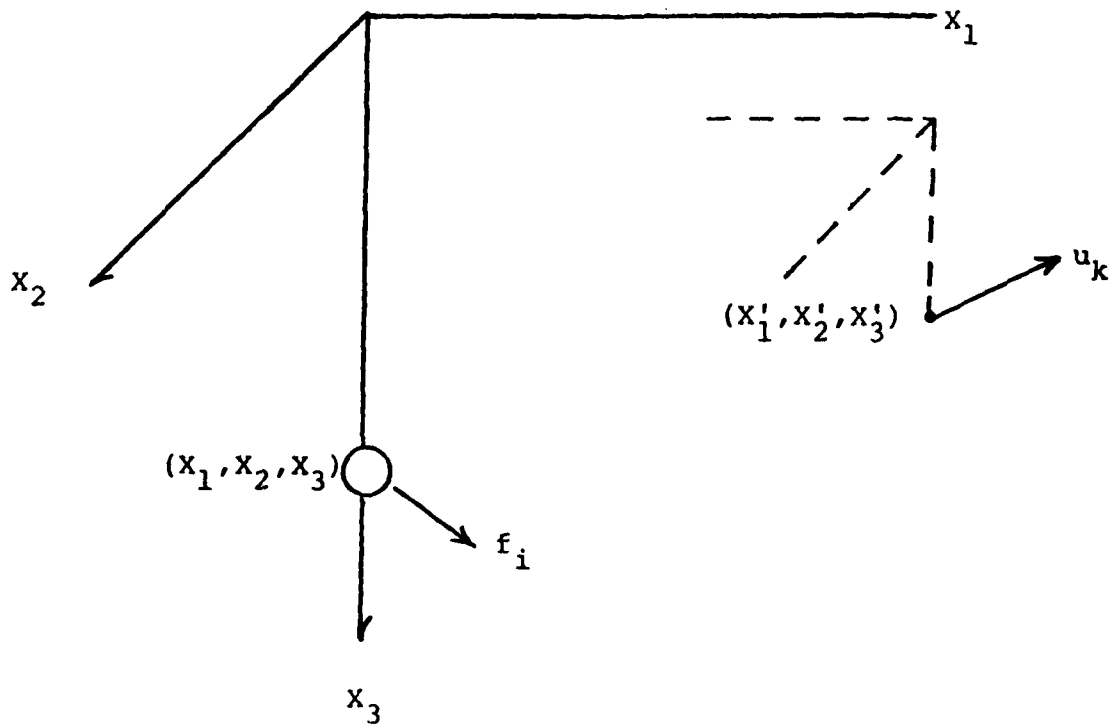
SEISMIC NOISE SPECTRA: RAILROAD VALLEY

Figure 4-2

$u_k \sim$ DISPLACEMENT

$f_i \sim$ FORCE

$$u_k(X', T') = \iiint_{-\infty}^{\infty} G_{ki}(X'; T'; X, T) * f_i(X, T) dV dT$$

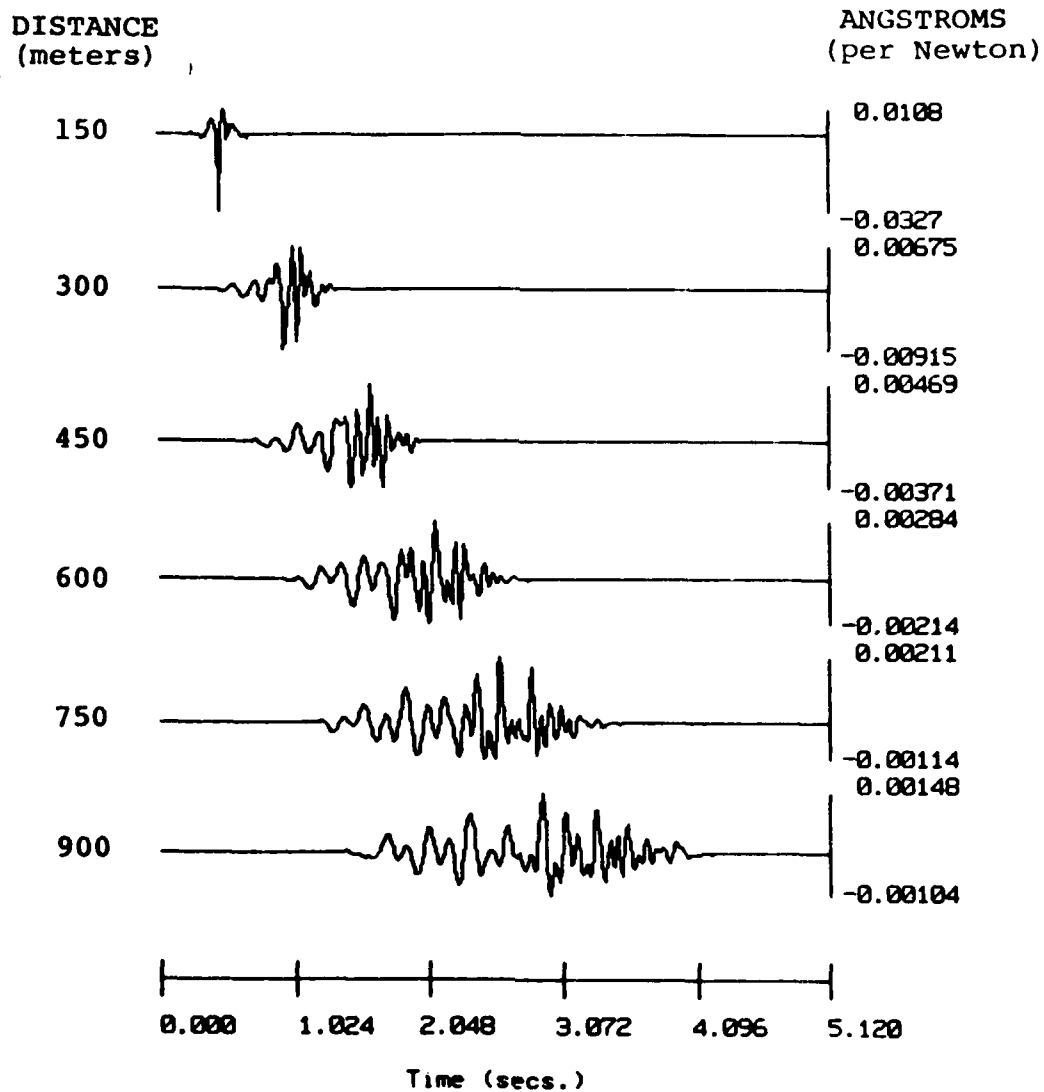


* TEMPORAL
CONVOLUTION

GREEN'S FUNCTION REPRESENTATION

Figure 4-3

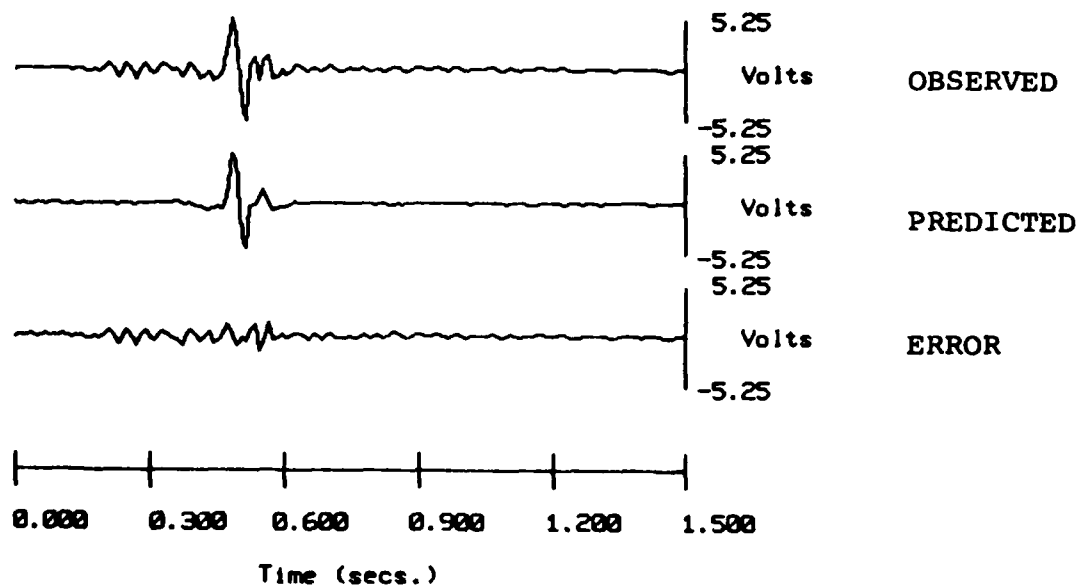
GROUND DISPLACEMENT



PREDICTED RESPONSE-RAILROAD VALLEY (270°)

Figure 4-4

Railroad Valley 270°
Response to a hammer blow
Distance 150 meters



ERROR WAVELET

Figure 4-5

LATERAL INHOMOGENEITIES IN RAILROAD VALLEY

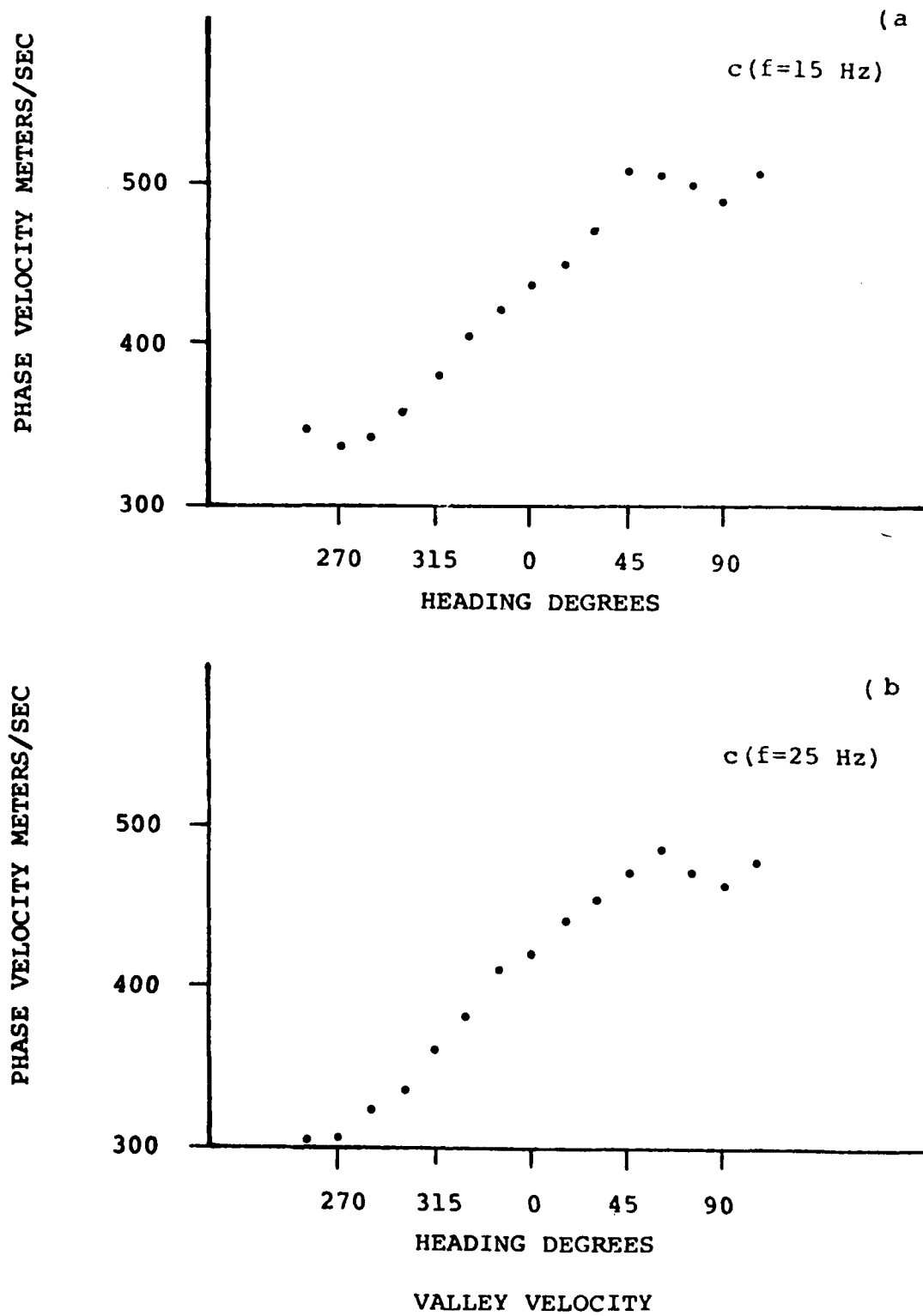
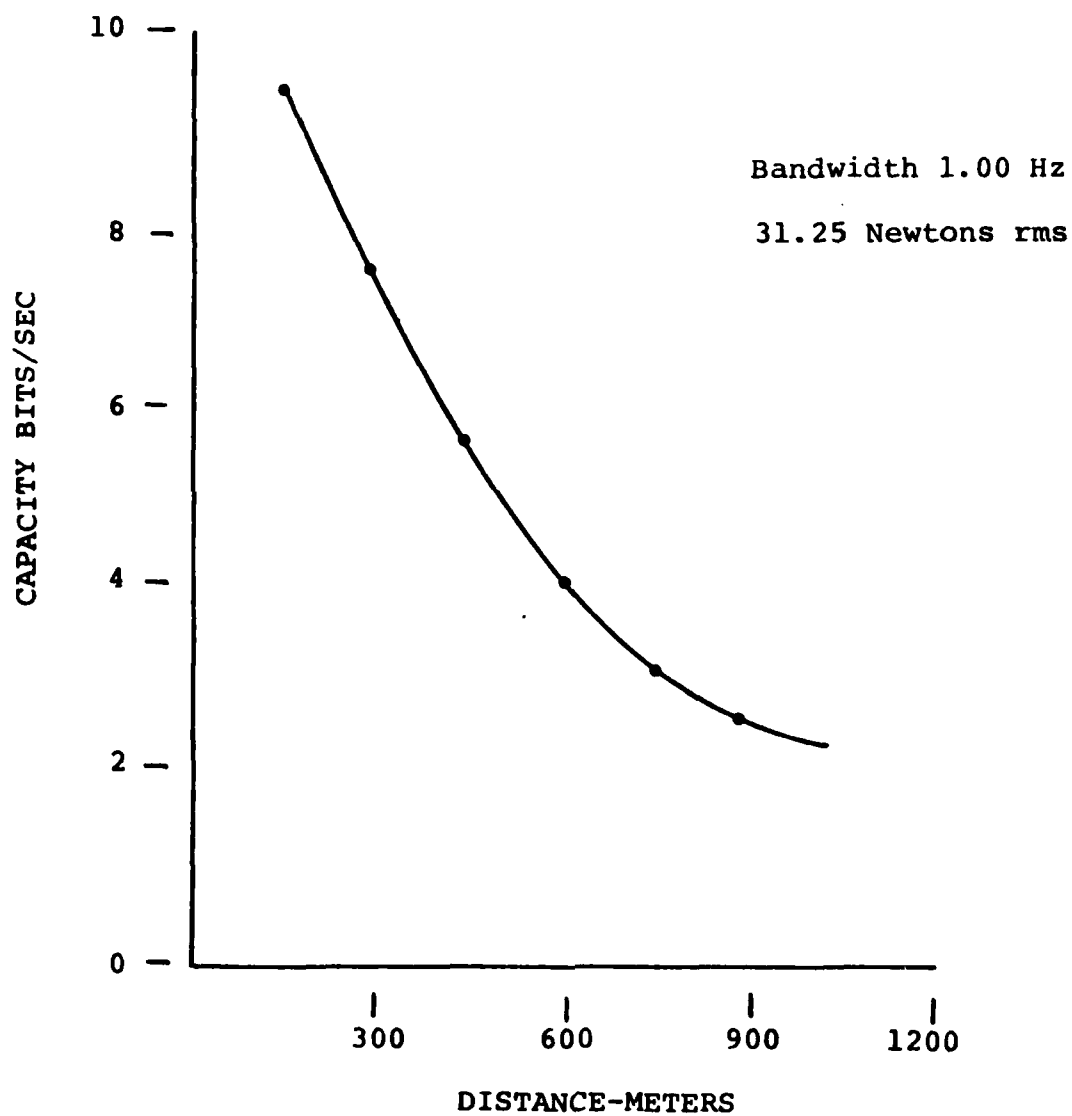
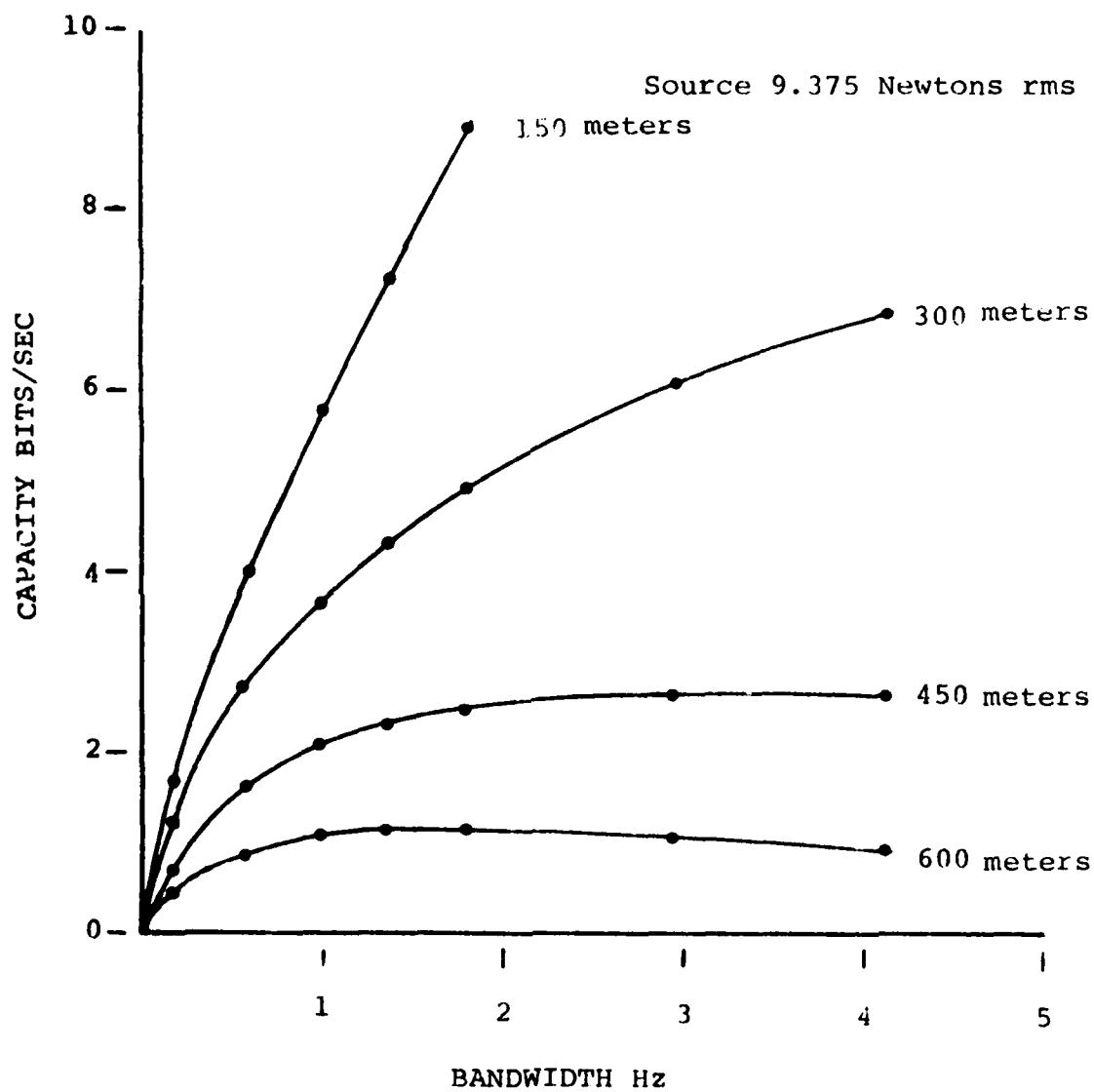


Figure 4-6



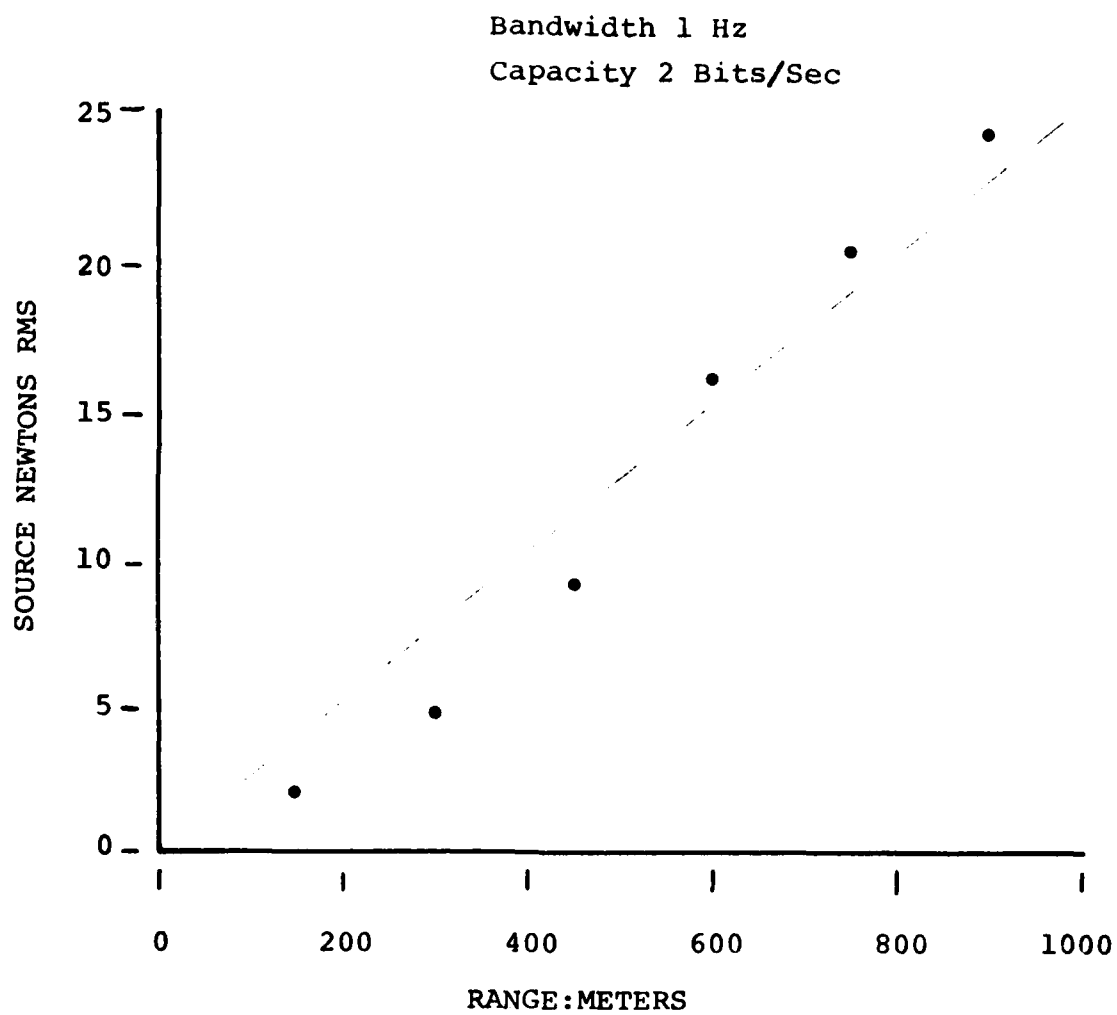
CHANNEL CAPACITY: RRV (270°) NARROW BAND SOURCE

Figure 4-7



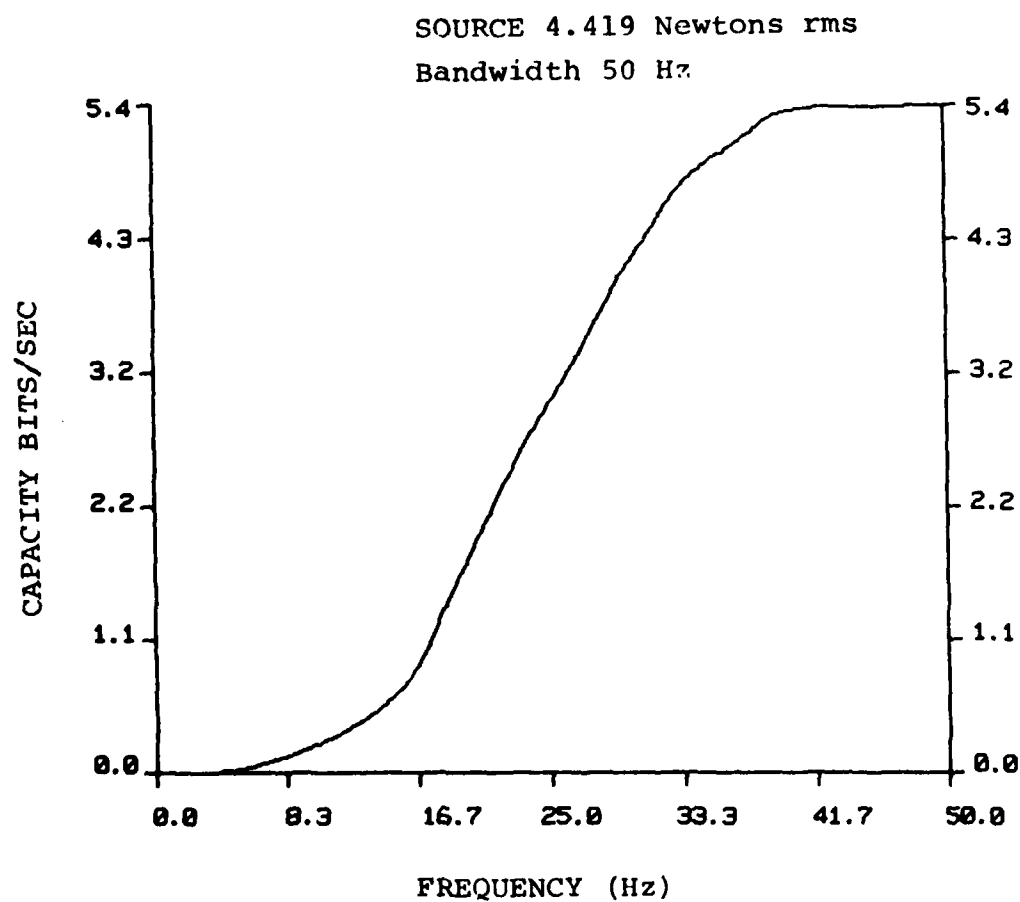
EFFECT OF BANDWIDTH

Figure 4-8



EFFECT OF SOURCE STRENGTH

Figure 4-9



GROUND BANDPASS CHARACTERISTIC: RRV 150METERS

Figure 4-10

Useful Bandwidth (98%)
Source 31.6 Newtons rms
Bandwidth 0-50 Hz

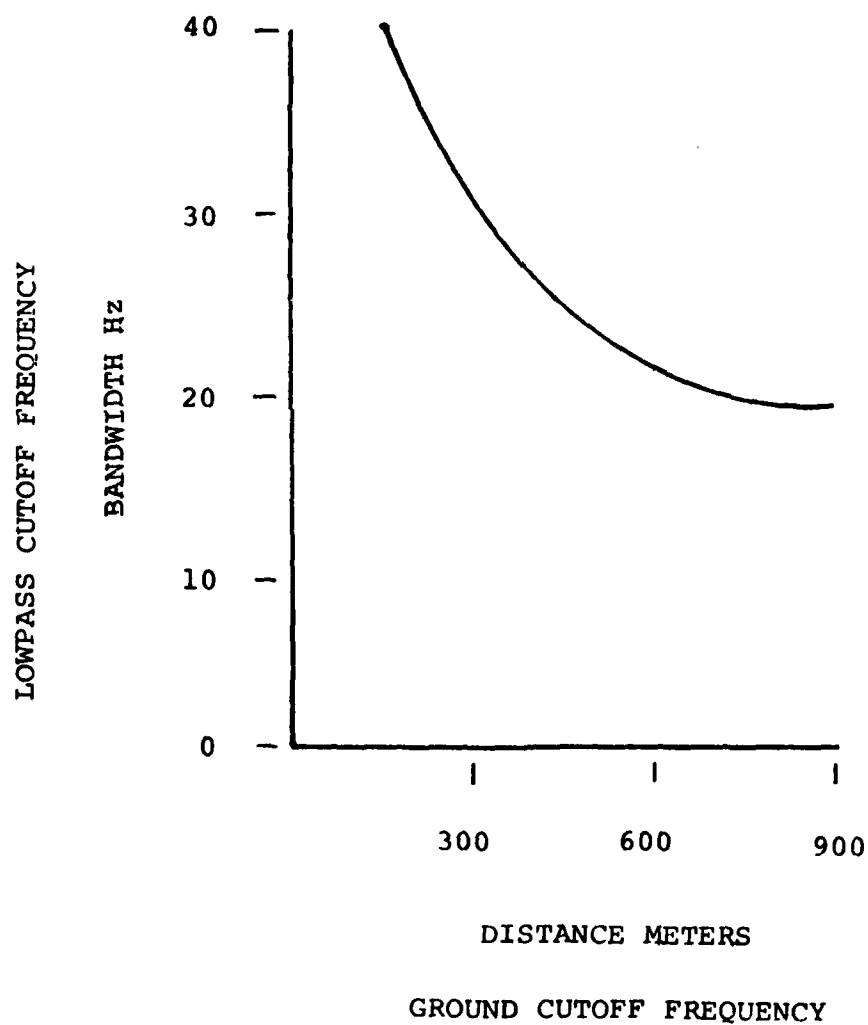
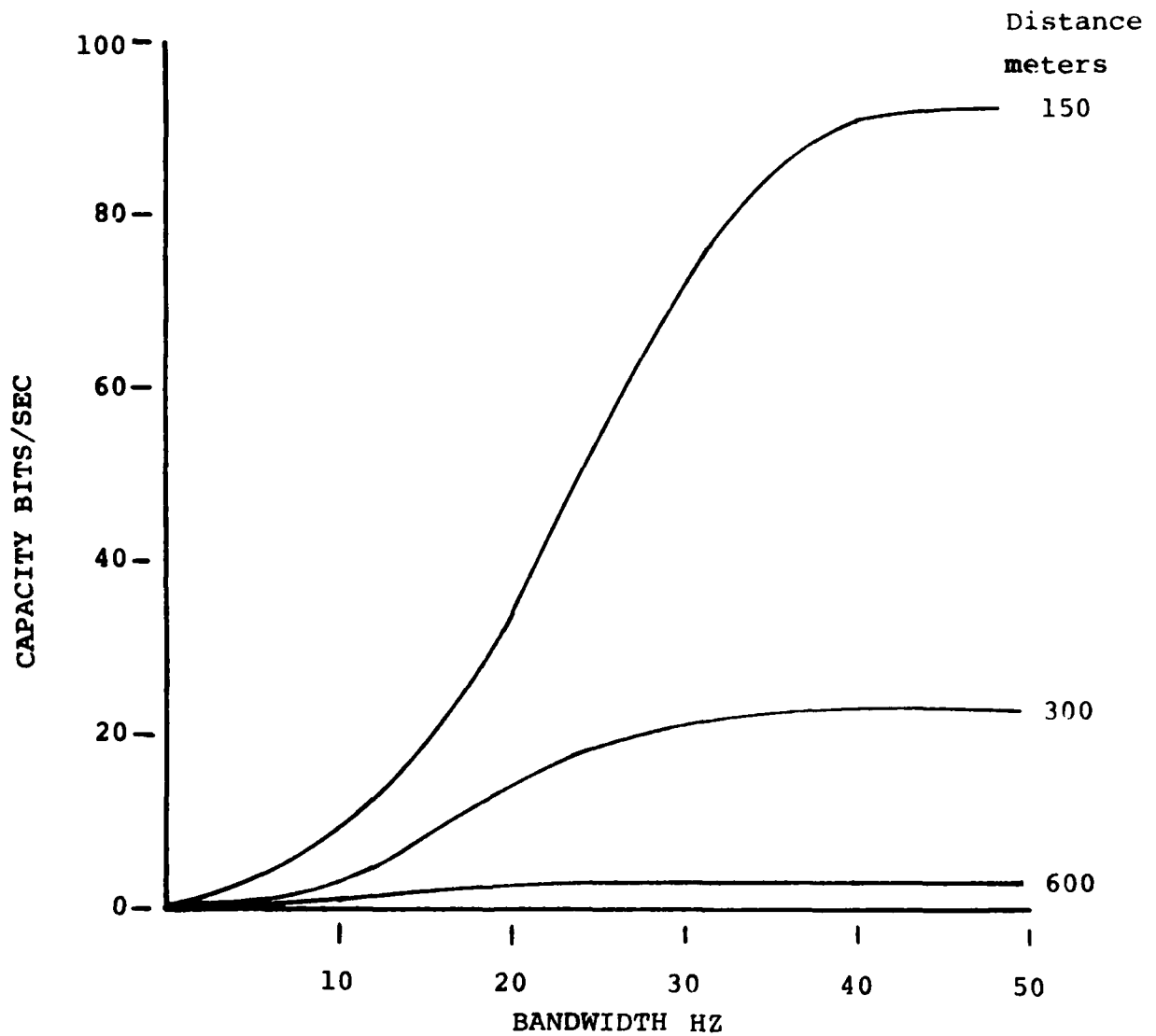


Figure 4-11

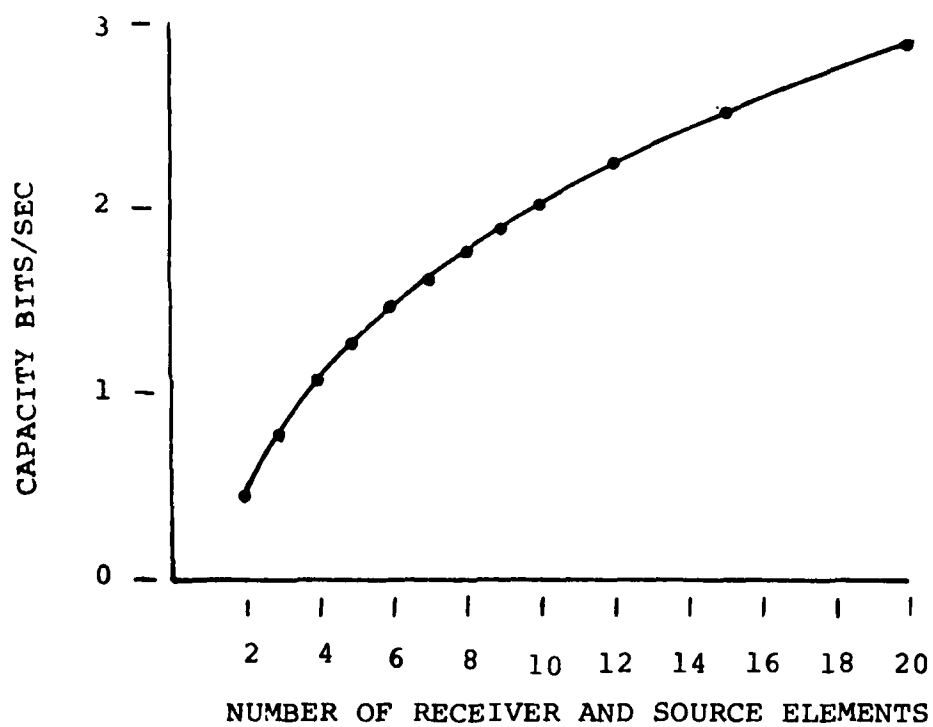
Source 31.6 Newtons rms



CHANNEL CAPACITIES: WIDE BAND SOURCE
RAILROAD VALLEY

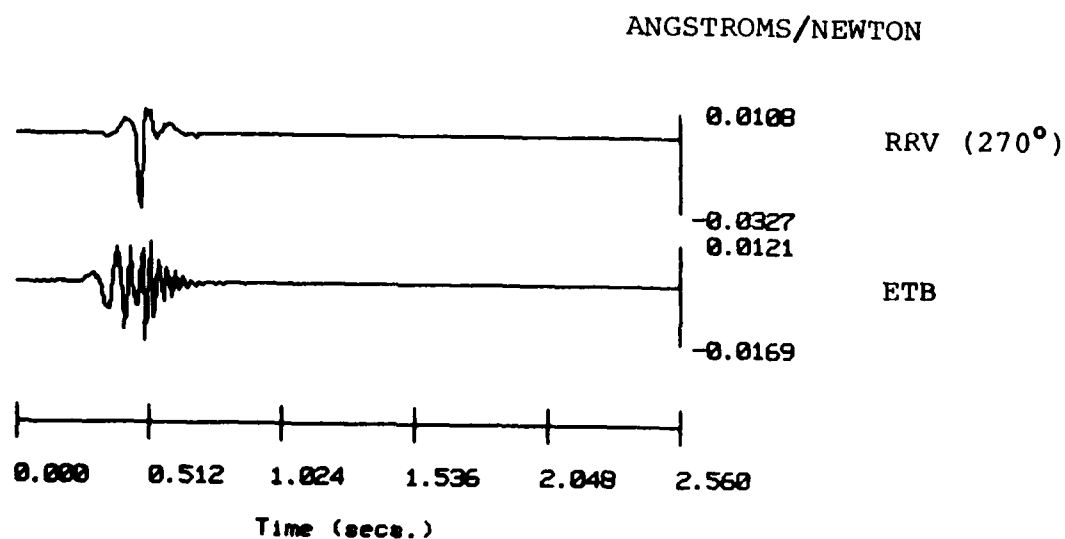
Figure 4-12

Source Strength 1.5625 Newtons rms
Range 300 meters
Bandwidth 1.0 Hz



EFFECT OF ARRAYS

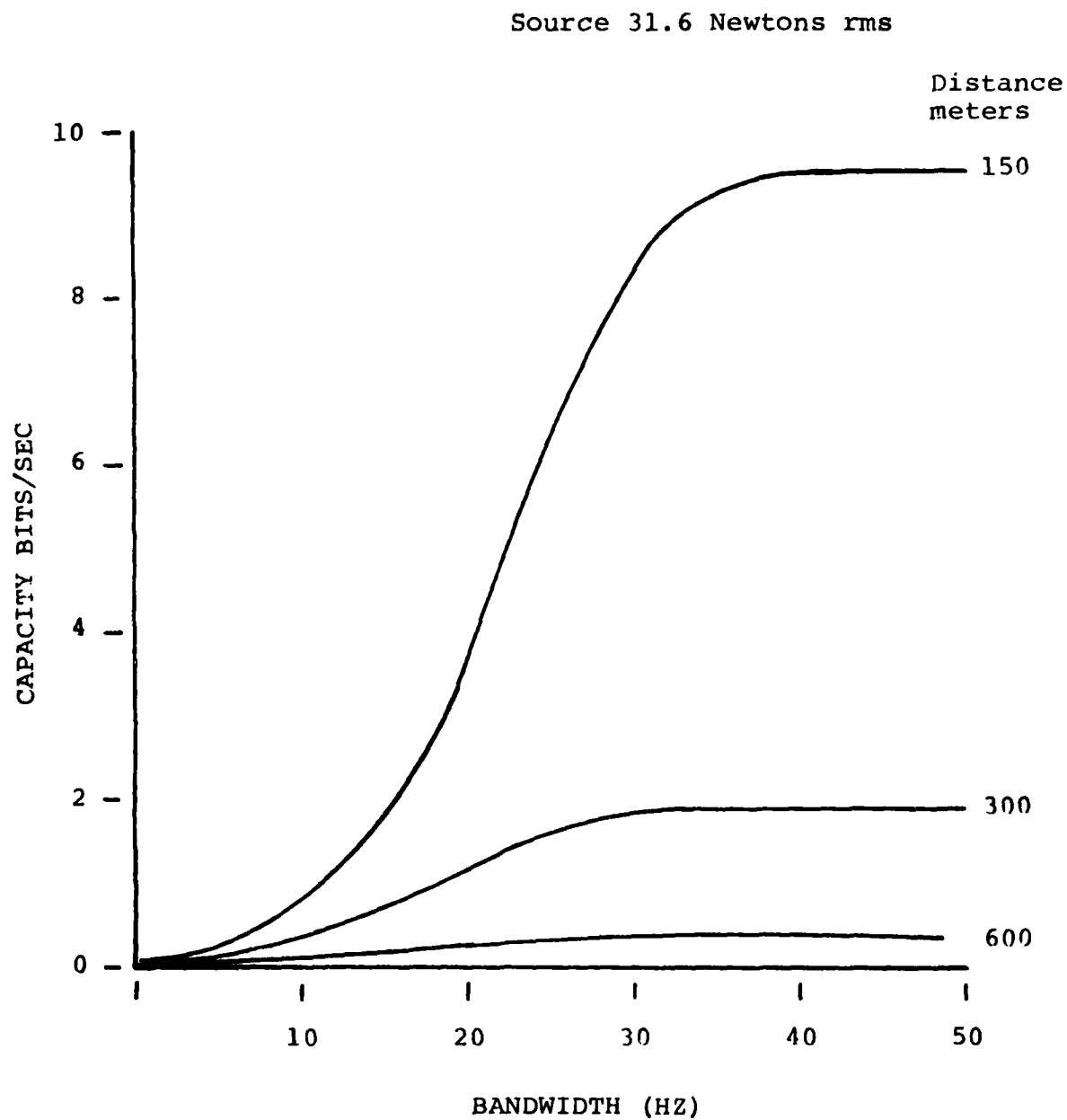
Figure 4-13



Range= 150 meters

EFFECT OF SITE

Figure 4-14



CHANNEL CAPACITIES: WIDE BAND SOURCE
JACKASS FLATS

Figure 4-15

5.0 SPACE TRANSPORTATION SYSTEM

There is a requirement to forecast the vibro-acoustic environment for Space Transportation System (STS) launches at Vandenberg (VAFB), California. Data from STS launches at Kennedy Space Center (KSC) are not directly applicable to Launch Complex 6, VAFB due to considerable differences in Ground Support System configurations at the two locations. Specification of pressure level and phase is essential to vibration forecasts which influence facility design, verification, and lifetime predictions. Model responses of VAFB structures are sensitive to the phase of the applied load. A workable model of both the shuttle source and facility response allows a forecast of the motion environment in the neighborhood of the pad at launch time.

Surface pressures produced at distances of 150-500 meters from the launch of STS-5 at Kennedy Space Center, Florida were analyzed. The calculated attenuation, phasing and spacial coherence of surface pressure observations are consistent with the pressure produced by acoustics propagating outward from a single, small source moving with the rocket. The Overall Sound Power Level (OASPL) estimates, calculated from standard form spectra, point to low acoustic efficiency or axially asymmetric acoustics for shuttle launches at KSC.

5.1 APPROACH

Array measurements of surface pressure taken during the launch of STS-5 permit a determination of the amplitude and phase of pressure excited by a launch over an area, and at an orientation and distance of interest

to Space Division. The measurements were used to evaluate a point source model. Of particular concern to vibration forecasts are the level, spacial coherency and effective source height for plume generated pressures at a range of 150-500 meters.

5.2 MEASUREMENT SYSTEM

Measurements were taken by the Air Force Geophysics Laboratory Geokinetic Data Acquisition System (GDAS), a unit that collects, displays, stores and analyzes geophysical data (1).

5.2.1 Sensor Locations - In its configuration at KSC for STS-5, Figure 5-1, GDAS accepts the output of an array of 12 pressure sensors. Each pressure observable is converted into a 12 bit binary word at a rate of 100 conversions per second. These data were merged with identification, error suppression, time, and status codes for storage on magnetic tape with a backup dump to disk. Measurements of Mission 5 started 3 minutes prior to lift-off and continued for a period of 15 minutes.

The orientation, size and distance to the array mirror the orientation, size and distance to major structures at VAFB. The array was deployed to determine the level, phase and spacial coherency of the acoustic load around the time of the sound power level maximum for VAFB structures at a range of 150-300 meters.

5.2.2 Data Quality - A number of error sources that determine the quality of measurement was explicitly considered. This heightened concern about data quality was prompted by the fact that pressure values measured for STS-5 are significantly smaller than those measured by NASA (2) and anticipated by AFGL for an STS propulsion system of standard acoustic

efficiency (3).

5.2.3 Uncorrelated Additive Noise - Measurements are used to isolate additive noise caused by atmospheric and hardware sources from launch generated acoustics. Total and incoherent spectra obtained for low level, colocated measurements were calculated, Figure 5-2. These estimates used periodogram smoothing that called for interval doubling by concatenating zeros to the original data set. The technique reduces the variance of the estimate and suppresses spectral leakage (4). Coherency estimates, Figure 5-3, used to separate the spectra were based on auto and cross spectra calculations of 10 data segments (5). The signal-to-noise (S/N) estimate for low level measurements, Figure 5-4, is the ratio of the square root of the coherent and incoherent spectra.

Confidence bounds for S/N values calculated from coherency estimates have been determined by Fay (6) for a stationary, Gaussian process. For the high coherencies found here at frequencies of 30 Hz or less, Figure 5-3, stable coherency and S/N estimates can be obtained by ensemble averaging over a small sample set. To illustrate, the interval for a coherency estimate, $\text{Coh}(f) = 0.9$, using an ensemble average of 8 samples, is calculated to be $0.8 \leq \text{Coh} \leq 0.96$ at the 95% confidence level for Gaussian variates.

The entire sequence used to estimate the dynamic range of GDAS at low levels was repeated for high level measurements, see Figures 5-5 through 5-7. The signal-to-noise level for an individual channel is found to be in excess of 10 in the bandpass $2 \leq f \leq 30$ Hz. Above 30 Hz, measurements are degraded by an additive, uncorrelated noise term.

5.3 ANALYSIS OF SURFACE PRESSURE

5.3.1 Space Shuttle Main Engines - The analysis of main engine acoustics is based on data samples of 2.56 seconds duration starting at 0718:57. The pressure spectrum, Figure 5-8, is a periodogram average over seven samples taken at locations 3-6 and 8-10 inclusive, see Figure 5-1. For frequencies below 30 Hz, the spectrum is well separated from system noise. Much above 30 Hz, the data are dominated by uncorrelated, additive noise. Below 2 Hz, pressure fluctuations expected for the 5 knot wind reported at the time of launch rapidly become a significant factor. A spectrum of pressure fluctuations for a 5 knot wind condition reported by Kimball (7) is included in Figure 5-8.

The pressure, $p(R,t)$ caused by an acoustic disturbance propagating outward from a small source located at the origin of a windless, isothermal, unbounded atmosphere is completely coherent along any radial segment with an amplitude and phase determined from its Fourier transform. In contrast, distributed, independent sources invariably lead to incoherent fields for separated observers. The magnitude of the coherence loss generally increases with the magnitude of the separation.

Main engine pressure measurements $p(r_q, t)$ at distances $r_q, q = 1, 2, \dots, 12$ are taken to be a spacially coherent acoustic term corrupted by independent additive noise. Under this construction the magnitude of the ratio of vector and scalar sums of $p(r, \omega)$, the transformed pressure measurements

corrected for hardware response are:

$$v(k, \omega) = \left| \frac{\sum_{\ell=1}^{12} p(r_{\ell}, \omega) e^{ikr_{\ell}}}{\sum_{\ell=1}^{12} |p(r_{\ell}, \omega)|} \right|$$

For a coherent acoustic field, $v(k, \omega)$ approaches unity for large S/N measurements with $C_0 = \omega/k$ and $\omega = 2\pi f$.

The absolute maxima of $v(k', \omega)$ for k weighted Fourier coefficients of the measured pressure samples in the band where additive noise was small is close to unity, Figure 5-9. The measured pressures are coherent under a phase shift given by $(k'r_0 = \omega r_0)$.

The absolute maxima $v(k, \omega)$ values establish the propagation characteristics for main engine pressure over the array, Figure 5-10. The median c value for frequencies in the band $2 \leq f \leq 30$ Hz is 350.6 meters/second. Within this band, surface pressure measurements can be well represented by a coherent, non-dispersive, acoustic disturbance propagating outward from a single small source region located near the launch pad. For frequencies much above $f=30$ Hz, the scatter is consistent with errors due to measurement noise.

5.3.2 Solid Rocket Booster Ignition Pulse - The ignition of the solid engines produced a conspicuous transient over the array at 0719:01. The spectral density for a 2.56 second time gate starting at 0719:00.25 EST includes the ignition transient, Figure 5-11. The energy spectrum of the transient resulting from the ignition of the solid engines peaks near 3 Hz. The spacial coherency and phase velocity of the sample located by the

absolute maxima of $v(k, \omega)$ shows that the ignition pressure wavelet propagates over the array as a coherent, non-dispersive disturbance at a velocity of 347 meters/second, Figures 5-12 and 5-13.

As well recognized by NASA, the need to predict pressure spacially is essential to vibration forecasts for large class structures (8). We predict pressure by phase shifts obtained from (k, ω) pairs and $1/R$ attenuation in Figure 5-14. The residue not represented by a spherically divergent acoustic term incident on a smooth ground of constant reflectivity is quite small.

Secondary sources arising from reflections off structures and topography are minimal at KSC. The measurement is well satisfied by an outward propagating acoustic and additive hardware noise. Pressure predictions at VAFB, in contrast, must anticipate secondary sources caused by reflections from a number of major structures. The launch pressure environment at the two sites will differ.

5.3.3 Plume Sound Level Maximum - A major objective of this effort was the determination of the magnitude, phase and coherence of launch generated pressure around the time of maximum loading over distances and azimuths to major structures at VAFB. For our measurements of STS-5 the maximum occurred some 11 seconds after lift-off. At this time the rocket plume was taken to be close to vertical and in an undeflected, steady-state condition. The vehicle just commenced its roll maneuver. Water suppression originally was assumed (probably incorrectly) to be ineffective in attenuating pressure in the array area over this time.

The average spectrum, Figure 5-15, for surface measurements south of the shuttle (aligned with the Columbia's vertical stabilizer) is well above

additive noise for frequencies less than 30 Hz. The measured spectrum has the expected bell shape when plotted in log-log format (9). A spectral maximum somewhat in excess of 130 db is located around 5 Hz. The S/N estimate for measurements near the maximum is in excess of 100.

As before, the single source nature of the pressure field was tested, Figure 5-16. Pressure, particularly near 5 Hz, is well represented as a spacially coherent, acoustic disturbance. This feature continues to hold true for times well after lift-off. At these later times there is some evidence of dispersion consistent with the notion that longer waves "appear to" originate from a point lower in the plume.

Phase velocity estimates, Figure 5-17, for the STS-5 launch located by absolute $v(k, \omega)$ maxima values around the time of the load maximum show STS pressures can be modeled by acoustics coming from a small source located some 100-150 meters above the launch pad.

5.4 PLUME SPECTRA IN STANDARD FORM

After Hartnett, (10) stable broadband spectral estimates of surface pressure were constructed by fitting periodograms to a spectral form advocated by Powell (11) for undeflected, plume generated acoustics. The spectrum

$$G_{pp}(f) = \frac{4}{\pi} \frac{OASPL}{f_m} \left\{ f/f_m + f_m/f \right\}^{-2}$$

is fitted to periodograms by selecting values of OASPL and f_m , the frequency at the spectral maximum, that minimize the square of the residuals between periodogram coefficients and $G_{pp}(f)$. The best fitting

spectra for data 6 seconds or more after lift-off is summarized in Table 2.

Table 2 is a set of OASPL and f_m values that best fit data samples for times shortly after launch. The maximum OASPL for a surface measurement at 293 meters occurs 11 seconds after lift-off. The OASPL is calculated to be 139 db. The spectrum is a maximum at 4.37 Hz.

The overall acoustic power calculated for STS-5 is less than that measured for a Titan III-D, a vehicle with a thrust level less than half that of the shuttle (3).

5.4.1

TABLE 2. STANDARD SPECTRA PARAMETERS
(for 293 Meters)

Time After Lift-Off (Seconds)	fm Hz	OASPL ₂ PSI ²		Figure of Merit	OASPL (db)
6	10.86	2.652	$\times 10^{-4}$	3.25.9*	135
9	4.96	6.381	"	1.23	139
11	4.37	6.982	"	0.84	139
14	2.79	4.429	"	0.54	137
17	2.49	1.459	"	1.41	132
20	3.89	1.011	"	0.94	131

* Periodogram does not fit STANDARD FORM.

Two tests were run to evaluate when pressure periodograms could be represented as a stochastic process with the spectral form proposed by Powell. One test, Figure 5-18, plots the residuals against the distribution of a Chi squared variate with DOF=2, the expected distribution, had we fitted periodogram ordinates to the true spectra. The construction makes the acceptance criteria one of simply accepting the residuals to lie on the indicated straight line. This construction and a test based on a figure of merit supports the concept that measured periodograms are well represented by a spectrum of the form $G_{pp}(f)$ for all but the data set starting 6 seconds after lift-off. At this early stage in the launch, the acoustics do not exhibit the spectral form ascribed to an undeflected plume, and rightly so.

5.5 COMPARISON TO FORECASTED VALUES

It has long been widely accepted that the acoustic efficiency of an undeflected rocket exhaust, defined by the ratio of the OASPL to the exhaust's mechanical power, is about 0.5%, independent of thrust level (10). Indeed, the simple linear relation between maximum OASPL and thrust for an observer at a fixed distance over the wide range of thrust levels was the basis for AFGL's early forecasts for shuttle launches at VAFB. The OASPL calculated for STS-5 appears to be quite low, Figure 5-19. The "apparent" acoustic efficiency of this rocket based on surface pressures taken south of the pad is substantially lower than that of most large class rockets. Further, the location of the spectral maxima for a Strouhal number in harmony with the STS engine parameters differs from that forecast (3).

5.6 FINDINGS: STS-5

Overall Sound Power Level (OASPL) calculations for surface measurements south of the launch point in line with Columbia's vertical stabilizer were unexpectedly low.

STS-5 launch generated surface pressures were coherent in the sense that at any one time a unique range sensitive amplitude and phase factor exists to connect pressure observations.

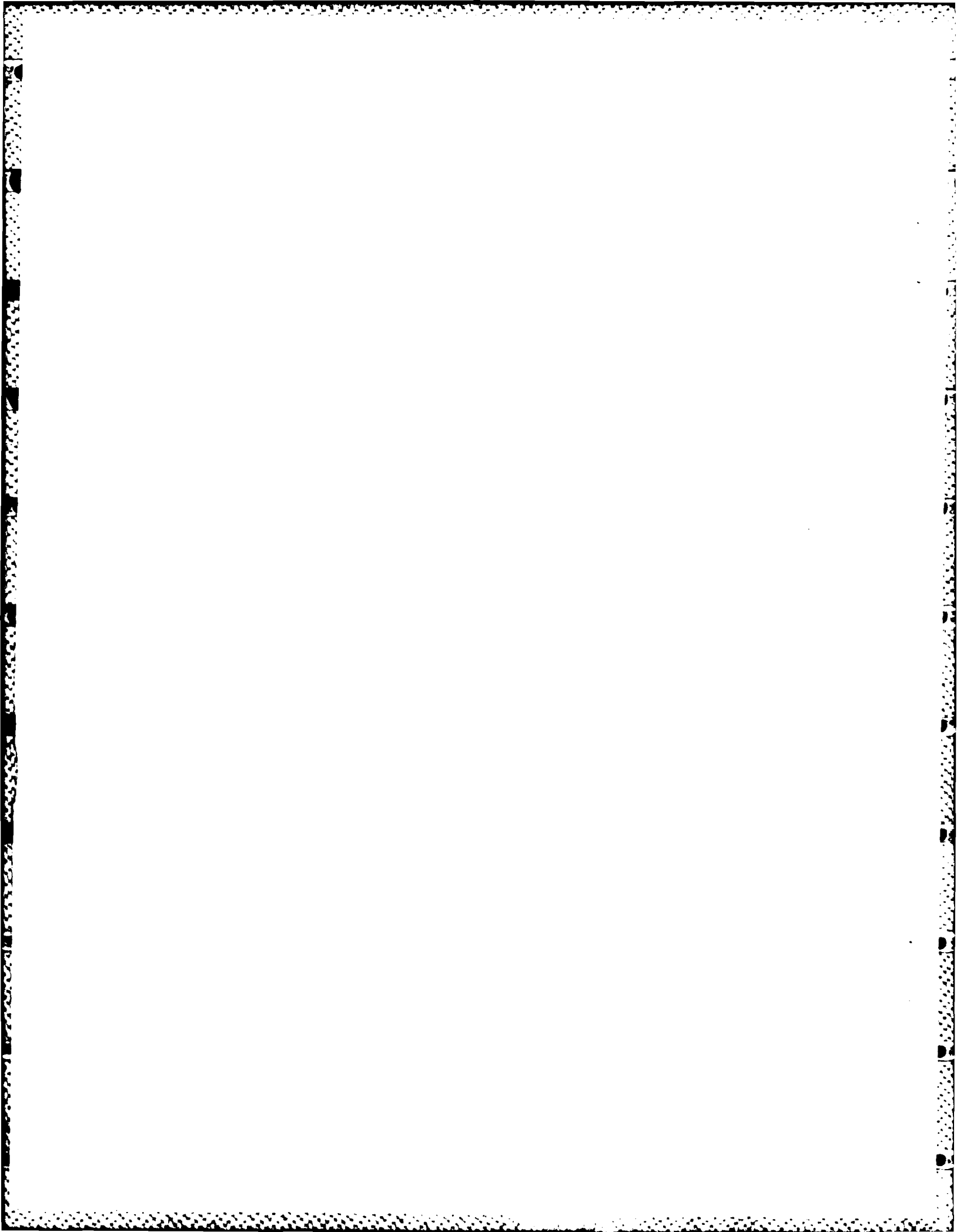
Calculated phase, attenuation and spacial coherency values for surface pressures generated by the STS-5 launch are entirely consistent with a surface pressure produced by an acoustic disturbance propagating outward from a single, small source moving with the rocket.

5.7 CONCLUSIONS: STS-5

The low pressure level found here indicates that the STS OASPL at KSC is asymmetric about the rocket's body axis. This lack of symmetry is quite likely due to asymmetries in the water suppression system.

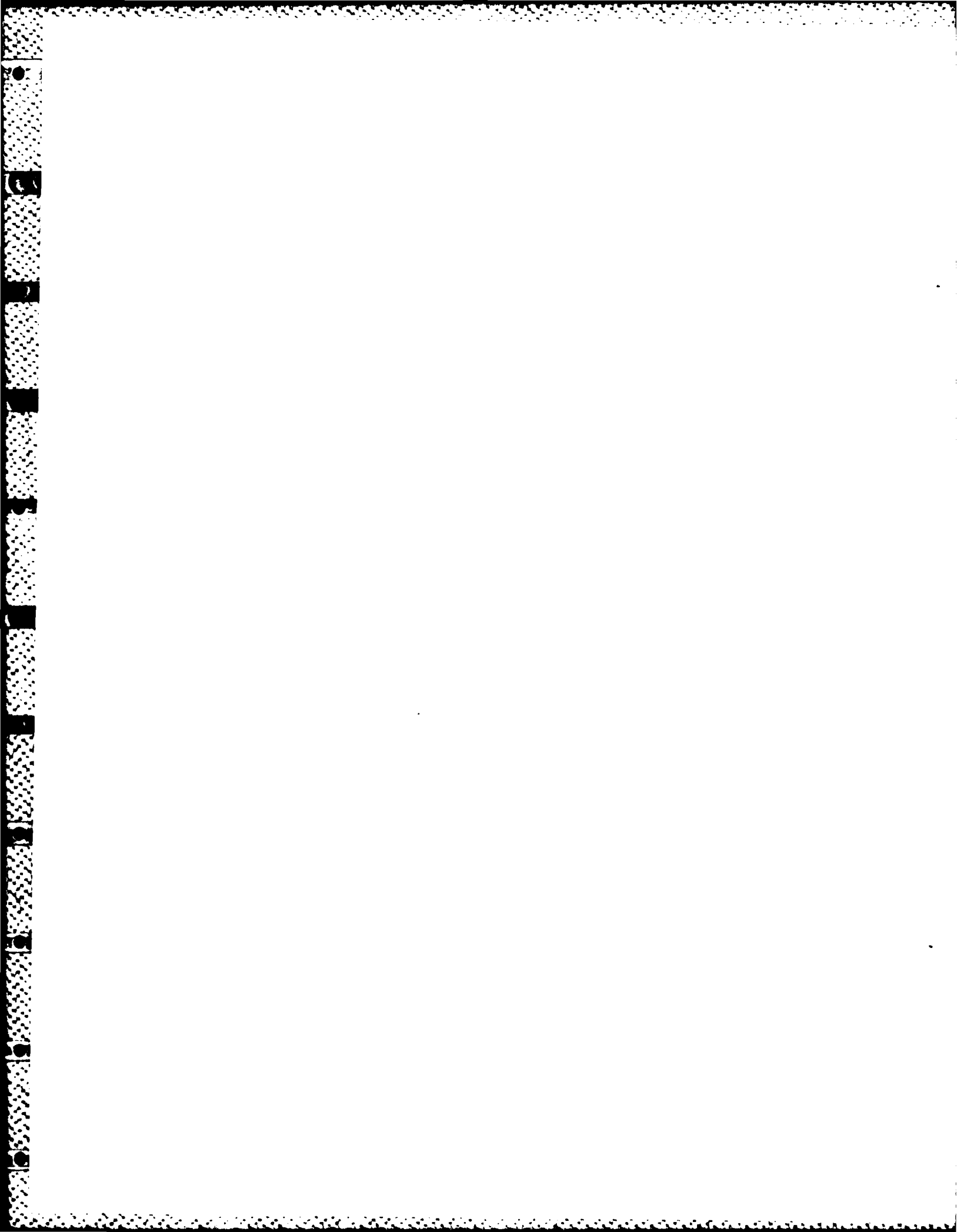
An "equivalent point source", essential to vibration forecasts can be located from the Kennedy Space Center (KSC) data to control facility response measurements at VAFB.

The location and construction of a plume source permits a forecast of pressures modified by the Air Force sound suppression system and reflections off nearby structures and topography at VAFB.



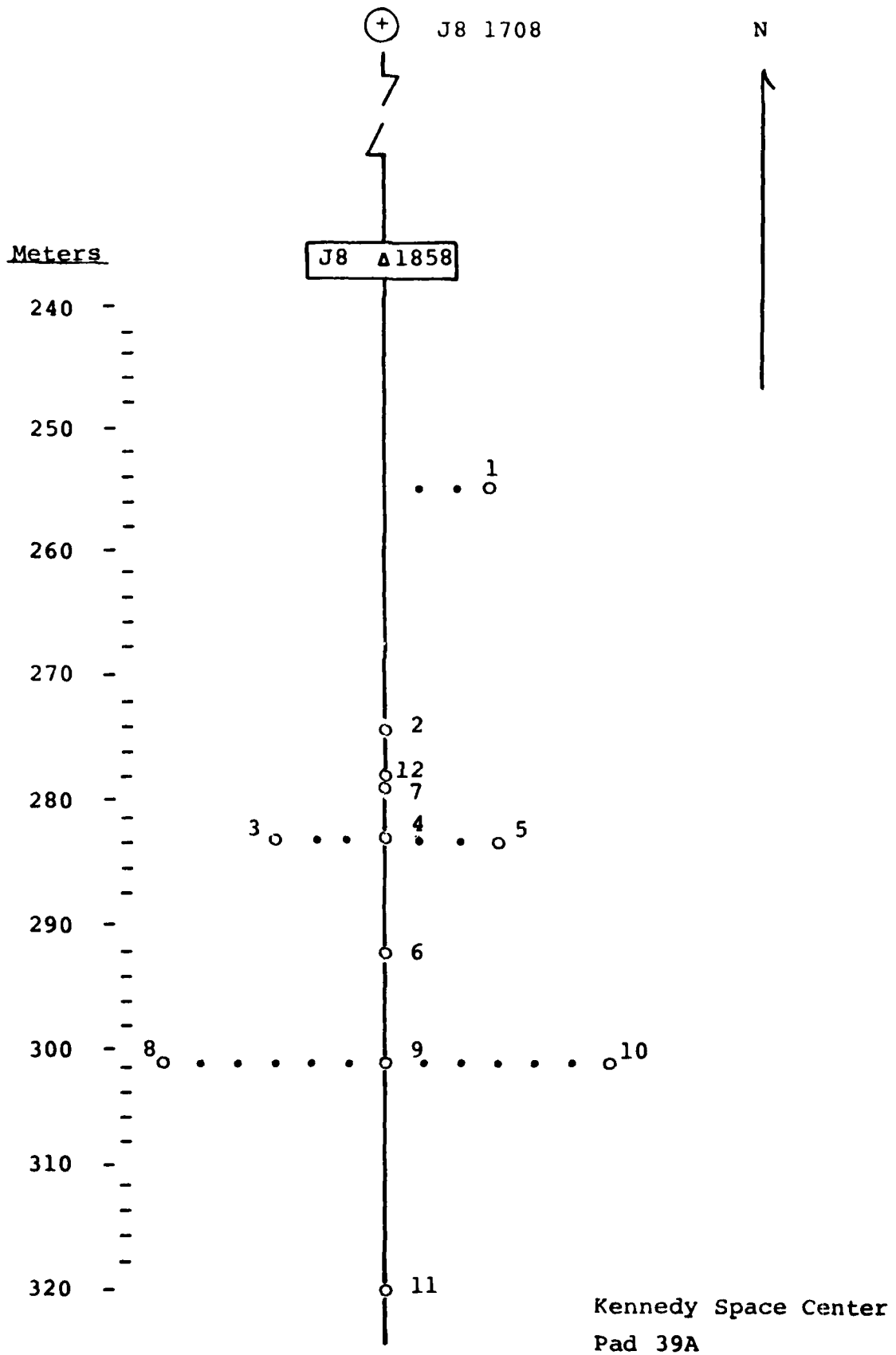
5.8 REFERENCES - SECTION 5

1. Von Glahn, P.G., The Air Force Geophysics Laboratory Standalone Data Acquisition System: A Functional Description, AFGL-TR-80-0317, Oct 1980. AD A100253.
2. NASA Report No. KSC-DD-457-TR, Space Shuttle STS-1 Launch Processed Ground Measurements, Vol I, Sep 1981.
3. Crowley, F.A., Hartnett, E.B. and Ossing, H.A., The Seismo-Acoustic Disturbance Produced by a Titan III-D with Applications to the Space Transportation System Launch Environment at Vandenberg AFB, AFGL-TR-80-0358, Nov 1980. AD A100209.
4. Yuen, C.K., On The Smoothed Periodogram Method for Spectrum Estimation, Signal Processing Vol I, No. 1, Jan 1979.
5. Bendat, J. and Piersol, A., Measurement and Analysis of Random Data, John Wiley and Sons, 1966.
6. Fay, J.W., Confidence Bounds for Signal-to-Noise Ratios from Magnitude Squared Coherence Estimates, IEEE Transactions on Acoustics, Speech and Signal Processing, Vol. ASSP-28, No. 6, Dec 1980.
7. Kimball, B.A. and Lemon, E.R., Spectra of Air Pressure Fluctuations at the Soil Surface, JGR Vol 75, No. 33, Nov 1970.
8. NASA Report no. GP-1059, Revision A, Environment and Test Specification Levels Ground Support Equipment for Space Shuttle System Launch Complex 39, Acoustic and Vibration, Vol. I, Sep 1976.
9. NASA Report No. SP-8072, Acoustic Loads Generated by the Propulsion System, 1971.
10. Hartnett, E. and Carleen, E., Characterization of Titan III-D Acoustic Pressure Spectra by Least Squares Fit to Theoretical Model, AFGL-TR-80-0004, Jan 1980. AD A083021.
11. Powell, A., Theory of Vortex Sound, Jour Acous Soc of America Vol. 36, No. 1, Jan 1964.



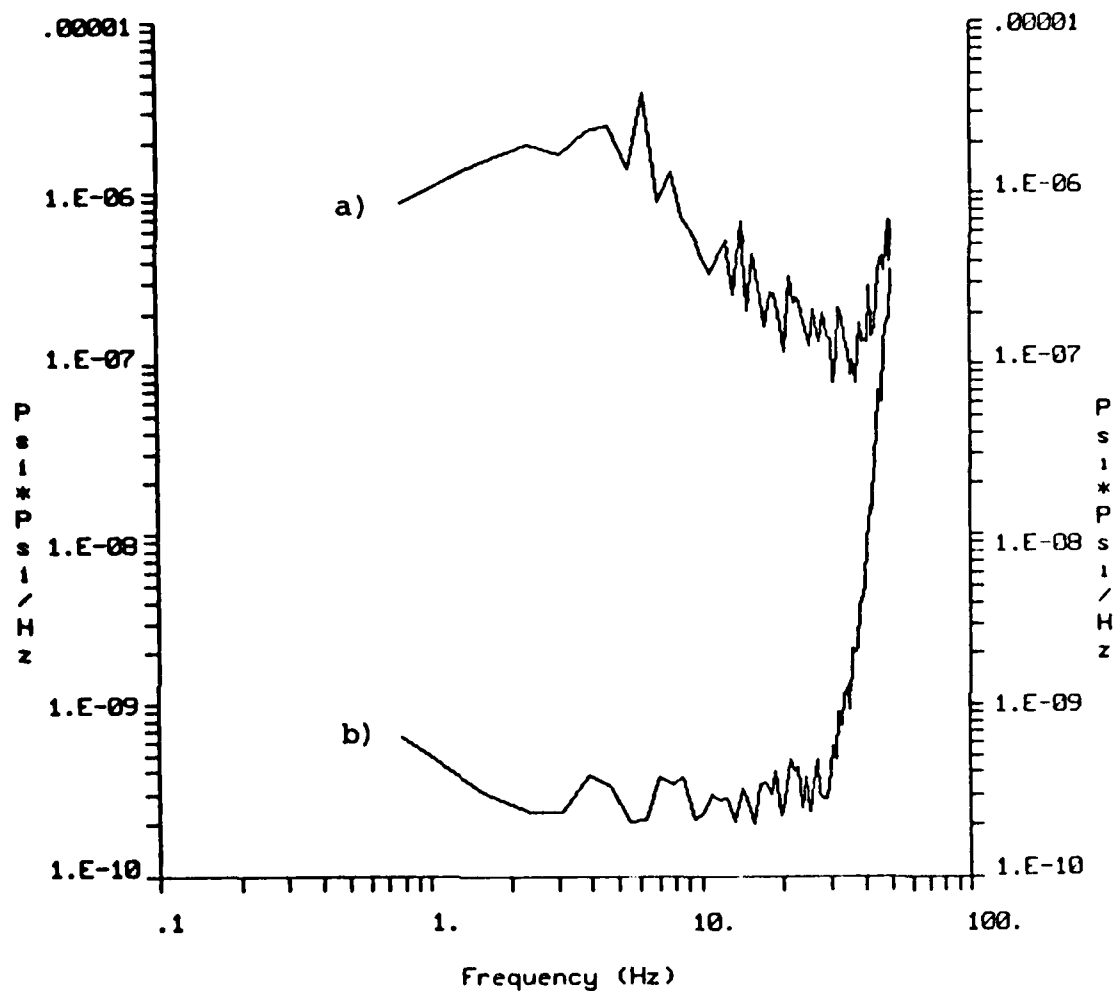
5.9 ILLUSTRATIONS - SECTION 5

1. Sensor Locations
2. Pressure Spectra (Low Level)
3. Channel Coherency - Low Level Measurements
4. S/N Estimate: Low Level Measurements
5. Pressure Spectra (High Level)
6. Channel Coherency - High Level Measurements
7. S/N Estimate: High Level Measurements
8. Spectra: Main Engine
9. Absolute Maxima: Main Engine
10. Propagation Characteristics: Main Engine
11. Spectra: Solids Ignition
12. Absolute Maxima: Solids Ignition
13. Phase Velocity: Solids Ignition
14. Pressure Prediction: Solids Ignition
15. Spectra: Solids Ignition
16. Absolute Maxima: Plume
17. Phase Velocity: STS-5 Launch
18. Spectrum Acceptance Test
19. OASPL Maxima



SENSOR LOCATIONS

Figure 5-1



DOF=20

a) Total Spectra

b) Incoherent Portion

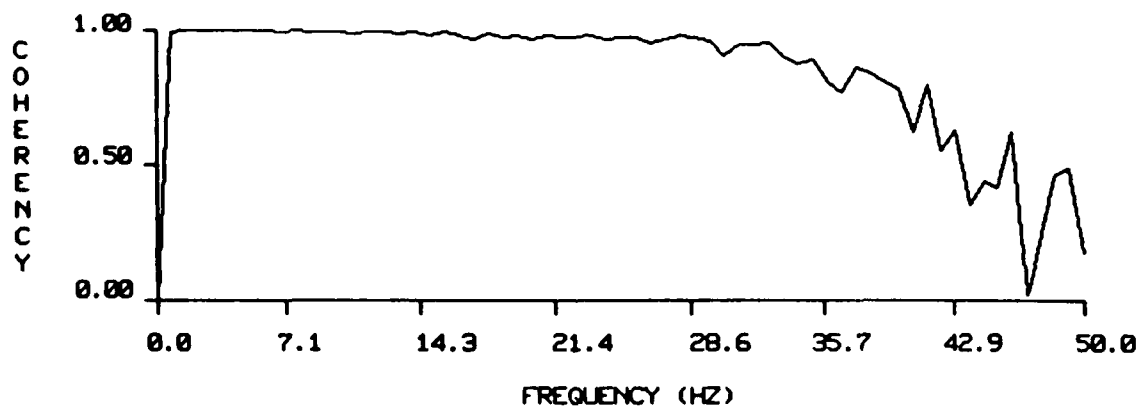
PRESSURE SPECTRA (LOW LEVEL)

Figure 5-2

COHERENCY TEST
STANDARD = CHANNEL 7

COMPARISON = CHANNEL 12

10 SEGMENTS



Sensor Separation \approx 1 Meter

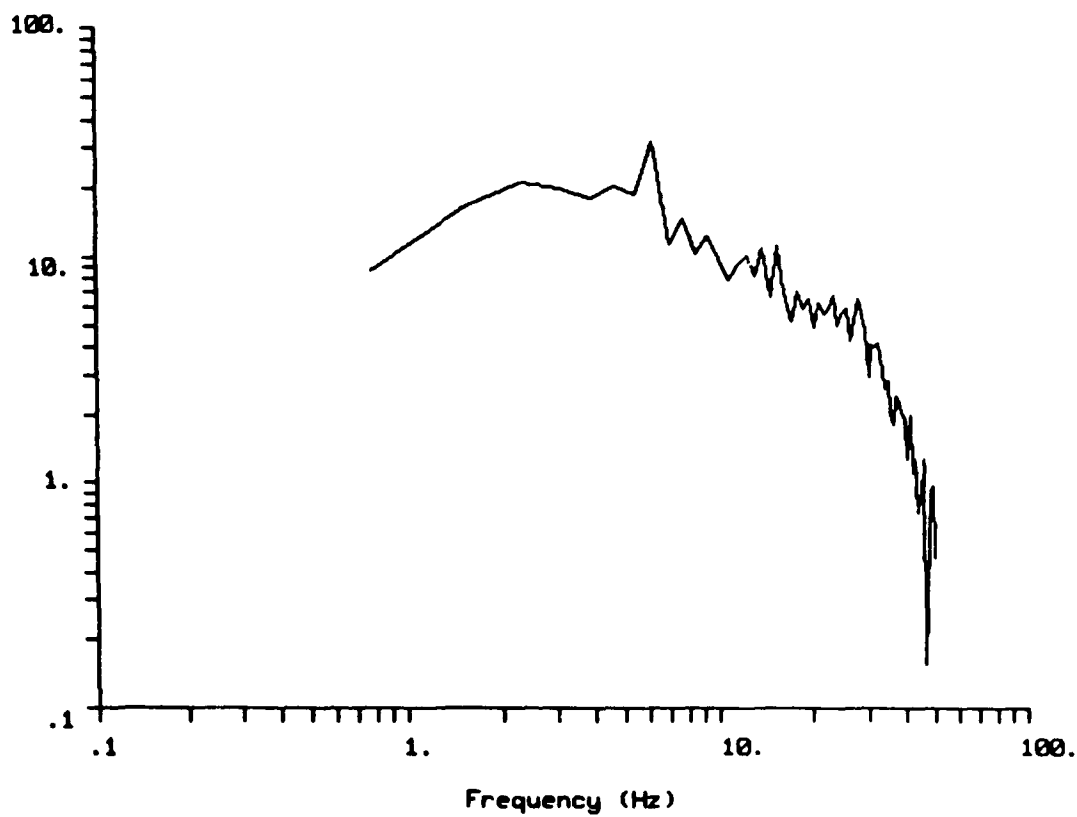
CHANNEL COHERENCY
LOW LEVEL PRESSURE MEASUREMENTS

Figure 5-3

SIGNAL TO NOISE RATIO
STANDARD = CHANNEL 7

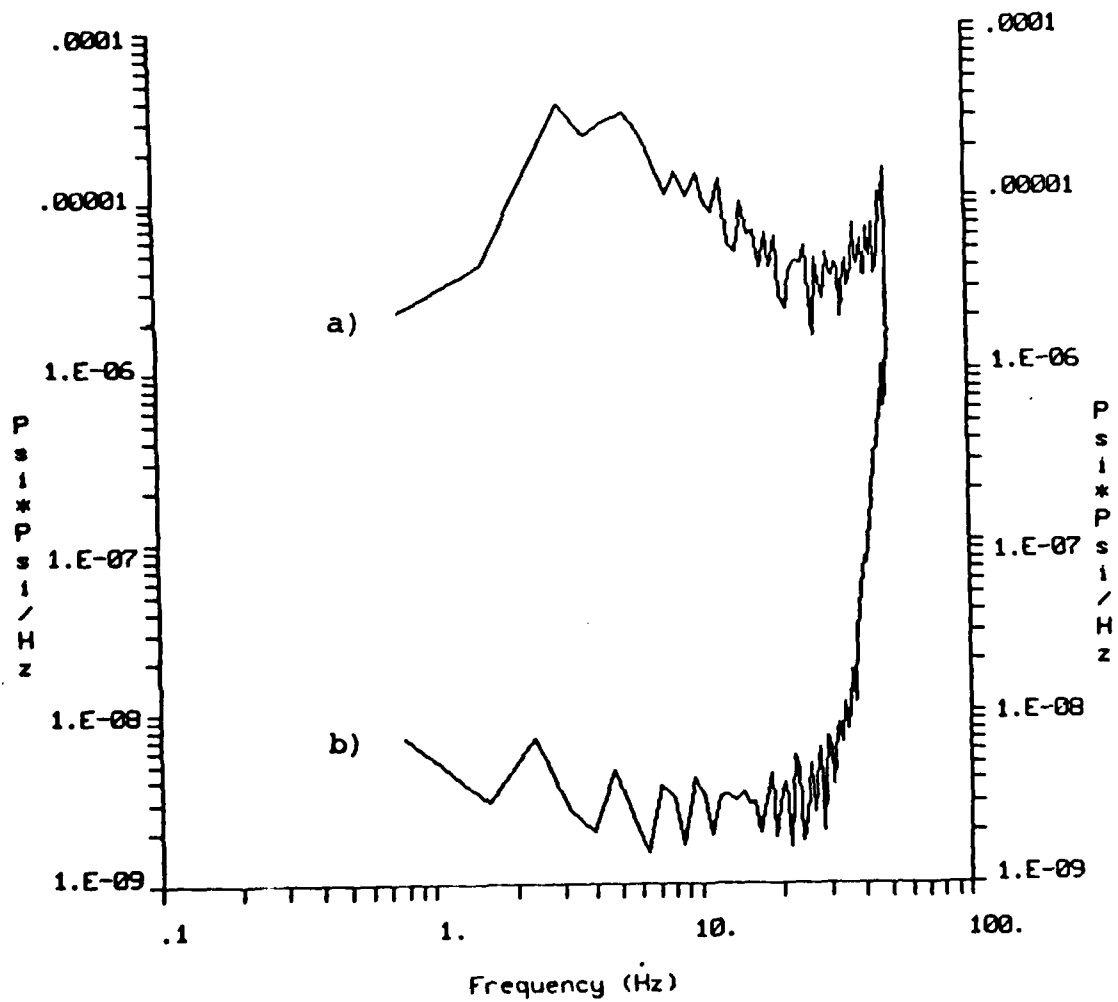
COMPARISON = CHANNEL 12

10 SEGMENTS



S/N ESTIMATE : LOW LEVEL MEASUREMENTS

Figure 5-4



DOF=2

- a) Total Spectra
- b) Incoherent Portion

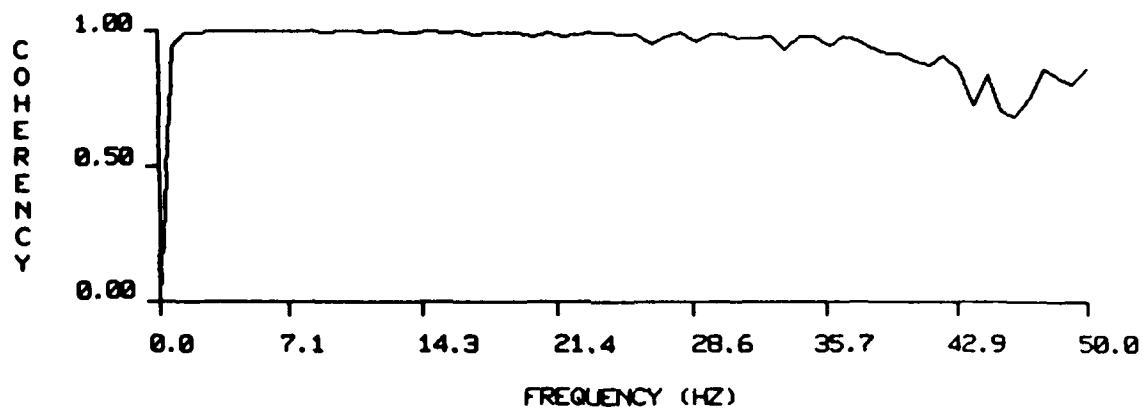
PRESSURE SPECTRA (HIGH LEVEL)

Figure 5-5

COHERENCY TEST
STANDARD = CHANNEL 7

COMPARISON = CHANNEL 12

10 SEGMENTS



Sensor Separation \approx 1 Meter

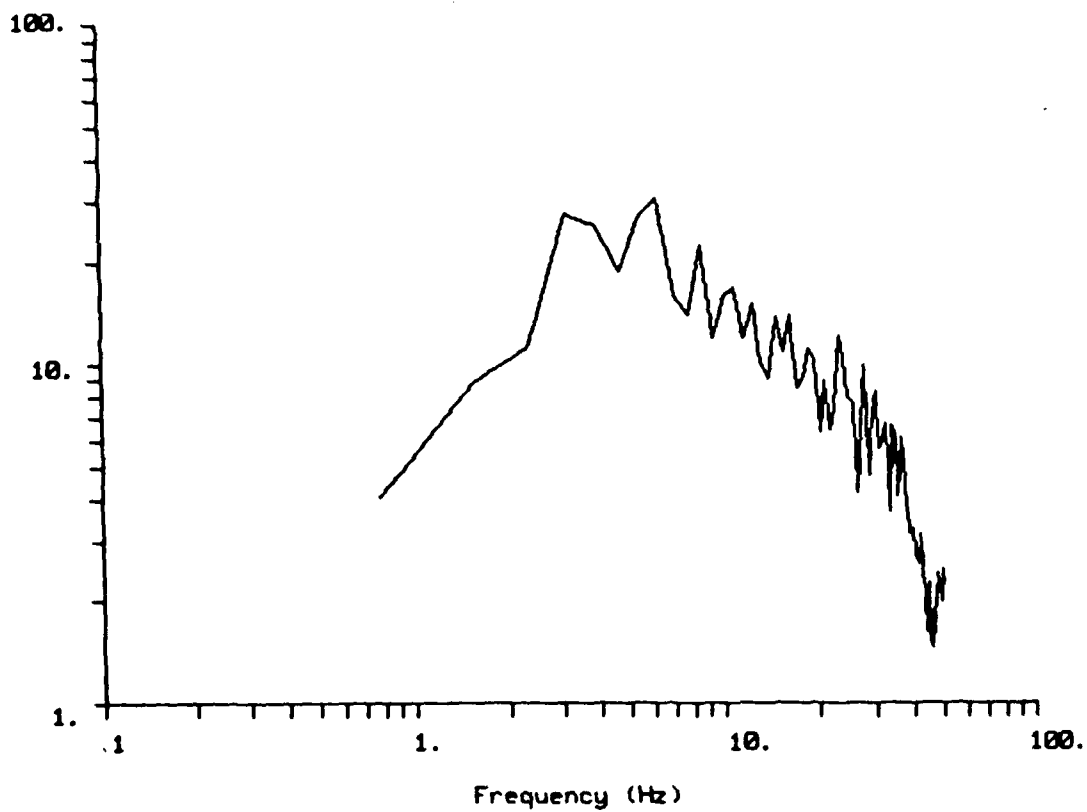
CHANNEL COHERENCY
HIGH LEVEL PRESSURE MEASUREMENTS

Figure 5-6

SIGNAL TO NOISE RATIO
STANDARD - CHANNEL 7

COMPARISON - CHANNEL 12

10 SEGMENTS



S/N ESTIMATE : HIGH LEVEL MEASUREMENTS

Figure 5-7

AD-R142 682

GEOKINETIC EFFECT ON MOTION SENSITIVE INSTRUMENTATION
SYSTEMS AND FACILITIES(U) WESTON OBSERVATORY MA
F A CROWLEY ET AL. 15 JAN 84 AFGL-TR-84-0031

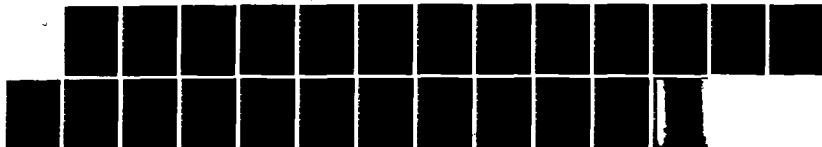
2/2

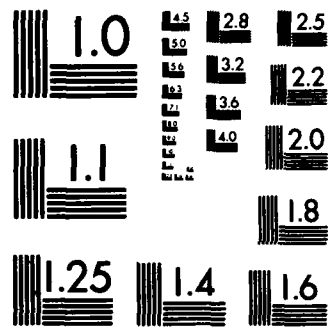
UNCLASSIFIED

F19628-81-K-0005

F/G 8/11

NL



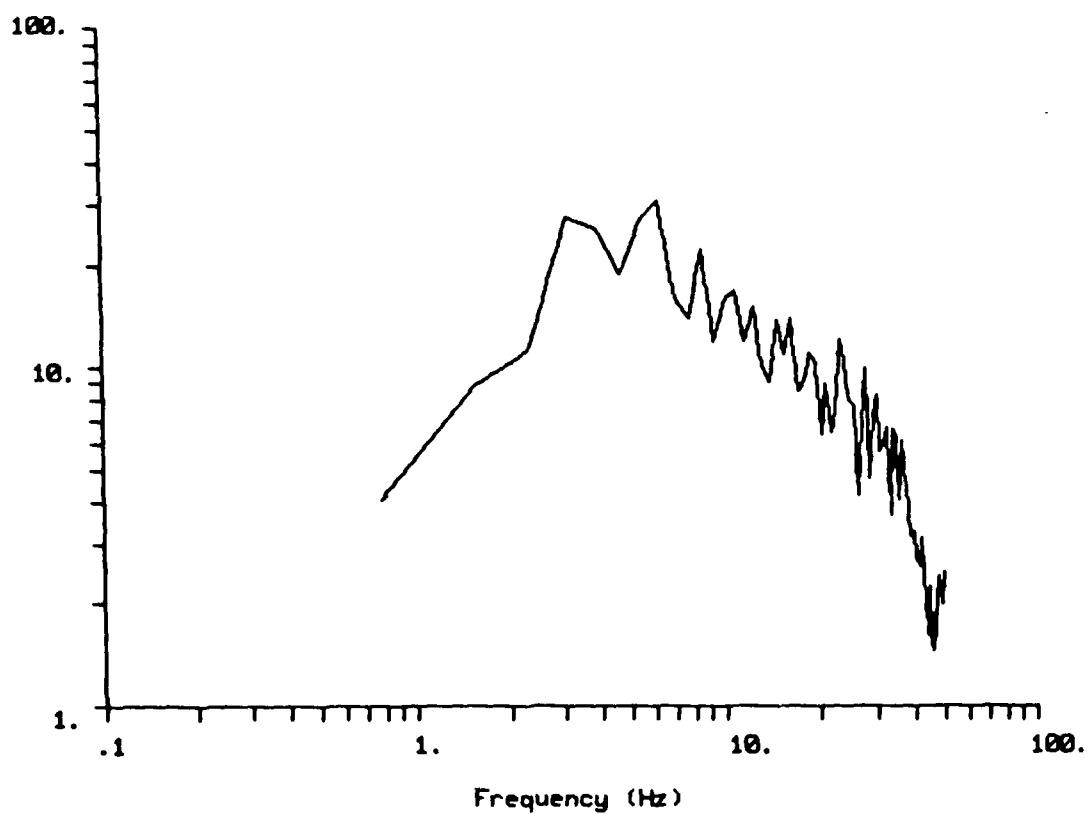


MICROCOPY RESOLUTION TEST CHART
NATIONAL BUREAU OF STANDARDS-1963-A

SIGNAL TO NOISE RATIO
STANDARD - CHANNEL 7

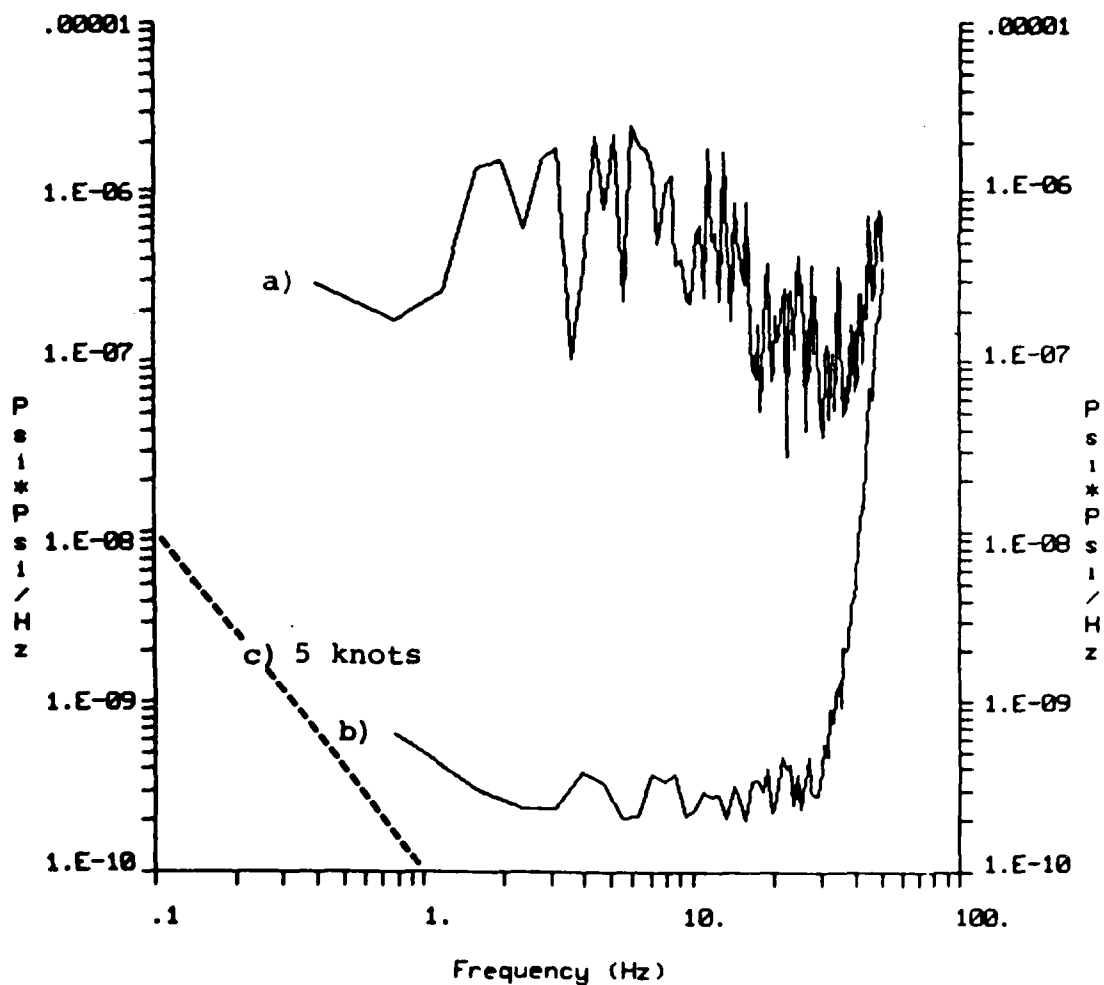
COMPARISON - CHANNEL 12

10 SEGMENTS



S/N ESTIMATE : HIGH LEVEL MEASUREMENTS

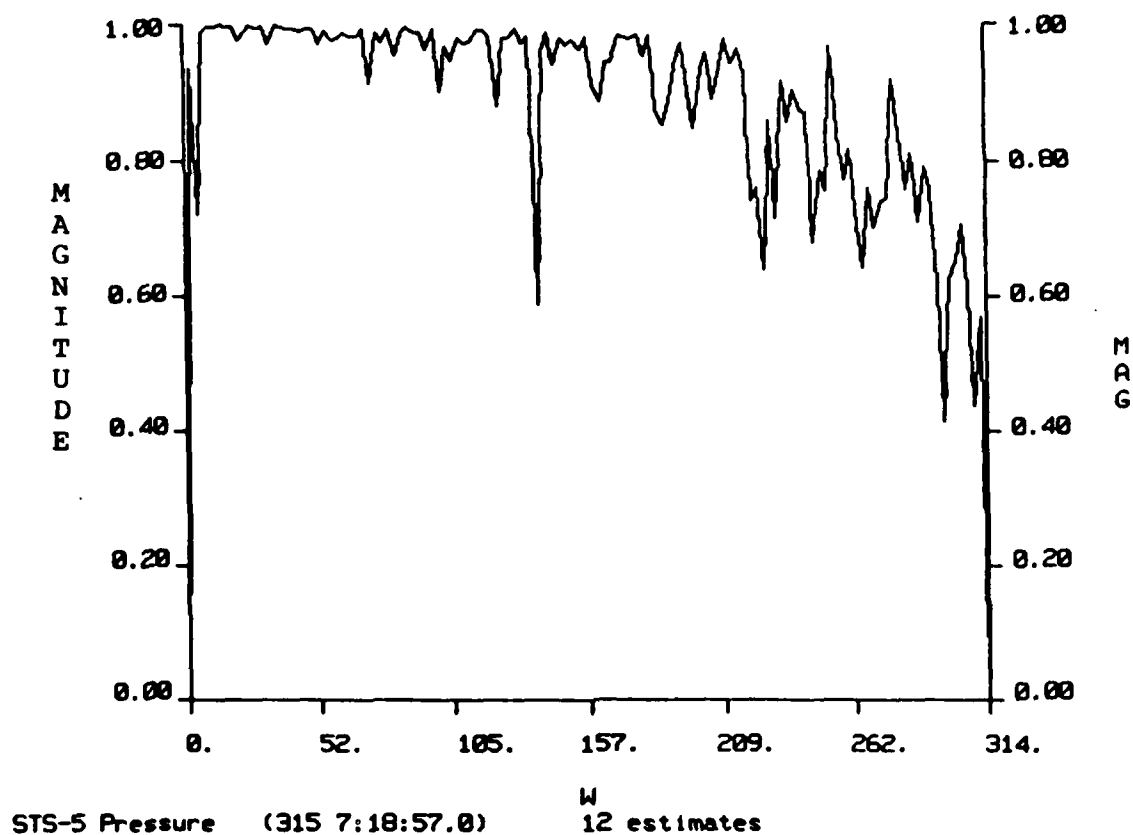
Figure 5-7



- a) Spectral Average, Distance 293 Meters
- b) System Noise Figure for Low Level Measurements
- c) Pressure Spectrum for 5 Knot Wind

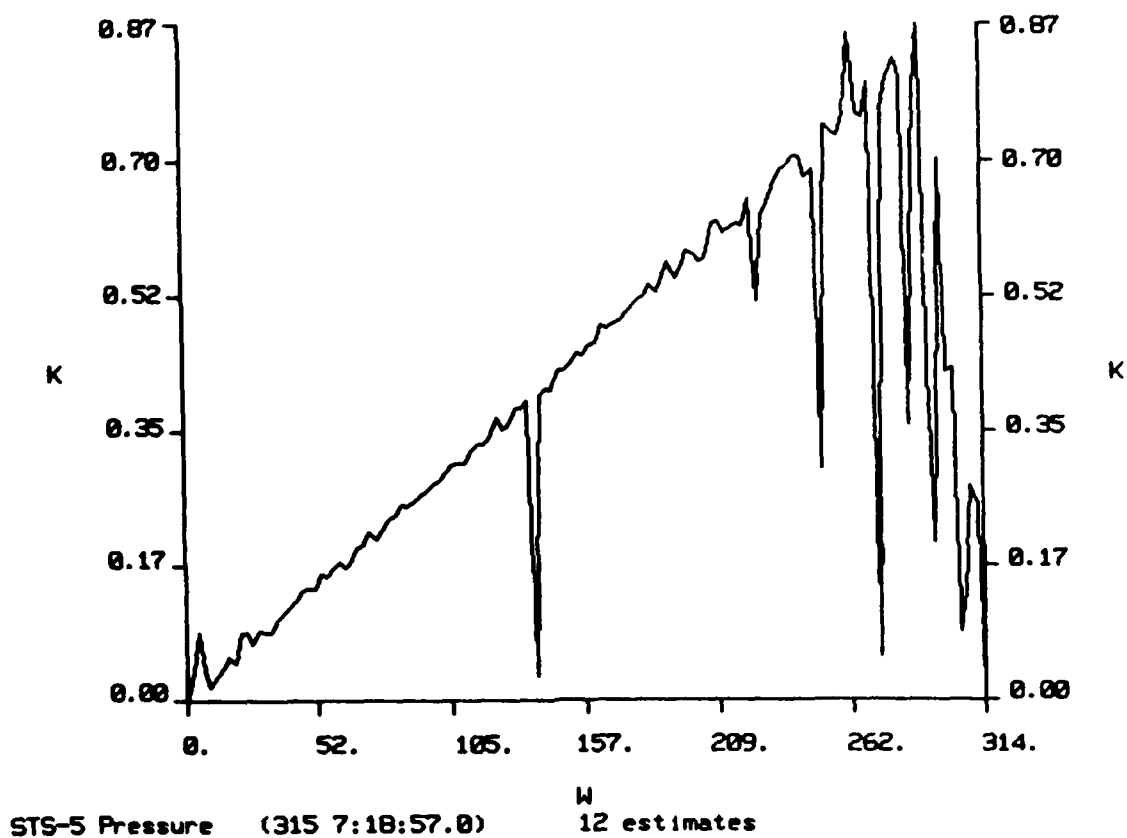
SPECTRA: MAIN ENGINE

Figure 5-8



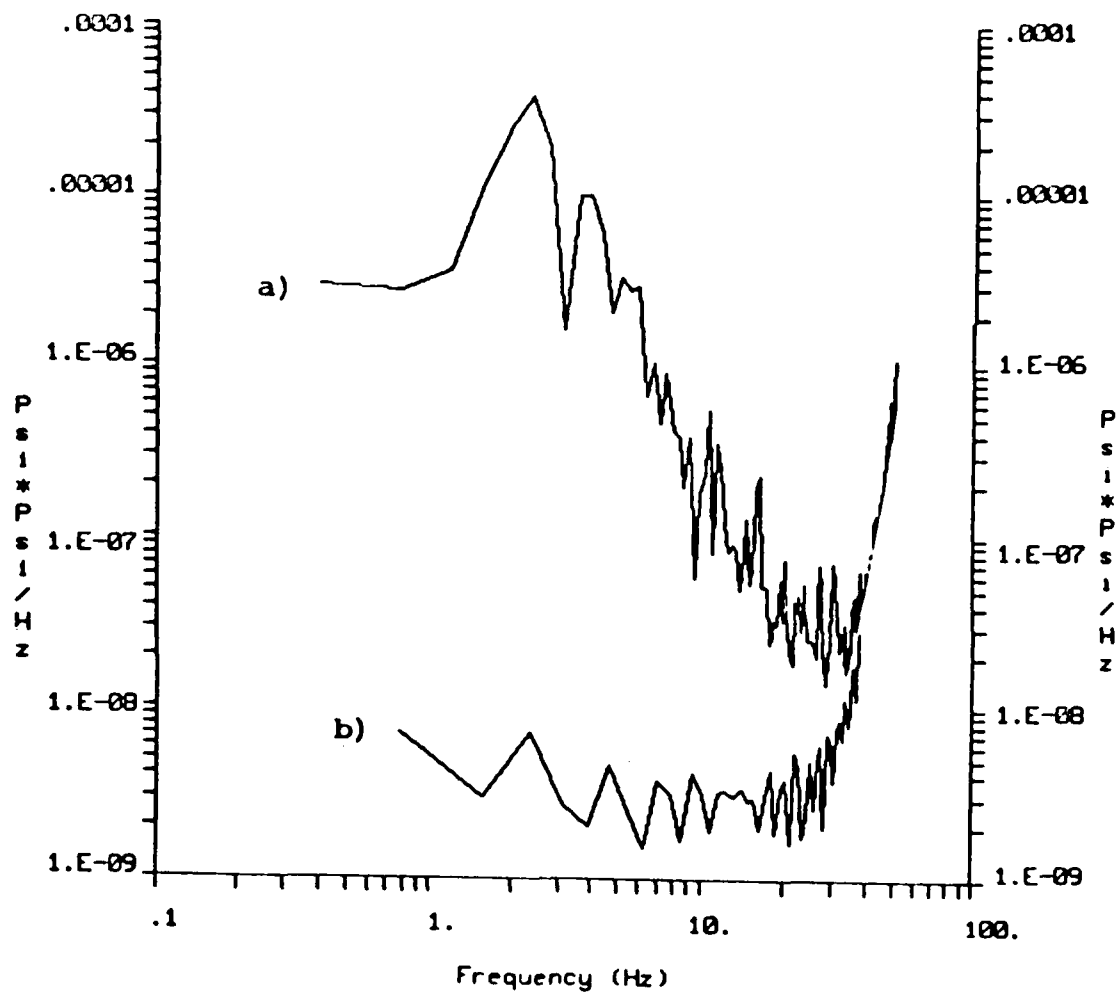
$\hat{v}(k, \omega)$: MAIN ENGINE

Figure 5-9



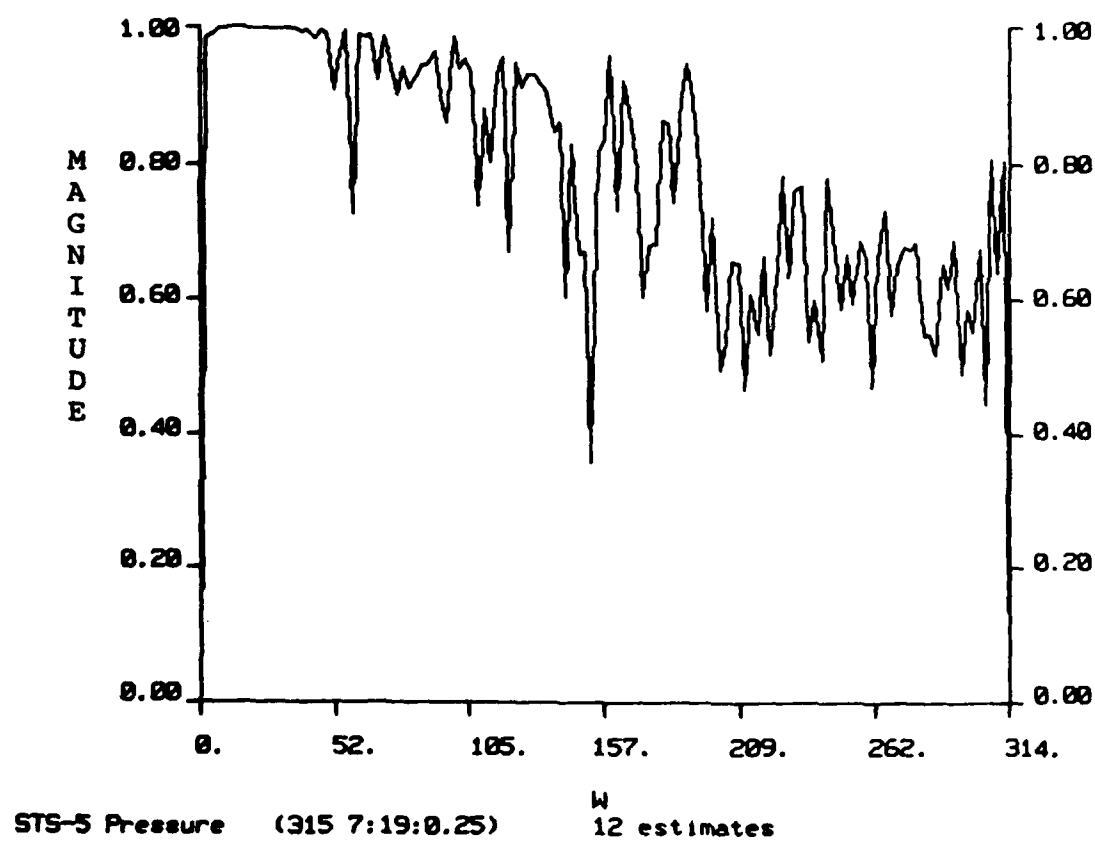
PROPAGATION CHARACTERISTIC: MAIN ENGINE

Figure 5-10



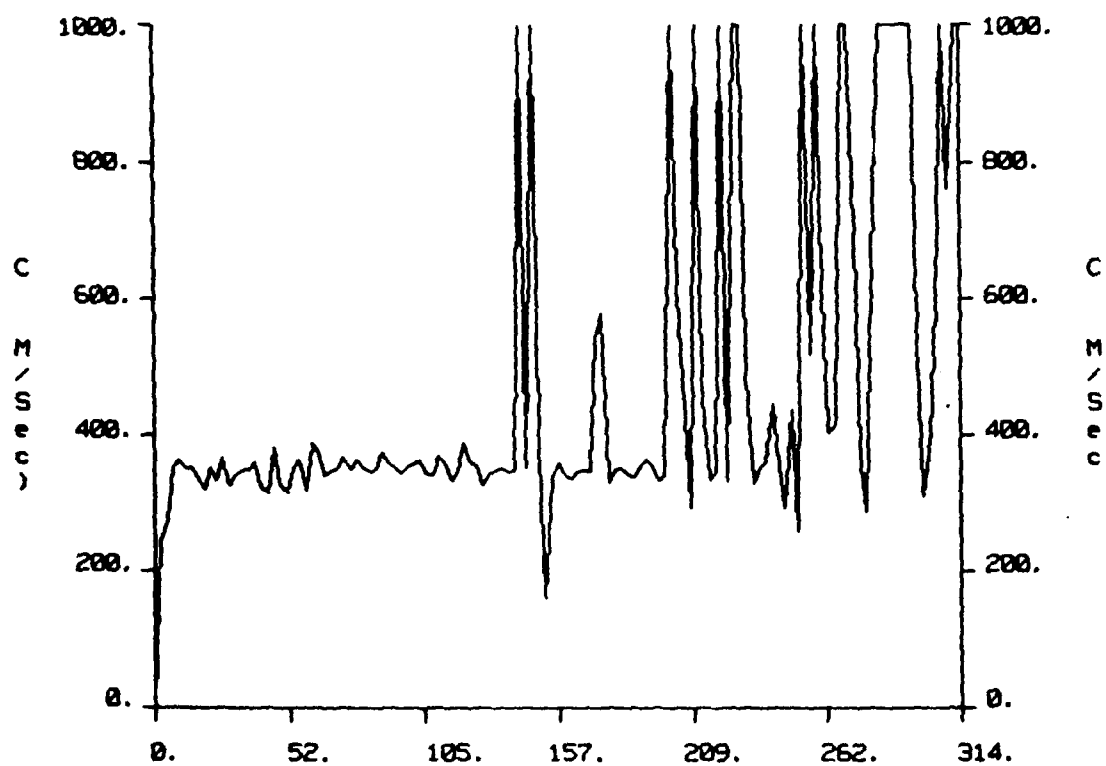
a) Spectral Average ~293 Meters DOF ~14
 b) Noise Figure for High Level Measurements

SPECTRA: SOLIDS IGNITION



$\hat{v}(k, \omega)$: SOLIDS IGNITION

Figure 5-12

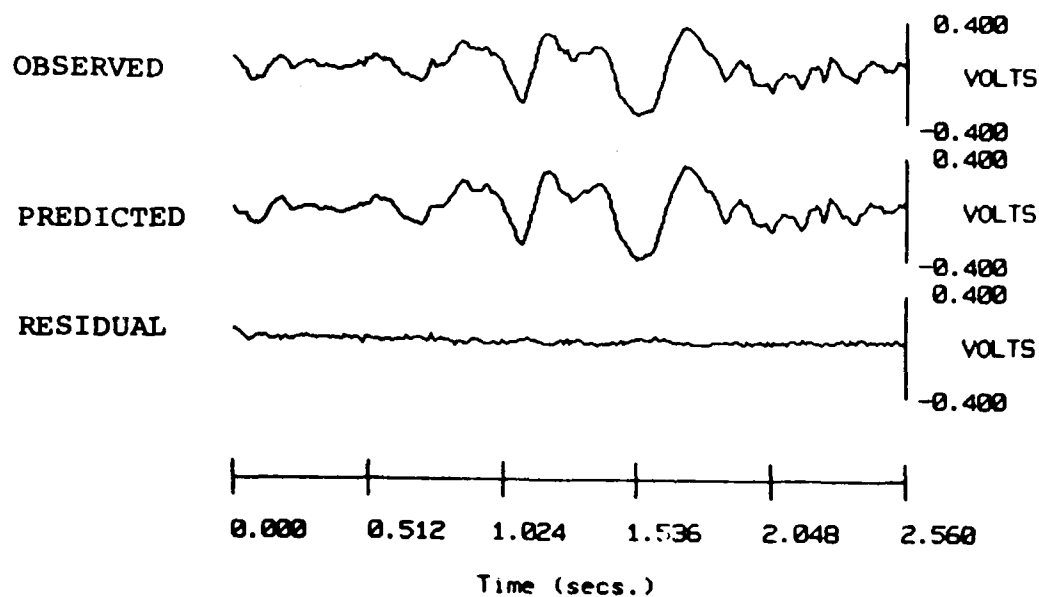


STS-5 Pressure (315 7:19:0.25) W
 Median= 347.4219 12 estimates

PHASE VELOCITY: SOLIDS IGNITION

Figure 5-13

293 meters

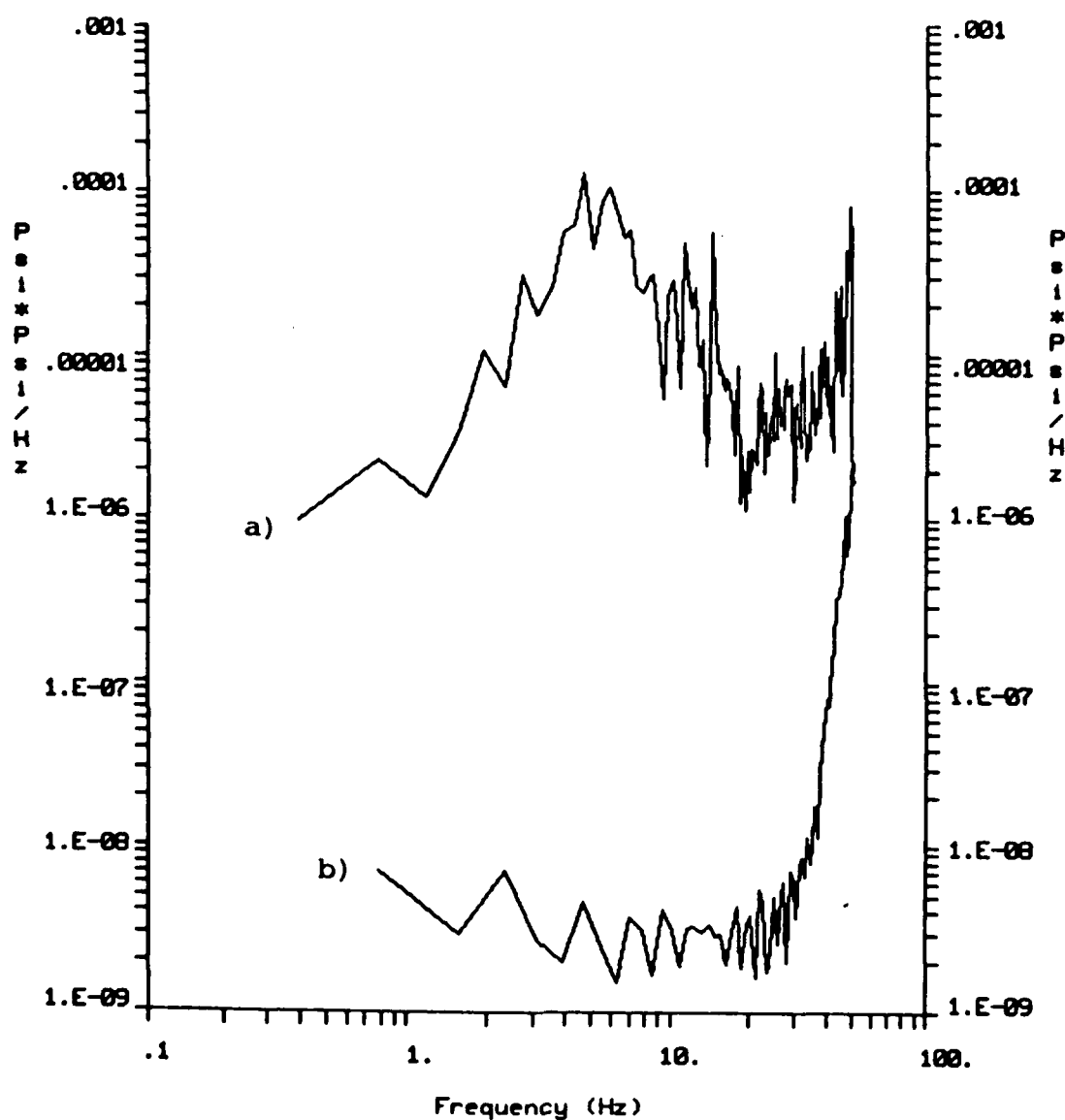


T=0.--> 315 7:19: 0.250
File: DTSSB3.DAI

(Predicted pressure passed through Ch 6 response)

PRESSURE PREDICTION: SOLIDS IGNITION

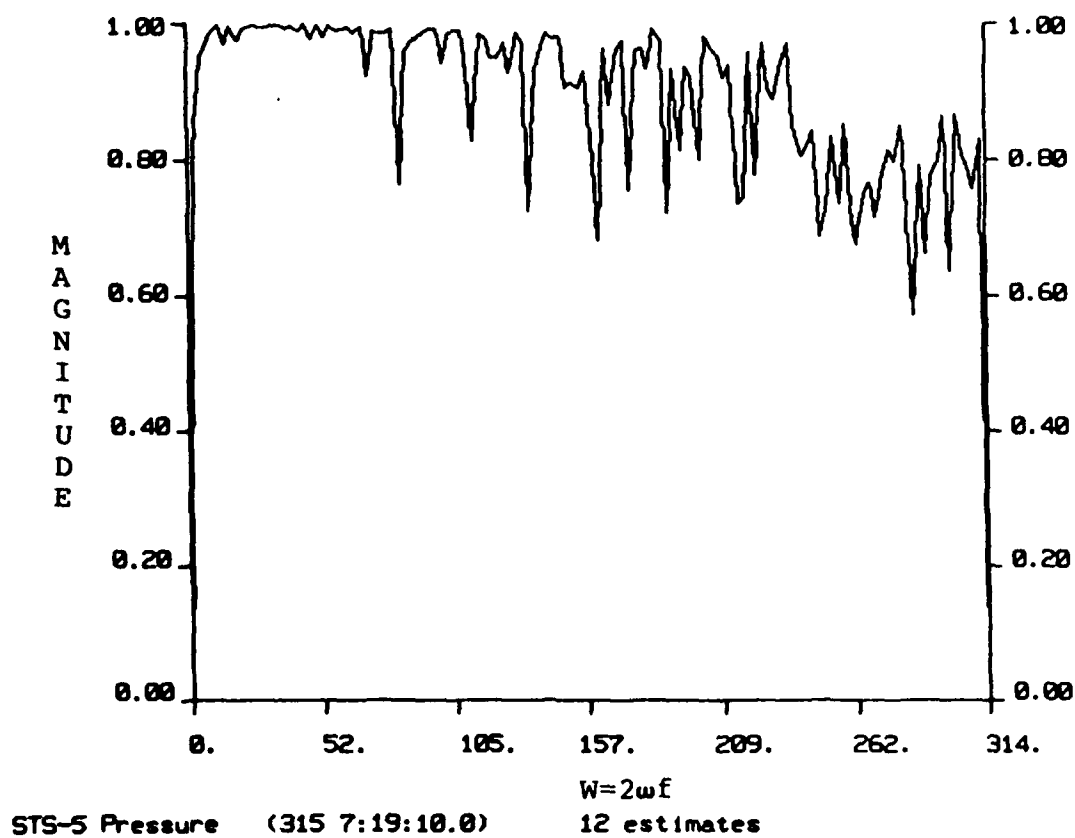
Figure 5-14



- a) Spectral Average ~293 Meters DOF ~14
 b) Noise Figure for High Level Measurements

SPECTRA: SOLIDS IGNITION

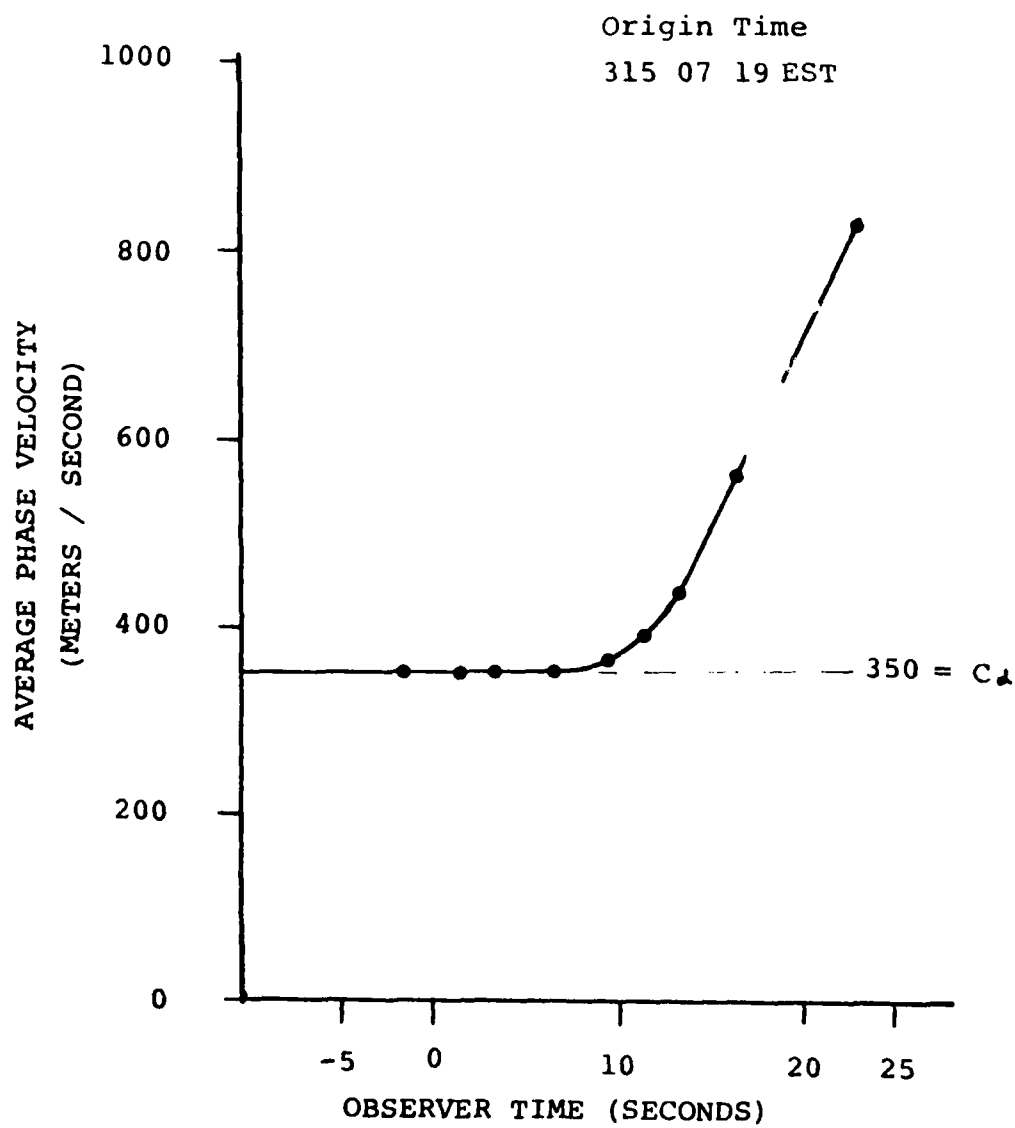
Figure 5-15



$\hat{v}(k, \omega)$: PLUME MAXIMUM

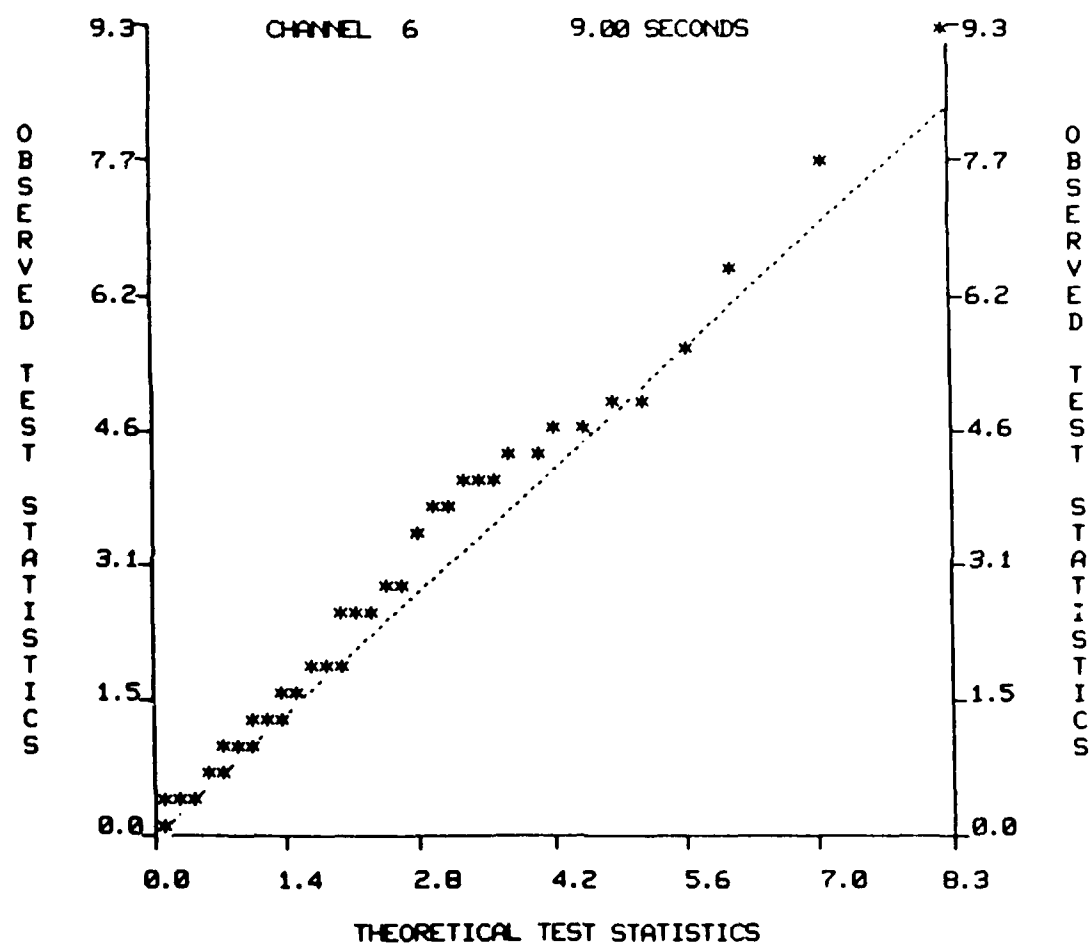
Figure 5-16

STS-5; KSC



PHASE VELOCITY: STS-5 LAUNCH

Figure 5-17



SPECTRUM ACCEPTANCE TEST

Figure 5-18

Maximum Power for a Ground Station at 300 Meters

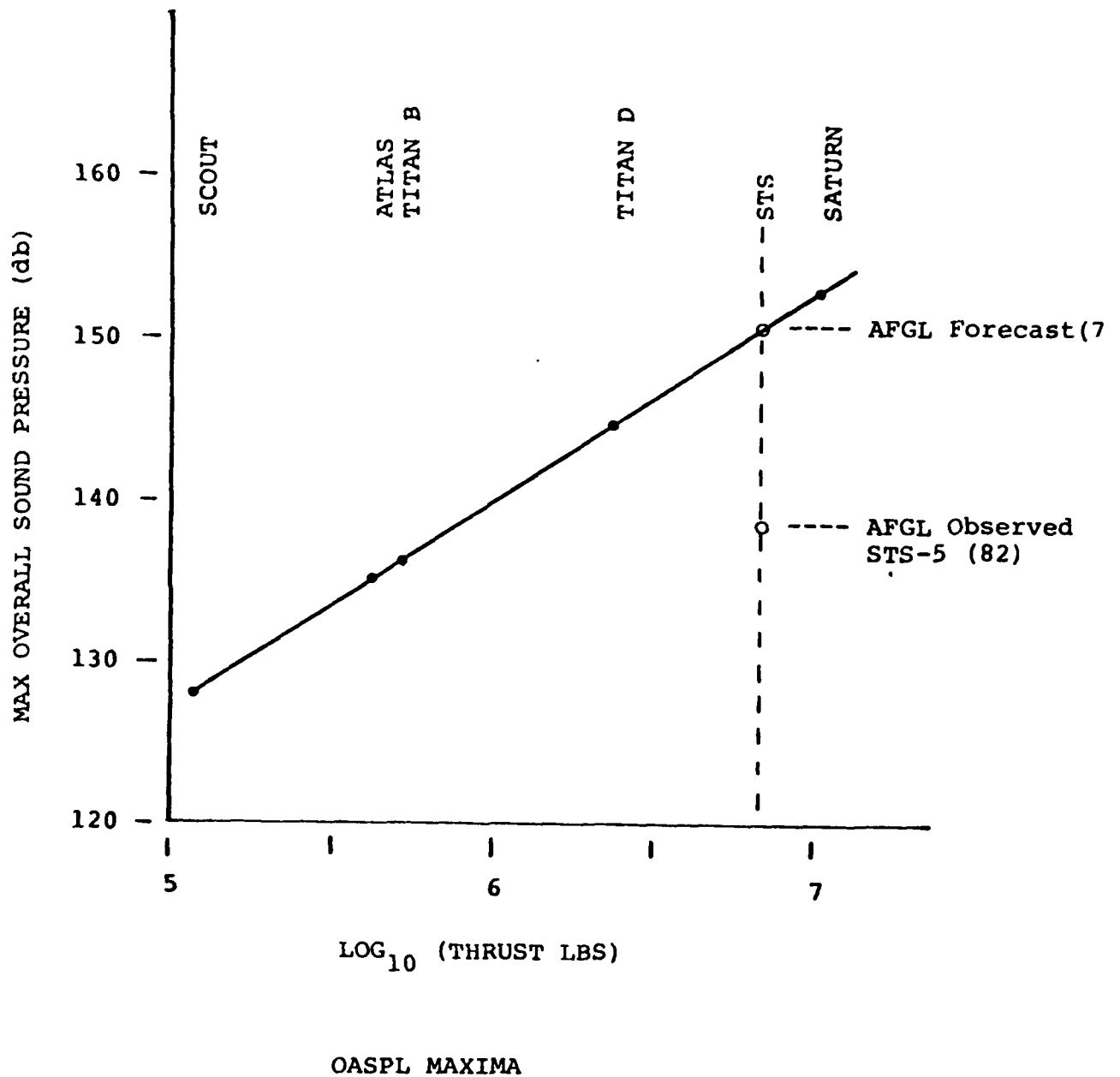


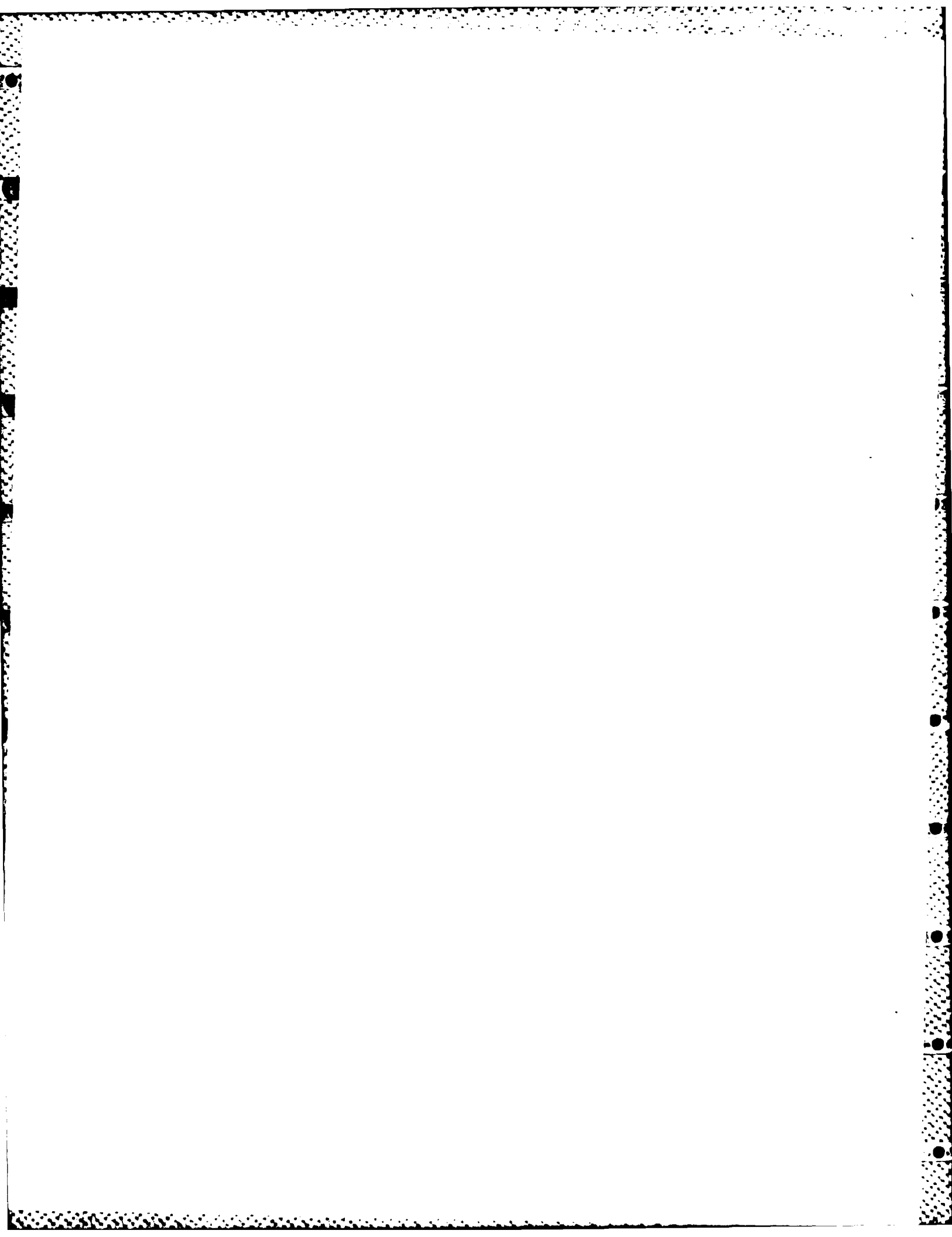
Figure 5-19

6.0 SEISMIC PIER ROOM

Progress has been made in upgrading a dedicated seismic pier room at the Weston Observatory for the systematic calibration of pressure sensors and seismometers. Individual test and calibration are particularly important before shipping instruments to remote field sites and after repair. Cabling between the pier room and the computer ensures test and calibration of sensors under computer control similar to that used by GDAS.

During 1983, AFGL/LWH personnel were instructed in the test and calibration of seismometers at the Weston Observatory.

A dedicated instrument calibration facility provides assurance that all measurements are referenced to a common standard, using fixed procedures and known test piers. This improves the overall quality of our field data and also permits ready diagnosis of unreliable sensors.



7.0 SONIC BOOMS

Reduction of sonic boom data acquired during supersonic overflights of Railroad Valley has been completed. The work expands AFGL's technical data base of vibro-acoustic phenomena, particularly in deep, dry alluvial areas. The data applies directly to the response of this landform to surface loads produced by atmospheric explosions or rocket firings. The immediate objective of this effort is to establish ground response to a known source. Of greater interest is the inverse problem, namely the description of source parameters, (e.g. height of burst, burst yield, distance and bearing for explosions; or altitude, distance, bearing, speed for aircraft) from vibro-acoustic measurements.

Large ground responses to acoustic sources, when they occur, are invariably dominated by air-coupled seismics (1,2). Air-coupled seismics are ground resonances excited when a surface pressure travels at a speed coincident with the speed of the Rayleigh Wave (3). The frequencies of these ground resonances are sensitive to the elastic parameters and densities in the region. In practice, air-coupled seismics appear as a narrowband, near surface ground disturbance in the wake of an acoustic load (4). Areas with level, uniform, dry alluvial surface layers best support air-coupled seismics. This is a common landform used for basing missiles and aircraft.

Sonic boom experiments in Railroad Valley proceeded in two steps. The initial study treated the affect of heading on ground response produced by MACH 1.1 overflights. The follow-on effort concentrated on the affect of aircraft speed on ground response. Our study found that the local ground response, determined from hammer blows, readily located the frequency of the air-coupled term when the heading and speed of the aircraft were known.

Clearly, the frequency of the air-coupled term produced by an overflight can be extrapolated to obtain information as to aircraft speed.

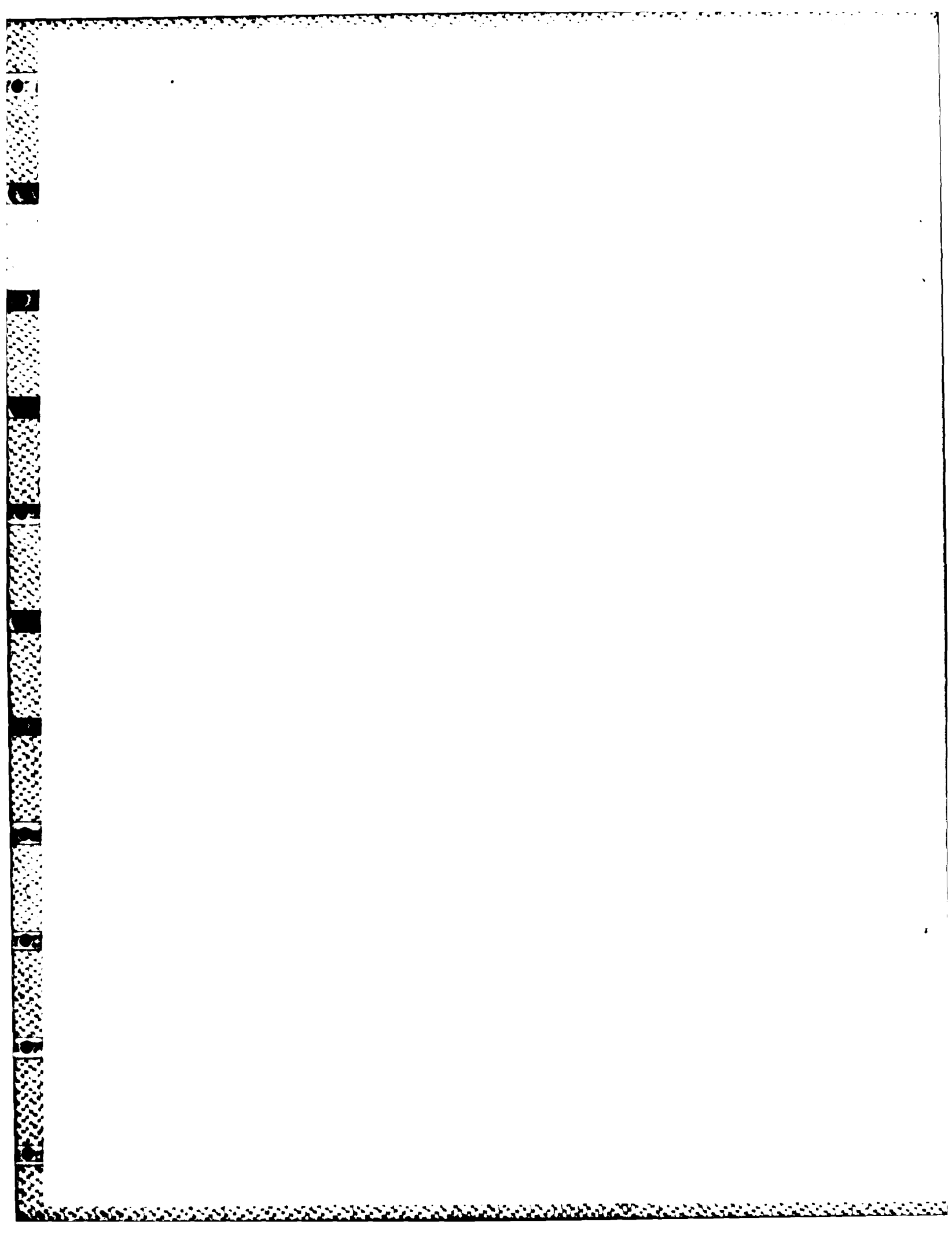
Air-coupled seismics can be used to remove location and speed ambiguities (ghosting) in network analysis.

A five element, small aperture seismo-acoustic array was used to measure flights made over Railroad Valley during June 1981 and later in June 1982. The aircraft pressure waves exhibit the usual N wave characteristic of sonic booms. In turn, ground disturbances invariably lagged the sonic boom (5). When the ground term was strongly excited, it had the properties of a narrowband Rayleigh wave.

The ground response of each overflight was calculated in terms of the normal admittance of the ground. The ratio of the amplitude of the seismics and pressure coefficients defines admittance. An admittance value in excess of 100mm/sec/psi was typical for the air-coupled term.

7.1 REFERENCES-SECTION 7

1. Oliver, J. and Isacks, B. (1962), Seismic Waves Coupled to Sonic Booms, Geophysics, 27, pp 528-530.
2. Espinosa, A. and Mickey, W. (1968), Observations of coupled Seismic Waves from Sonic Booms, A Short Note, Acustica, 20, pp 88-91.
3. Haskell, N. (1951), A Note on Air-Coupled Surface Waves, Bull. Seis. Soc. Am., 41, pp 295-300.
4. Ewing, W., et al., (1957), Elastic Waves in a Layered Media, McGraw-Hill, N.Y.
5. Wyle Laboratories Report WR68-2, (1968), Sonic and Vibration Environments for Ground Facilities - A Design Manual.

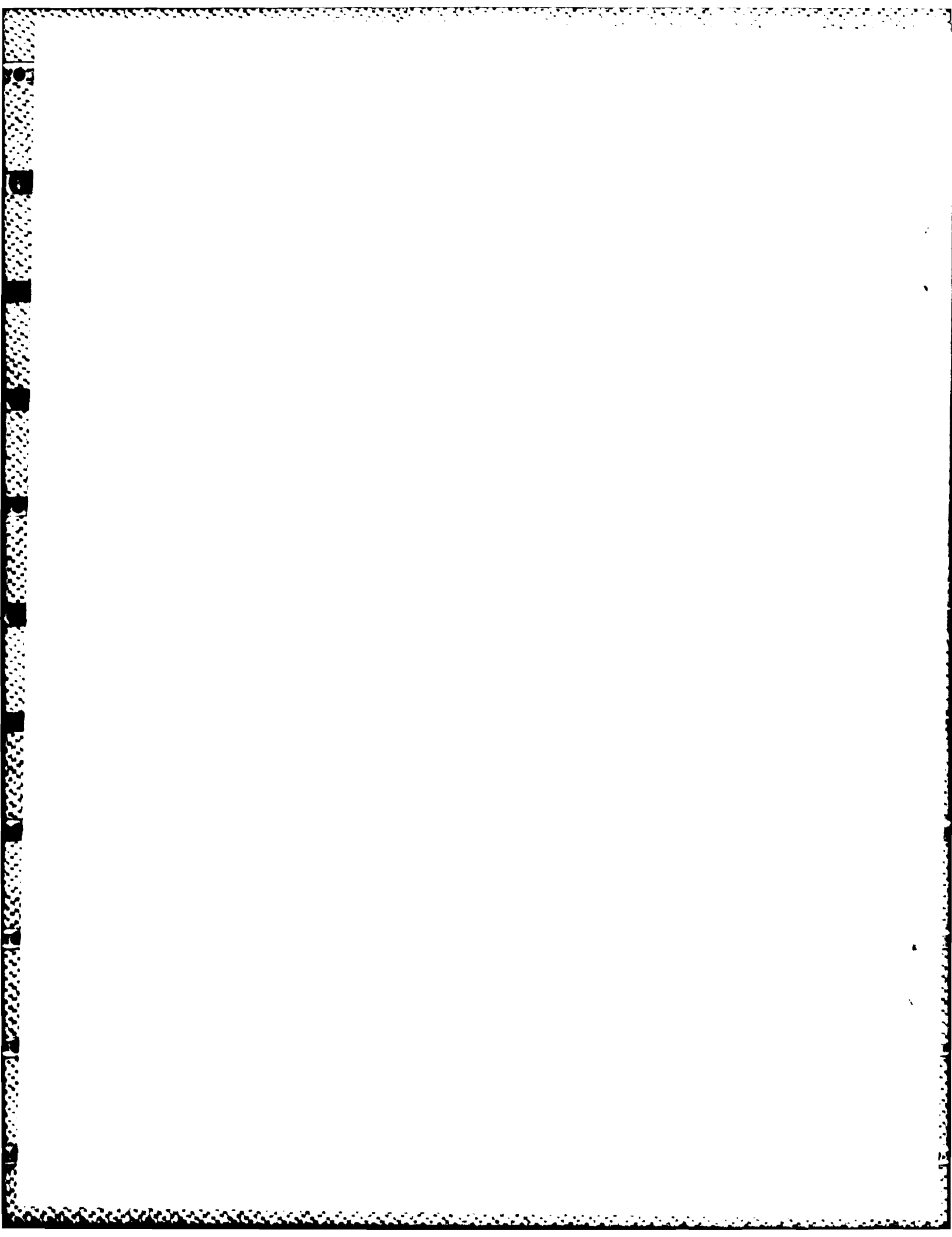


APPENDIX A - DEFINITIONS

A	Angstroms or Source Amplitude
AFGL	Air Force Geophysics Laboratory
AFGL/LWH	Terrestrial Sciences Division
c	Capacity or Phase Velocity
C_a	Speed of Sound in Air
D	Distance
db	Decibel
DOF	Degrees of Freedom
E	Goodness of Fit
EO	Voltage Constraint
ERC	Electronics Research Corporation
EST	Eastern Standard Time
f	Frequency, Hertz (Hz)
f_m	Frequency of G_{pp} (f) maximum
F_N	Nyquist Frequency
G	Green's Function
GDAS	Geokinetic Data Acquisition System
$G_{pp}(f)$	Theoretical Undelected Plume Spectrum
G_{33}	Vertical Displacement of Ground Surface at a "Large" Distance
i	$\sqrt{-1}$
j	Mode Number
K or k	Wave Number
k'	Trial Wave Number

km	Kilometer
KSC	Kennedy Space Center
LASA	Large Area Seismic Array
LCC	Launch Control Complex
NASA	National Aeronautics and Space Administration
$N(o,s^2)$	Zero Mean, Normal Process
OASPL	Overall Sound Power Level
PPR	Payload Preparation Room
P_{nn}	Power Spectra of Noise Process
P_{ss}	Power Spectra of Signal Process
$p(p-p)$	Peak to Peak Pressure
$p(r_l, t)$	Pressure at Distance r_l at Time t
$p(r_l, \omega)$	Fourier Transform of $p(r_l, t)$
PSI	Pressure, Pounds Per Sq. In.
Q	Material Quality Factor
r	Distance
RC	Resistor/Capacitor
rms	Root Mean Square
KRV	Railroad Valley, Nevada
ScF	Scale Factor
s^2	Variance
SD	Space Division
S/N	Signal to Noise Ratio
STS	Space Transportation System
T	Source Time

T'	Time
t	Retardation Time
t_p	Wave Phase Delay
t_g	Wave Group Delay
U	Group Velocity
VAFB	Vandenberg Air Force Base
VIC	Voltage to current inverter
$V_o(p-p)$	Peak to Peak Volts
$(2\pi f)$	Angular Frequency
ω	2π of Angular Frequency
$\mathcal{L}(k, \omega)$	Ratio of Magnitude of k weighted sum to scalar sum for $p(r_{\mathcal{L}}, \omega)$
$\hat{\mathcal{L}}(k, \omega)$	Absolute Maximum of $\mathcal{L}(k, \omega)$
ϕ_s	Source Phase



11-22-72

REPROD

FILMED

8